TÉCNICO LISBOA

Evaluation of Train Communications in Bridges and other Metallic Structures

Pedro Oliveira Jorge Delgado

Thesis to obtain the Master of Science Degree in

Electrical and Computer Engineering

Supervisor: Prof. Luís Manuel de Jesus Sousa Correia

Examination Committee

Chairperson: Prof. José Eduardo Charters Ribeiro da Cunha Sanguino

Supervisor: Prof. Luís Manuel de Jesus Sousa Correia

Members of Committee: Prof. Custódio José de Oliveira Peixeiro

Eng. Fernando Manuel Lopes Santana

November 2018

I declare that this document is an original work of my own authorship and that it fulfils all the requirements of the Code of Conduct and Good Practices of the Universidade de Lisboa

To my family

Acknowledgements

Firstly, I would like to express my sincere gratitude to my thesis supervisor, Professor Luís M. Correia, for allowing me to work under his supervision and giving me the possibility of developing this work in collaboration with Thales. It has been amasing to work with such a great person and amasing professor with immense knowledge to share. Over the several meetings we had during the development of this work, Professor Luís M. Correia not only gave me precious advice on how to correct and develop my work, but also enlightened me on the mentality an engineer should have, giving me important tips that will definitely shape my professional life. Thank you for all your support and guidance.

To Thales, namely Engineers Fernando Santana, Nuno Frigolet and Sérgio Rodrigues, who provided me with precious insights regarding the railway area and gave valuable input towards my work.

To my fellow partners at GROW, for their valuable friendship, input, support and motivation along our countless meetings. I would like to address special thanks to my colleagues André Ribeiro, for showing me the ropes to CST, and Kenan Turbic, for his patience, his readiness to help and for providing me access to the group's workstation.

My thanks to all of my other friends who encouraged me and gave me tips on how to overrun this challenge.

Last but by no means least, I would like to thank my family: my parents, brother and grandmother, for supporting me throughout not only this journey but for the rest of my life as well. I am forever grateful for their everlasting love, trust, advice, unconditional support, as well as their investment in my education and for making me the person I am today.

Abstract

The objective of this work was to develop a model in order to analyse the effect of a metallic bridge in different telecommunications systems, working in the 900 (GSM), 2600 (LTE) and 5900 MHz (WiFi/BBRS) frequency bands, for railway environments. The strategy adopted in this work evolved around two main directions. The first one was simply to implement propagation models in order to calculate path loss for the various environments under study. The novelty of this work comes with the second one, which consists of an electromagnetic model, based on CST software, for the analysis of penetration losses through a metallic bridge. The model was based on the schematics of a real bridge and different configurations were tested in order to reach a compromise between an accurate representation of the real problem and limited computational resources. It is then possible to estimate maximum communication distances for given configurations, as well as performance degradations that come with the inclusion of the metallic obstruction. In what concerns GSM, viaduct environments lead a range decrease roughly from 19% to 44% relative to their maximum communication distances, whereas other scenarios can see deteriorations from 45% to 56%. For BBRS, it is concluded that the currently used distances of around 300 m between BSs are conservative. This is also the scenario where the metallic bridge yields the biggest performance decrease, with communication distances reduced around 86%.

Keywords

Railway Communications, Metallic Bridges, Path Loss, CST Throughput.

Resumo

O objectivo deste trabalho foi desenvolver um modelo capaz de analisar o efeito de uma ponte metálica em diferentes sistemas de telecomunicações a operar nas bandas de frequências dos 900 (GSM), 2600 (LTE) e 5900 MHZ (WiFi/BBRS), para diferentes cenários de vias férreas. A estratégia adoptada neste trabalho prende-se directamente com dois módulos principais. O primeiro trata-se simplesmente de implementação de modelos de propagação para calcular perdas de propagação em vários cenários. A novidade desde trabalho vem com o segundo módulo, que consiste num modelo eletromagnético baseado no software CST com o principal objetivo de analisar as perdas de penetração através de uma ponte metálica. O modelo é desenvolvido com base numa ponte real e diferentes configurações foram testadas de modo a chegar a um compromisso entre uma representação precisa do problema e recursos computacionais limitados. É então possível estimar distâncias máximas de comunicação para certas configurações, assim como degradações de desempenho devido à inclusão da obstrução sob a forma de ponte metálica. No que se refer a GSM, cenários de viaducto têm perdas entre 19% e 44% relativamente a distâncias máximas de comunicação, enquanto que outros cenários podem ver estas distâncias reduzidas desde 45% até 56%. Para o caso do BBRS é concluído que as distâncias actualmente usadas, da ordem dos 300 m, entre estações base são conservativas. Este é também o cenário onde se observam as maiores reduções no que toca a distâncias máximas de comunicação, em cerca de 86%.

Palavras-chave

Via Férreas, Pontes Metálicas, Perdas de Propagação, CST, Ritmo de Transmissão.

Table of Contents

List of Figures

List of Tables

List of Acronyms

2G	2nd Generation
3G	3rd Generation
3GPP	3rd Generation Partnership Project
AP	Access Point
BBRS	Broad Band Radio System
BPSK	Bipolar Phase Shift Keying
BS	Base Station
BSS	Base Station Subsystem
CCTV	Closed Circuit Television
CDMA	Code-Division Multiple Access
CS	Circuit Switching
CST	Computer Simulation Software
DL	Downlink
DQPSK	Differential Quadrature Phase Shift Keying
E-GSM-R	Extended Global System for Mobile Communications
EIRENE	European Integrated Railway Radio Enhanced Network
EM	Electromagnetic
eNB	E-UTRAN Node B
EPC	Evolved Packet Core
EPS	Evolved Packet System
ERTMS	European Rail Traffic Management System
ETCS	European Train Control System
ETSI	European Telecommunications Standard Institute
E-UTRAN	Evolved Universal Terrestrial Radio Access Network
FDD	Frequency Division Duplex
FDMA	Frequency Division Multiple Access
FSS	Frequency Selective Surface
GI	Guard Interval
GMSK	Gaussian Minimum Shift Keying
GPRS	General Packet Radio Service
GPS	Global Positioning System
GSM	Global System for Mobile Communications
GSM-R	Global System for Mobile Communications-Railway
HSR	High Speed Railway

HSS	Home Subscriber Service
IEEE	Institute of Electrical and Electronics Engineers
IN	Mobile Intelligent Network
IoT	Internet of Things
IP	Internet Protocol
ISDN	Integrated Services Digital Network
LOS	Line of Sight
LS	Least Squares
LTE	Long Term Evolution
LTE-R	Long Term Evolution-Railway
MCS	Modulation and Coding Scheme
MIMO	Multiple Input Multiple Output
MME	Mobility Management Entity
MMS	Multimedia Message Service
MORANE	Mobile Radio for Railway Networks in Europe
MSC	Mobile Switching Centre
MT	Mobile Terminal
NLOS	Non-Line of Sight
NSS	Network Subsystem
OCC	Operation Control Centre
OFDMA	Orthogonal Frequency Division Multiple Access
OSS	Operation and Support Subsystem
PAPR	Peak to Average Power Ratio
PCRF	Policy and Charging Rules Function
PDN	Packet Data Network
PEC	Perfect Electrical Conductor
P-GW	Packet Data Network Gateway
PS	Packet Switching
PSTN	Public Switched Telephone Network
QAM	Quadrature Amplitude Modulation
QPSK	Quadrature Phase Shift Keying
RAN	Radio Access Network
RB	Resource Block
RBC	Radio Block Centre
RMS	Root Mean Square
RMSE	Root Mean Square Error
RRM	Radio Resource Management
Rx	Receiver
SC-FDMA	Single Carrier Frequency Division Multiple Access
S-GW	Serving Gateway

SISO	Single Input Single Output
SMS	Short Message Service
SS	Subsystem
SSS	Mobile Switching Subsystem
TCH	Traffic Channel
TD	Terminal Device
TDD	Time Division Duplex
TDMA	Time Division Multiple Access
TETRA	Terrestrial Trunked Radio
Tx	Transmitter
UE	User Equipment
UL	Uplink
UMTS	Universal Mobile Telecommunications System
VoIP	Voice Over IP
VoLTE	Voice Over LTE

List of Symbols

A	Fitting Parameter
B	Intercept Parameter
B_W	Bandwidth
C	Path Loss Frequency Dependence
$C_{A,B,C,D}$	Path Loss Expression's Coefficients
C_{ch}	Channel Capacity
d	Distance between Transmitter and Receiver
d_0	Reference Distance
d_{BP}	Breakpoint Distance
E	Electric field magnitude
E_{dir}	Electric field emitted by dipole at a given point
E_{fs}	Electric field for free space propagation
F	Noise Figure
f_c	Centre Frequency
H	Viaduct's Height
h_{AR}	Distance between the Antenna and the Roof of the Train
h_{BS}	Base Station's Height
h_{MS}	Mobile Station's Height
h_t	Train's Height
l	Dipole's Length
L_{bridge}	Losses due to the insertion of a metallicbridge
L_p	Path Loss
M_I	Interference Margin
M_S	System Margin
N	Noise power
P_t	Power fed to the transmitting antenna
P_{Tx}	Transmitter output power
R_b	Throughput
R_{ff}	Far field Region
w_t	Train's Width
X	Environment Specific Parameter
x	Standard Normal Distribution
y	Normal Distribution defined in He *et al.* 2011 model

μ	Average
$\Delta_{1,2}$	He *et al.* 2014 model correction factors
θ	Elevation in Spherical Coordinates
λ	Wavelength
ρ	Radius in Spherical Coordinates
ρ_N	Signal to Noise Ratio
$\sigma_{u,su}$	Standard deviation (urban, suburban)
φ	Azimuth in Spherical Coordinates

List of Software

Antenna Magus	Antenna Design
CST	Electromagnetic Simulator
Draw.io	Flowchart editor
Excel	Computing and Processing Tool
GetData	Data Digitiser
MATLAB	Numerical Computing
Microsoft Word	Text Processor
MS Paint	Image Editor

Chapter 1

Introduction

This chapter gives a brief overview of the thesis. In order to understand the relevance of this work, a contextual perspective is given in Section 1.1, which approaches the most common railway networks, as well as the current investment in some European countries' infrastructure. In Section 1.2, the motivation for the work is established, explaining some of the most important points that are focused on this work, followed by a detailed work structure.

1.1 Overview

Over the last years, High Speed Railways (HSRs) have been developed in order to improve the quality of life of train passengers. This method of transport can drastically reduce the cost and duration of passengers' trips, but it also comes with new needs in what concerns technology, infrastructures and safety.

This development emerges as an improvement in different areas, such as railway infrastructure deployment (railway tracks, overhead wires, tunnels, bridges and stations), the rolling stock, training facilities and all the required equipment to supply the tracks with telecommunication systems.

The constant need for communications inside trains and along stations (whether it comes from the trains' own communications systems or the passengers' devices) has led to increasing investments by many entities (railway infrastructure owners, managers and service providers) in order to supply the currently existing networks with not only voice and data transmission but also different passenger safety and cargo tracking systems.

Mobile communications are an essential part of this investment, which comes with special needs in what concerns signalling and safety compared to standard personal communications. Like these systems, railway telecommunications evolved from the analogue 1G system and currently operate using mostly a 2G system with special railway functionalities.

In 2000, European railway companies finalised the specifications for the Global System for Mobile Communications – Railway (GSM-R), an international communications standard for railway communications based on the second-generation GSM with specific railway functionalities, with the objective of replacing all analogue systems then in use. It is implemented with dedicated Base Stations (BSs) along the railways in the specific frequency bands: GSM-R and E-GSM-R.

Nokia, Huawei and Kapsch are the main suppliers of GSM-R infrastructure. In most implementations, the BSs are usually located 7 to15 km apart from each other, however, countries such as China opt to use lower distances (3 to 5 km) in order to achieve higher levels of redundancy, which guarantee higher network availabilities. Countries such as Germany and Italy have GSM-R networks with between 3 000 and 4 000 BSs.

GSM-R is essentially the same system as the 2nd generation GSM, with additional railway functionalities, such as group calls, broadcast calls, emergency calls, shunting mode, functional and location-dependent addressing. Its specifications are defined by the European Integrated Railway Radio Enhanced Network (EIRENE) and approved by Mobile Radio for Railway Networks in Europe (MORANE). Nowadays it is mainly used in Europe, Asia, North Africa and Australia, replacing the majority of the older railway communications standards. It provides a secure platform for voice and data communication for trains, control centres, rail staff and user devices; however, it has the same limitations of the GSM standard, that is, the low maximum data rate (172 kbps), the high levels of interference from

other users operating in the same bands and of course, disadvantages related to circuit switch techniques.

Terrestrial Trunked Radio (TETRA) is a private communications system of trunked mobile radio. Like GSM-R, it provides data and voice transmission, however, as a private network, its focus revolves around entities such as security forces, emergency services, military, transport companies and governments. Its specifications are defined by the European Telecommunications Standards Institute (ETSI) and it aims to provide a radio system for a closed group of users. It features voice encryption and emergency call reliability and its unique services include wide-area fast call set up and direct mode operation, mainly useful in emergency situations.

TETRA uses a low frequency band, which allows the coverage of large areas with a reduced number of BSs. In the absence of a network, radio terminals can use the direct mode, which allows the direct communication amng different channels. It provides a point-to-point function, enabling users to have trunked radio links between each other without the direct involvement of an operator. Operation modes include transmission from one mobile terminal (MT) to another and one MT to many MTs (Broadcast or user groups), useful for railway communications. Some limitations of this technology are related to the limited available bandwidth. Interference from other services is expected and acceptable and the allowed transfer rates are low (up to 36 kbps). Besides data and voice, signalling is also transmitted, enabling the distinction of different MTs, which are identified by their phone numbers. This is important when the group of users using the service follows a hierarchy, which is the case of most, if not all, of the aforementioned entities. Overall, this system has low installation and maintenance costs and offers a reliable service to its users, albeit with low data rates.

Broad Band Radio System (BBRS) is a proprietary system, mainly used in metro and railway scenarios, which uses WiFi technology (802.11n) and allows the transmission of data between the rolling stock and the wayside, as well as eventual existing stations or any other physical infrastructure. It provides data rates close to the ones of 802.11n (theoretical maximum of 75 Mbps for a single 20 MHz channel data stream with no guard interval) and serves the need of systems asking for real time information, such as live video transmission, public addressing, passenger live information and help points, as well as train management and maintenance services.

Long Term Evolution – Railway (LTE-R) is the emerging platform for railway communications, featuring high data rates and the possibility of performing handovers with no data loss. The system operates using single sector cells and possible frequency bands to be used are the 450, 800, 900, 1400, 1800 and 2600 MHz ones. Since it is fully built on packet switch, it suits better data communications and offers reduced delays on signalling, useful for train specific operations and systems such as the European Train Control System (ETCS). More efficient spectrum usage and higher throughputs (peak rates of almost 100 Mbps) are consequences of upgrades in what concerns modulation and access techniques over 2G systems, making LTE-R the current stand-out winner in what concerns data rates in railway communications.

Even though 2G railway networks are present in most developed countries, implemented via GSM-R,

the same is not true for newer generations. On the one hand, the standards for 4G LTE-R are being finalised and therefore operators may be waiting on their release in order to fully plan their networks, and on the other hand, perhaps there is currently no real demand for this technology in order to justify the investment needed to upgrade the existing railway networks to their successors.

Figure 1.1 shows the value of road and railway structures for different European countries.

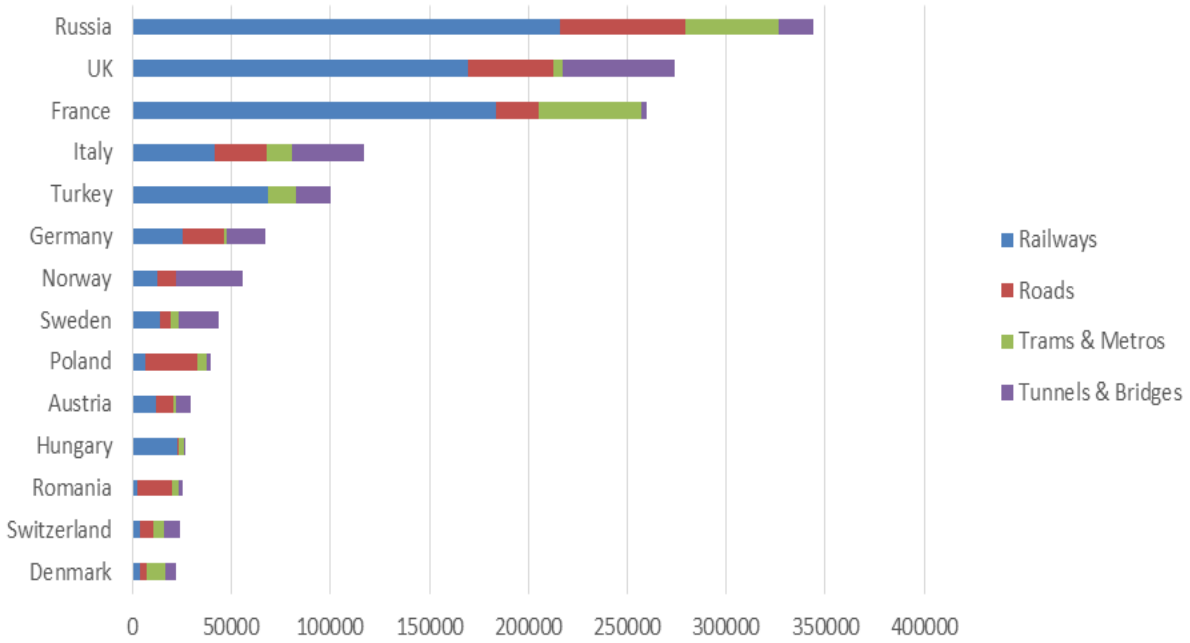

Figure 1.1 - European Investments in Road and Railway Businesses, values in US$ Million (extracted from [Cons17]).

One can see the majority of European countries are underdeveloped in what concerns railway and road investments, and even the ones with the most efforts in the area (UK and France) struggle to compete with the eastern world. Germany stands out as a noteworthy scenario, with under $67.5 \cdot 10^6$ $ in value split among railways, roads, trams, metros, tunnels and bridges.

The first LTE-R network launched in the world is located in the Korean city of Busan, providing communications to a 40 km long subway line, as a partnership between SK Telecom and Samsung. With the approach of the XXIII Olympic Games, held in Korea in the Winter of 2018, Samsung in partnership with Korea Telecom provided visitors of the games with safer train trips. As seen in [Sams17], this LTE-R network went live in December 2017, in the Korean line of Wonju-Gangneung, which has an extension of 120 km and enables access to the LTE-R network onboard of its trains, operating at speeds of up to 250 km/h.

It is only a matter of time before other operators in Asia or even new ones in Europe and America start investing in this technology, and therefore this work is relevant in order to provide a context for the eventual problems that may occur when dealing with telecommunication systems in metallic environments.

1.2 Motivation and Contents

In what concerns the motivation of this study, metallic materials have specific properties that must be taken into account when they are present in communications systems. Usually, metallic materials can be avoided when projecting the networks, or their impact is so small that they do not affect the standard analyses, however, in railway environments, metallic structures are present in the majority of the existing infrastructure and they have to be dealt with specifically. Examples of these are train stations, tunnels, bridges and viaducts, which are some of the environments approached within this work.

The main idea approached in this thesis consists of the fact that metallic structures are excellent reflectors of EM waves, which leads to high levels of attenuation and phenomena such as radiation scattering and diffraction along the metallic media.

This work focuses on the impact of metallic structures, such as bridges and viaducts, on the different telecommunication systems already presented. EM simulations were performed in order to simulate the behaviour of a specific scenario, where a train is crossing a metallic bridge and different propagation models are implemented in order to properly estimate path loss and consequently obtainable throughputs for different systems and modulations. The main contribution of this work resides in the fact that the metallic bridge problem is modelled with CST software, which allows the development of an attenuation model for different work frequencies.

The work presented in this document is subdivided into five main chapters. The present one contains the overview of the thesis, along with its contents, as well as the motivation to do this kind of study. The evolution of the different communications systems at hand is approached here, as well as the main ideas that are approached in the remaining chapters of this thesis.

The second chapter contains the fundamental concepts that need to be explained in order for one to fully understand the developed work. Topics such as the architectures and radio interfaces of the different analysed networks (GSM-R, LTE-R and BBRS), as well as significative differences regarding their usual counterparts (standard 2G GSM, 4G LTE and 802.11n WiFi) are explained here and a brief overview regarding railway communications is given. The core scenarios that are encountered in railway environments are also presented and explained. The chapter ends with the state of the art, where one can check the works have been published so far in what concerns the approached thematic.

The following (third) chapter contains specific tools and methods that are needed in order to reach the objective of this work. It starts with a brief introduction regarding link budget and how it is calculated, through the introduction of important parameters that are needed in order to estimate path loss. Different propagation models approached in this work are also analysed in this section, with their parameters and scenarios detailed. Furthermore, throughput models for both LTE-R and WiFi are introduced so one can estimate the obtainable data rates in the analysed scenarios and an introduction to the simulator (CST) is given. This introduction consists of an overview that details some important aspects regarding the simulator, as well as a brief explanation of the different electromagnetic solvers that are available. In addition, the modelling of the simulated scenario is presented in this chapter, with considerations

regarding signal measurement and explains the approximations that were made. The chapter ends with a model assessment, which is needed in order to ensure the validity of the results that were obtained and shown in the following chapter.

The fourth chapter consists of the presentation of the results obtained with the developed models and the EM simulator, as well as their treatment and analysis. It begins with the definition of the scenario at hand, as well as the main requirements for the different networks in analysis. After these initial definitions, the process of modelling the attenuation introduced by a metallic bridge is explained. This is where the EM simulator's results are presented and analysed. Finally, the different networks are approached with distinct methodologies based on their capabilities and requisites. Path loss is the key parameter which is analysed in this section. GSM results are split into viaducts and other types of scenarios whereas LTE and WiFi first need some considerations regarding their signal to noise ratios and modulation levels.

Finally, the fifth and last chapter contains the conclusion of this work, as well as the main points that can be developed in future works. It contains a collection of the main conclusions drawn in the previous chapter and the core ideas one should retain from this work.

At the end of this work, a group of annexes exists in order to present additional information that is useful to complement some of the contents presented in the main work.

Chapter 2

Fundamental Aspects

This chapter provides an overview of the GSM-R, TETRA, LTE-R, BBRS systems, focusing on their architectures and radio interfaces. Some railway-specific points regarding telecommunications are given and the main scenarios to be analysed are stated. An introduction regarding the simulator in use is also given, followed by some of the released works regarding the thematic of this work.

2.1 GSM-R and TETRA

This section contains aspects regarding GSM and is based on [Corr15], [HaRM13], [HAWG16] and [ZAZW17].

GSM-R's network is the same as GSM's with antennas placed next to the railways every 7 to 15 km. It is constituted by 4 different subsystems: Base station (BSS), Network (NSS), Public Networks and the mobile terminal (MT). The NSS includes the Mobile Switching (SSS), as well as the General Packet Radio Service (GPRS) subsystems. These components and their main interfaces are illustrated in Figure 2.1.

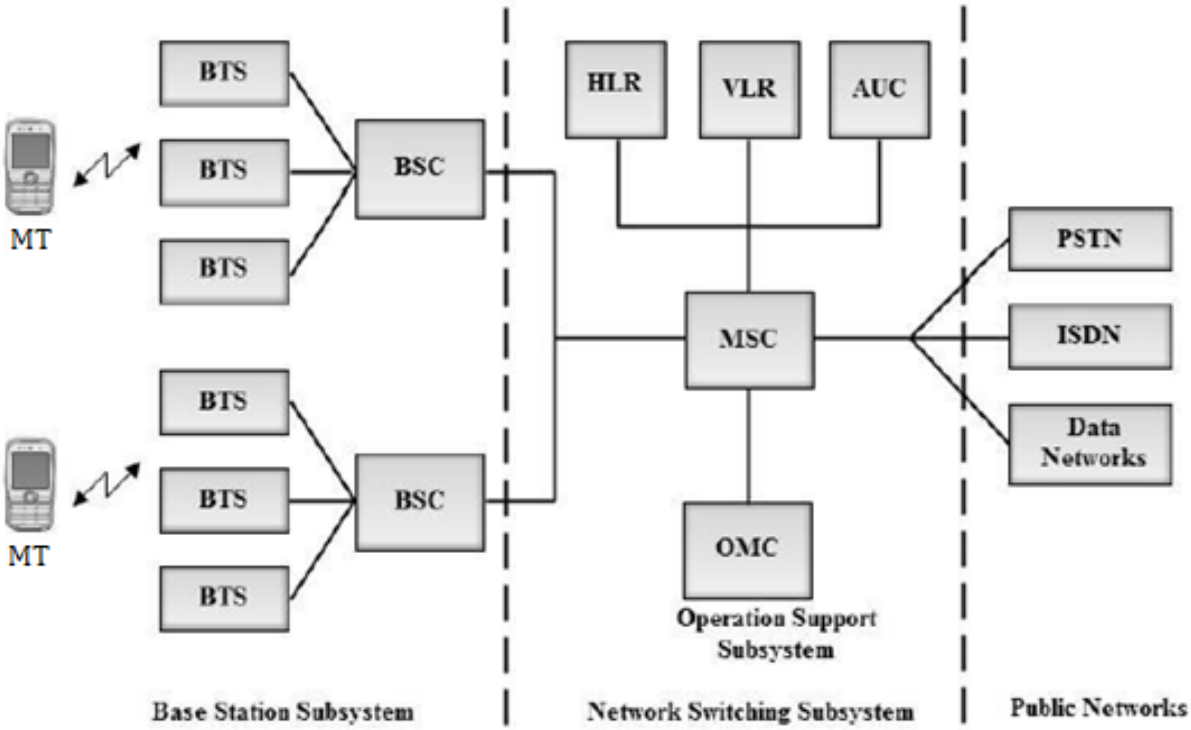

Figure 2.1 - GSM's Architecture (extracted from [BANI14]).

The SSS manages the user server switching, as well as user data, mobility and security functions. It contains GSM's primary node, the Mobile Switching Centre (MSC), which is responsible for the routing of services such as voice and SMS and Circuit Switched (CS) data.

GPRS includes a core layer as well as an access one. It is responsible for the users' packet traffic. The access layer is based on GSM-R, and therefore it uses its resources.

Connecting the mobile stations, the BSS receives and transmits their signals and handles radio resource management. It is also responsible for the communication among users and the transmission of

signalling and user information. It also enables the access to public networks such as the Public Switched Telephone Network (PSTN) and the Integrated Services Digital Network (ISDN).

Finally, the MT is the physical device that is used in order to access and use the system.

GSM is based on Time-Division Multiple Access (TDMA) and Frequency-Division Duplex (FDD), allowing a bidirectional transmission of information. In TDMA, users are periodically assigned time-slots in a frame structure. The whole frequency band is shared among all users, so a synchronised time-slot mechanism is essential. With this technique, multiple channels per carrier are achievable, along with high inter-symbolic interference.

Interference from simultaneous transmissions is negligible, since users are separated in time and the devices experience high battery lives due to the periodical transmission nature of TDMA. Even though it is a cheap multiple access technique, TDMA comes with limitations, such as users being limited to a fixed number of time-slots at any given moment, which can be a constraint, depending on the quantity of devices using the network, resulting in calls dropping if the network is congested. Table 2.1 shows the standardised GSM frequency bands and Figure 2.2 presents GSM-R's band allocation.

Table 2.1 - GSM's Frequency Allocation (adapted from [HaRM13]).

GSM Band [MHz]	Available Frequencies [MHz]	Location
400	[450.4 - 457.6] U [460.4 - 467.6] [478.8 - 486] U [488.8 - 496]	Europe
800	[824 - 849] U [869 - 894]	America
900	[880 - 915] U [925-960]	Europe, Asia, Africa
1800	[1710 - 1785] U [1805 - 1880]	Europe, Asia, Africa
1900	[1850 - 1910] U [1930 - 1990]	America

GSM-R maintains the GSM's 200 kHz carrier spacing and Gaussian Minimum Shift Keying (GMSK) modulation, allowing transmission rates of up to 270.833 kbps. A TDMA frame has a duration of 4.615 ms, which is split into 8 time-slots, each with 156.25 bits and a duration of 577 µs, being assigned to traffic (TCH) or control channels. The minimum power at the receiver for the system to operate correctly (receiver sensitivity) is -104 dBm.

Data is transmitted in time-slot as bursts. There are 5 different types of bursts: the normal burst, the frequency correction burst, the synchronisation burst, the access burst and the dummy burst. The format and content of each burst depends on its type.

CS is used to ensure a constant flow of information between trains and control centres. This is possible due to the use of a digital modem, which operates with a higher priority than users. No sectorisation is used (Single-Sector cells) and hard handover is employed, that is, a user's connection with a BS is totally broken before the user connects to another BS. In order to guarantee system's performance, maximum train speeds should be below 500 km/h.

Figure 2.2 shows the GSM-900 frequency band, including where GSM-R and its extended band, E-GSM-R, are located.

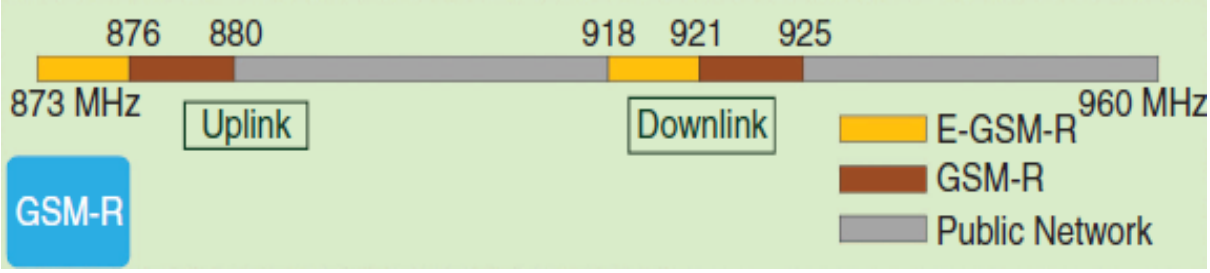

Figure 2.2 - GSM-R's Band Allocation (adapted from [HAWG16]).

When analysing technical aspects, the most impactful difference between GSM and its railway counterpart concerns the usage of spectrum. Operators have full freedom to use their spectrum according to their needs, whereas GSM-R faces a much stricter frequency planning problem. GSM-R's frequency range is very close to public frequency resources and therefore adjacent frequency interference should be carefully analysed when deploying and optimising networks.

Another factor one should consider is that GSM-R focuses a lot more on safety and operational efficiency than the public GSM network and consequently its reliability is naturally higher. Additionally, GSM-R does not use adaptive modulation and coding, which is a very common, although hard to implement, requirement in other railway networks.

The main difference in what concerns user experience is related to the services offered by the systems. While the regular GSM offers voice and data services and is mainly concerned with the first, GSM-R provides functions specifically developed for railway environments, such as functional and location dependant addressing, emergency and priority calls, voice group and broadcast services and enhanced multilevel precedence and pre-emption.

One might face capacity issues when dealing with high traffic scenarios, but the priorities are to minimise interference and maximise coverage in order to ensure trains' and passengers' safety by providing permanent signalling and control uptime.

Figure 2.3 schematises the GSM-R's elements added to the core GSM standard.

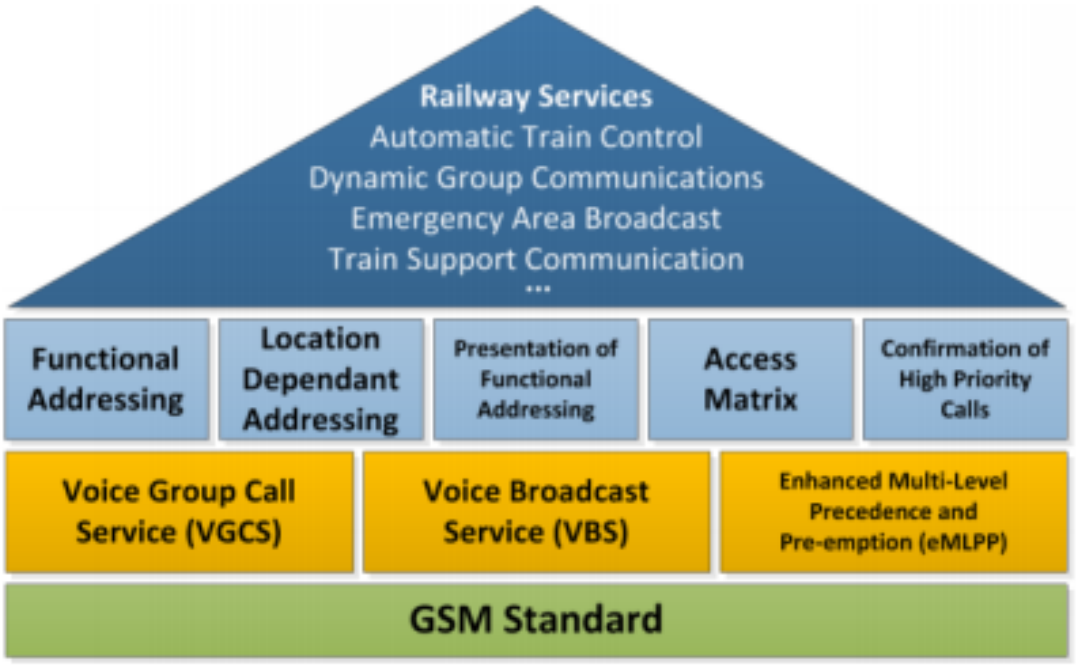

Figure 2.3 - GSM-R's Services Added on the GSM's Standard (extracted from [SnSo12]).

Even though Figure 2.3 states the different system capabilities in the shape of a pyramid, the available functionalities depend on the system's MT in use and its software. Not every single one of these features needs to be present in every GSM-R system.

TETRA is a possible alternative to GSM-R. This system requires a receiver sensitivity of -103 dBm and allows high cell ranges in the order of 60 km. It is capable of handover, uses CS for voice and Packet Switching (PS) for data.

[DuGI99] expresses TETRA's architecture in terms of 6 different interfaces, which ensure different provider interoperability, interworking and network management. These are represented in Figure 2.4 and explained bellow:

- Radio Air Interface (I1) assures the compatibility of different terminal equipment over the air interface;
- Line Station Interface (I2) for terminals connected over the wireline connection, such as ISDN;
- Inter-System Interface (I3) allows the connection of TETRA networks from different manufacturers;
- Terminal Equipment Interface (I4 and I4´) supports the independent development of mobile (I4) and line station (LS) to terminal equipment (I4´);
- Network Management Interface (I5) provides the management of network equipment inter-working within the TETRA network;
- Direct Mode Interface (I6), also known as walkie-talkie, is used when MTs need to communicate directly with each other, without the need of the TETRA network.

As seen in [Hart07], the TETRA radio air interface standard provides secure communications channels through the use of a digital algorithm, which prevents data from being intercepted by unwanted listeners and radio scanners.

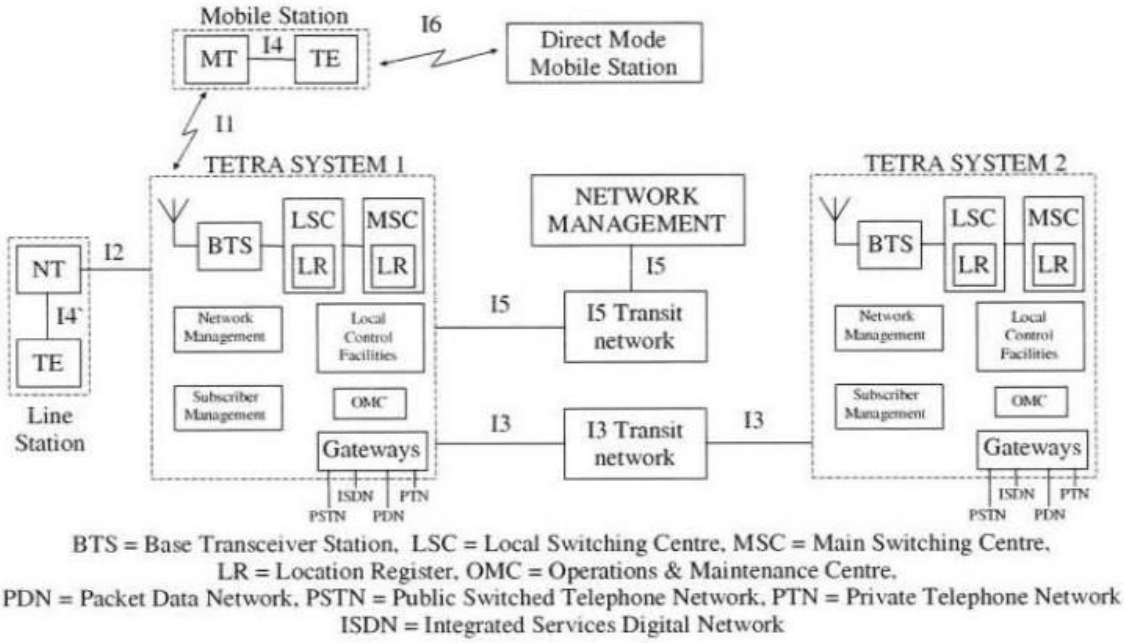

Figure 2.4 - TETRA Network Architecture (extracted from [DuGI99]).

Additional encryption standards can be utilised as part of TETRA in order to make it suitable for Governments and Military organisations.

Following [Corr15], TETRA's most commonly used band is [380, 470] MHz, however, depending on the spectrum availability and the intended coverage area, the higher frequency band [870, 923] MHz can also be used. FDD is employed and the most common configuration uses the [380, 390] MHz range for uplink (UL) and [390, 400] MHz for downlink (DL). It uses TDMA with 4 time-slots per frame and 25 kHz channels with $\pi/4$-Differential Quadrature Phase Shift Keying (DQPSK) modulation.

2.2 LTE-R

This section approaches LTE system's basic concepts, as seen in [Corr15], [HAWG16] and [ZAZW17].

Like GSM/GSM-R, the distinction between LTE and LTE-R are the services that are offered by the technology and therefore LTE-R's network architecture is essentially the same as LTE's, Figure 2.5.

Following [HoTo11], the LTE system is constituted by 4 main domains: The Evolved Universal Terrestrial Radio Access Network (E-UTRAN), the Evolved Packet Core (EPC), the Services and the User Equipment (UE).

The IP Connectivity Layer groups the EPC, the E-UTRAN and the UEs. Also called Evolved Packet System (EPS), this group has the task of providing IP based connectivity, since all services offered in this layer are Internet Protocol (IP) based.

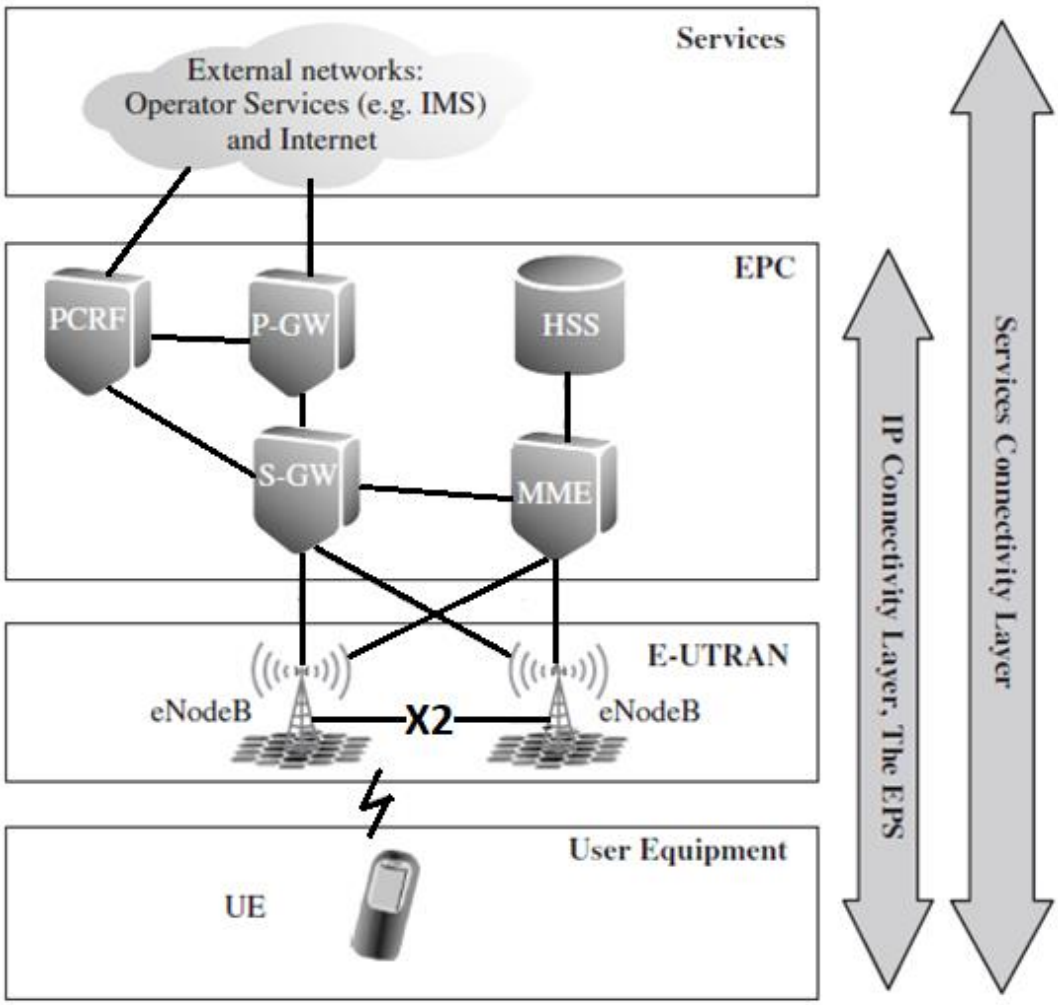

Figure 2.5 - LTE's Architecture (adapted from [HoTo11]).

The Services layer is connected to the EPC and provides utilities such as Voice Over IP (VoIP), Voice Over LTE (VoLTE) and access to the Internet.

According to [3GPP17], when developing the 4G systems, the 3rd Generation Partnership Project (3GPP) decided to use IP to transport services. With this change, LTE no longer uses the traditional CS as seen in GSM and the 3rd generation Universal Mobile Telecommunications System (UMTS) and EPC is basically a PS equivalent of these previous 2G and 3G systems, Figure 2.6.

The Policy and Charging Rules Function (PCRF) is composed of software that is responsible for policy, as well as charging functionalities. The two gateways, Packet Data Network (P-GW) and Serving (S-GW), are connected and transport the data between the UEs and the external networks. While the S-GW is responsible for routing the users' IP packets, the P-GW routes packets between the Packet Data Networks (PDNs).

The signalling for mobility and security in E-UTRAN access is handled by the Mobile Management Entity (MME) and the Home Subscriber Service (HSS) is a database that contains user information and provides support for mobility management, call set up, user authentication and access validation.

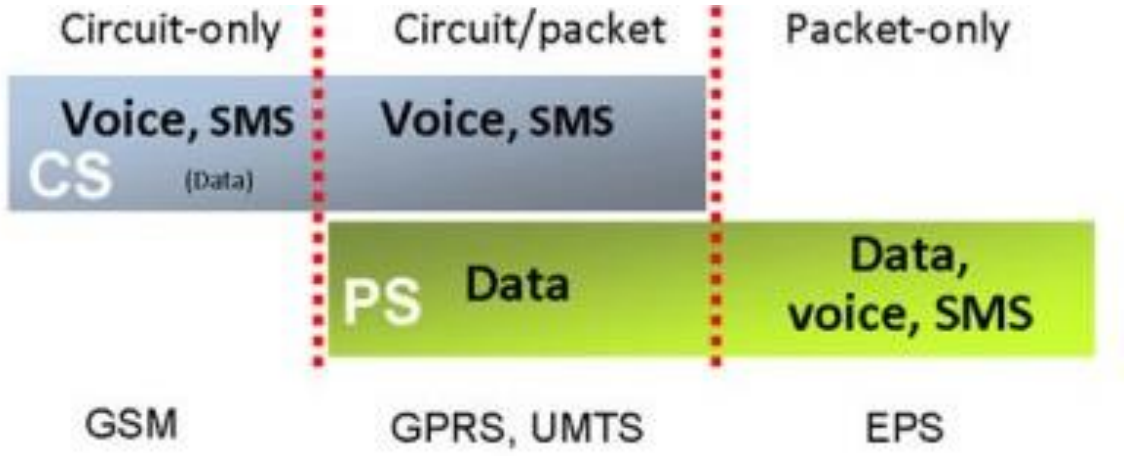

Figure 2.6 - Different Technologies' Domains (extracted from [3GPP17]).

The E-UTRAN implements the Radio Access Network (RAN) and has, as its main functions, the roles of Radio Resource Management (RRM), IP Header compression, as well as Security and Mobility Management. It is solely composed of nodes called E-UTRAN Node B (eNB), which are essentially base stations that control all radio functions in a fixed part if the system. These are connected to the EPC and can be connected to each other via the X2 interface.

LTE can use both duplexing modes, FDD and Time-Division Duplex (TDD), in order to achieve a bidirectional flow of information. For these reasons, one has more flexibility in what concerns to frequency allocation when choosing the TDD configuration, especially when spectrum scarcity is being dealt with.

When dealing with HSRs, additional planning should be made in order to account for the specific railway environment. Due to the train monitoring services, UL requirements are often much higher than DL ones. The FDD configuration for LTE defines extra UL-DL configurations, ensuring more flexibility when dealing with asymmetric transmissions. On the other hand, TDD LTE faces stricter synchronisation requirements compared to FDD, aggravated by fast-moving trains.

LTE employs Orthogonal Frequency Division Multiple Access (OFDMA) for DL and Single Carrier Frequency Division Multiple Access (SC-FDMA) for UL. The first technique consists of splitting the information into several narrow, closely-spaced (15 kHz) orthogonal sub-carriers in order to transmit the information, which are then assigned to different users. For UL the former technique is no longer employed since the combining of the different subcarriers can lead to a high Peak to Average Power Ratio (PAPR), which needs additional power back-off techniques, leading to power constraints. This is not significative in fixed applications but can be a major hindrance when dealing with MTs. For this reason, SC-FDMA is used in UL, as it is more energy efficient, leading to jointly transmitted subcarriers, instead of OFDMA's separated ones.

LTE-FDD is the most common duplex mode used in Europe and the most used bands are located around 800, 1800, and 2600 MHz. Table 2.2 shows these bands with detail.

Table 2.2 - LTE-FDD's Bands in Europe (adapted from [HoTo11]).

Band Designation	UL Band [MHz]	DL Band [MHz]
20	[832, 862]	[791, 821]
3	[1710, 1785]	[1805, 1880]
7	[2500, 2570]	[2620, 2690]

The physical resources that are allocated to users are called resource blocks (RBs). They consist of 12 subcarriers and, given the previously mentioned carrier spacing, have a resolution of 180 kHz in frequency, which corresponds to a time-slot with a duration of 0.5 ms.

An example of an LTE-FDD frame can be observed in Figure 2.7. It is composed of 10 subframes, each containing 2 slots with a duration of 0.5 ms each and up to 7 OFDM symbols are transmitted per subframe. In LTE-TDD there are also 10 subframes, however, since the total bandwidth must be shared between UL and DL, along with guard frequencies, a fewer number of symbols (usually 6) may be transmitted.

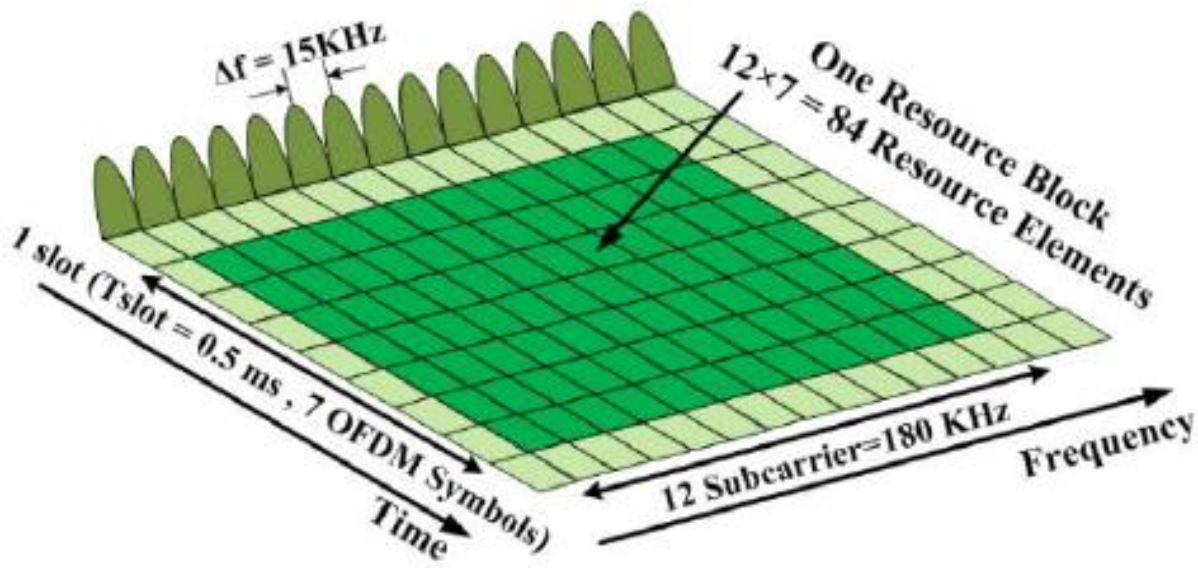

Figure 2.7 - LTE-FDD Resource Block (extracted from [ChSh14]).

Increasing the bandwidth of the system has no effects on the carrier spacing, but instead increases the number of subcarriers that can be allocated to users. Table 2.3 presents 3GPP's bandwidth configurations, as well as their corresponding number of available RBs or subcarriers.

The employed modulation schemes are Quadrature Phase Shift Keying (QPSK) and Quadrature Amplitude Modulation (QAM): 16-QAM or 64-QAM and 256QAM in DL, which is not considered in this work.

Table 2.3 - LTE Physical Channels (adapted from [Corr15]).

Bandwidth [MHz]	1.4	3.0	5.0	10	15	20
Number of RBs	6	15	25	50	75	100
Number of Subcarriers	72	180	300	600	900	1200

Table 2.4 shows LTE's peak UL single stream throughputs for different configurations of MCSs.

Table 2.4 - LTE's Peak UL Throughputs [adapted from [Alme13]).

UL maximum throughput [Mbps]	**Bandwidth [MHz]**					
MCS	**1.4**	**3.0**	**5.0**	**10**	**15**	**20**
QPSK, ½	1.0	2.5	4.2	8.4	12.6	16.8
16QAM, ½	2.0	5.0	8.4	16.8	25.2	33.6
64QAM, ¾	4.5	11.3	18.9	37.8	56.7	75.6

Aside from the frequencies, which are not standardised yet, what differentiates LTE-R from its LTE counterpart is related to the services it offers and the fact that its more oriented toward reliability rather than capacity, in order to ensure permanent system availability.

[HAWG16] presents 5 LTE-R services described below:

- Information transmission of control systems is a feature that enables the compatibility of ETCS level 3 through real-time information wireless transmission.
- Real-time monitoring provides imaging of the cabinets, tracks and equipment, as well as weather conditions. This information is shared between both the control centre and the train in real-time.
- Train multimedia dispatching allows the transmission of text, data, voice, image and video to the dispatcher. It supports features such as voice trunking, dynamic grouping, temporary group calling, short message (SMS) and multimedia message services (MMS).
- Railway emergency communications.
- Railway Internet of Things (IoT) provides with services such as real-time querying and tracking.

Other services are also mentioned such as in-station communications, wireless interaction of passenger information and mobile e-ticketing.

2.3 BBRS

Some aspects regarding WiFi/BBRS are described in this section, based on [Cisc10], [Stal05], [Thal12], [Thal17] and [Nati18].

BBRS' architecture is shown in Figure 2.8. It consists of several Access Points (APs) spread along the different stations, which provide radio coverage for onboard train systems. The network is maintained by central controllers, which are responsible for routing traffic from the different APs to their destinations and has additional redundancy in order to guarantee passenger and cargo safety.

The Network Management System (NMS), as part of the Operation Control Centre (OCC), is responsible for the supervision of the individual equipment inside the network and can perform operations such as device discovery and monitoring and performance analysis. It enables live monitoring and management of the network from the OCC. Functions such as traffic prioritisation and radio power controls are available.

Figure 2.8 shows that APs are set both at stations and along the track between stations. In a railway setting these are usually connected to a fixed BS through optic fibre and placed along the line, as close as possible to the rolling stock.

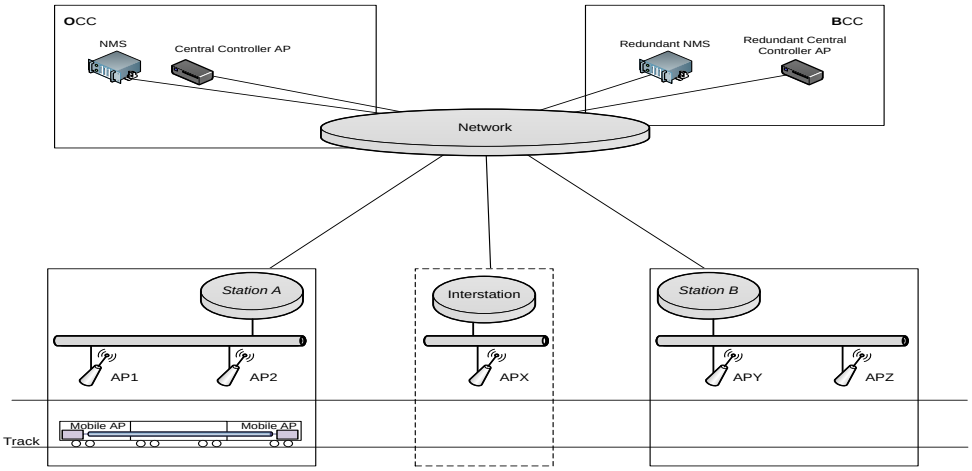

Figure 2.8 - BBRS' System Architecture (extracted from [Thal17]).

BBRS is based on Institute of Electrical and Electronics Engineers' (IEEE's) 802.11n WiFi. According to [LIEB11], the later uses OFDM and can operate in 2 distinct bands, the 2.4 GHz and the 5 GHz ones.

The channels, spaced 5 MHz from each other, are 20 or 40 MHz wide (this is achievable with the combination of a primary and secondary channels. Adjacent channels produce high levels of interference, so in order to guarantee the best performance, consecutive channels are usually not employed. Modulation possibilities are Bipolar Phase Shift Keying (BPSK), QPSK, 16QAM and 64QAM.

Even though [Wlan18] states that each country regulates their own bands, the most common channel configuration for the 2.4 GHz band is shown in Table 2.5.

Table 2.5 - Common Channel Allocation for 2.4 GHz 802.11n WiFi.

Channel Number	Centre Frequency [MHz]
1	2412
2	2417
3	2422
4	2427
5	2432
6	2437
7	2442
8	2447
9	2452
10	2457
11	2462
12	2467
13	2472

Using one or two 40 MHz channels for its communications, BBRS' handovers between the onboard equipment are intelligent and parametrised given the type of equipment and the quality of the links. It can operate using either licensed (the holder gets a legal right to interference-free data channels) or unlicensed WiFi, which can be standardised or not. It should be noted that, even though the system is based on 802.11n, it is not limited to the later frequency bands, being able to use other ranges of frequencies that do not belong in the 2.4 or the 5 GHz standardised bands, as seen in Table 2.6. It shows 4 possible frequency configurations, with the last one being the most common one.

A 20 MHz band contains 52 usable subcarriers and doubling the channel capacity to 40 MHz yields an increase in subcarriers higher than 100% due to the fact that the guard band does not need to be twice as big. 40 MHz channels can operate with up to 108 subcarriers, however this work only contemplates 20 MHz channels, which are often used in BBRS.

The system supports train speeds of up to 250 km/h and has a theoretical maximum throughput of 125 Mbps, however, due to the speed of trains, only 70 Mbps are guaranteed at any given moment. It is capable of providing handovers within 100 ms and has a maximum communication distance of 1 km, lowering to 300 m in urban environments.

Table 2.6 - BBRS's Frequencies (adapted from [Thal17]).

	Standard	Non-Standard
Non-Licensed	[2.405 - 2.495] GHz [5.150 - 5.825] GHz	[5.825 - 5.875] GHz
Licensed	-	[5.875 – 5.925] GHz

The 5 GHz 802.11n band has a similar configuration, with frequencies ranging from 5.000 to 5.835 GHz.

Figure 2.9 shows the available channel map for this band.

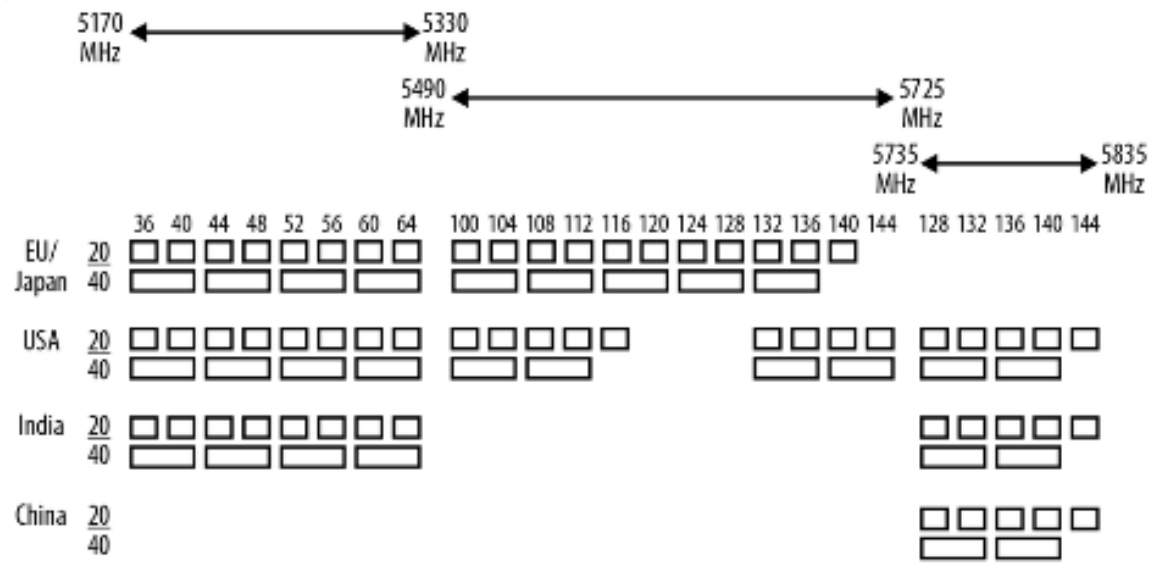

Figure 2.9 - Available Channel Map for the 5 GHz Band (extracted from [GAST12]).

Table 2.7 shows maximum 802.11n single stream data rates for different combinations of MCSs and bandwidths, depending on how long the Guard Interval (GI) is. Minimum levels of signal to noise ratios are also stated in order for each set of MCS to be used. One should note, however, that these ratios are not sufficient to reach peak data rates, but the bare minimum for the modulator to work correctly.

Table 2.7 - Maximum 802.11n Single Stream Throughputs (adapted from [Mcsi18]).

Throughput [Mbps]		**20 MHz Bandwidth**		**40 MHz bandwidth**	
MCS	$\rho_{N,min}$ [dB]	**800 ns GI**	**400 ns GI**	**800 ns GI**	**400 ns GI**
BPSK, ½	2	6.5	7.2	13.5	15
QPSK, ½	5	13	14.4	27	30
QPSK, ¾	9	19.5	21.7	40.5	45
16-QAM, ½	11	26	28.9	54	60
16-QAM, ¾	15	39	43.4	81	90
64-QAM, ⅔	18	52	57.8	108	120
64-QAM, ¾	20	58.5	65	121.5	135

In what concerns the railway environment, antennas are located at a height of 5 m and APs are usually spread around 300 m from each other, due to the high propagation losses originating from operating at such a high frequency. The data network is connected via optical fibre. Onboard the train, one or more radios are present, and the antennas are located on its top.

Many levels of redundancy are present in the system (among the controllers, the carriages and the railway) and quality of service is assured by assigning different priority levels to the equipment. System security is ensured via data encryption and access control. BBRS employs 5 main services in order to assure extra WiFi functionalities:

- The Train Maintenance System provides real-time onboard system visualisation and anomality alarms;
- Onboard Closed-Circuit Television (CCTV) Visualisation manages real-time imaging and access to recorded images through onboard cameras;
- Platform Camera Visualisation allows the real-time visualisation of train cabinets;
- Passenger Information Services is responsible for sending audio, text and video to the train;
- Passenger Internet Service is self-explanatory and provides internet connection to passengers.

2.4 Railway Communications

The increasing investment in the transports industry over the last years brought higher requirements for the communications systems present in vehicles. The railway transports scenario is an obvious case where this applies since, similar to other communications systems, what was suitable some years ago in what concerns available data rates is no longer acceptable for the majority of the most recent system requirements. This has even more important regarding data to transmit, such as train dispatching commands, train operation control commands, radio train number checking and dynamic monitoring information of signalling equipment.

From a telecommunications system view-point, the great advantage of a railway network is that it is fixed, and therefore, given that one has coverage along a certain area, one can always obtain the current positions and the possible paths of the different terminals. Since the costs involved in this kind of structures are very high and the requirements rarely change once the network is deployed, infrastructure planning in crucial.

Another advantage relate to this one is the fact that, in many situations, one knows beforehand where higher levels of data will be transferred. One location where this is expected to happen is at train stations, often needing more than 4 streams of data (different cameras covering the platforms), which are usually near a BS (and therefore path loss is low, resulting in high signal to noise ratios), which poses no problem regarding signal strength whatsoever. It should be noted, however, that situations where the train is leaving its station can temporarily produce exceptionally high attenuation levels (higher than 30 dB as seen in the state of the art) and therefore this case should be carefully analysed.

On the other hand, environments such as tunnels or metallic bridges introduce higher losses than the average ones and if they are present in areas where CCTV coverage is required, deployable BSs or base station amplifiers can be applied in order to provide a constant high transmission rate over all periods of time. Of course, if these locations are known beforehand, the distance between BSs can be

appropriately lowered. Services such as voice and signalling also need constant data rates, but they are generally low and therefore these are not the main problem at hand.

A major downside when dealing with these types of environments is the presence of MTs moving at speeds in the order of hundreds of kilometres, leading to coherence times lower than 1 ms, high doppler shifts (up to 300 Hz in GSM-R to almost 2 kHz at 5.9 GHz with speeds of 350 km/h) and the impossibility of tracking channels. However, as seen in [HAWG16], since the train moves along a scheduled route with a predictable and constant speed, it is possible to compensate for these levels of uncertainty via the use of real-time speed and position, as well as other pre-recorded data.

Should the symbol transmission rate be high enough, the channel will not be compromised by the movement of the terminal, however, other factors such as multipath delay spread could still introduce distortion into the system.

Factors such as diversity can be looked upon to solve this fading problem, however these are not always feasible due to the lack of spectrum or physical space to install the antennas on the trains (the roof is often occupied by antennas for different frequencies, air conditioning units, pantographs and solar panels). The BBRS system employs 2 antennas on its trains, however only one is actually being used at a given time, with the remaining one providing redundancy, should it be needed.

Looking at performance parameters, from a safety view-point, one is mainly concerned with coverage and not so much with capacity or interference, since the main concern is providing telecommunications to the train on-board equipment, in contrast to conventional 2G and 3G communications where capacity is often a major deal breaker and interference from different users far outweighs many other detrimental factors such as noise and fading.

Latency can be tolerated but service downtime in what concerns CCTV footage or train signalling is a problem. When dealing with railway situations the main concern is providing constant voice and video communications, which may require high data rates depending on video quality and number of streams, with other small data requirements such as train signalling and control commands.

Unlike LTE-R, GSM-R is vastly implemented on the majority of developed countries, and even though it is suitable for some of the operations listed above, other types of services such as automatic train operation and video surveillance need access to larger bit rates. GSM-R cannot easily handle these traffic flows, thus one expects its 4G successor, LTE-R, to supply the needed performance.

According to [ZAZW17], LTE-R emerges as the IoT platform for railways and the core of security operations for railways, however, for now, LTE-R is still being standardised and consequently the majority of railway telecommunications systems currently use TETRA or GSM-R.

The European Rail Traffic Management System (ERTMS) Standard consists of two main parts. First, it uses GSM-R for the communications existing between trains and railway tracks, along with any extra communications for eventual systems or services to operate. In addition, it also possesses a core signalling and train control component, the previously mentioned ETCS, responsible for railway safety and on-board train control.

The ETCS system is explained in [Thal18] and consists of the use of standardised train equipment according to the different ETCS levels (1 to 3, with 3 having the most requirements) in order to perform security tasks such as calculating maximum safe speeds for the trains, signalling for the drivers and automatic control of the vehicle, should it be needed.

The use of this system leads to increased train performance, track utilisation and passenger capacity and frequency through the use of on-board and trackside systems.

The first ETCS level provides cab signalling and can be built over the existing signalling system. It uses eurobalises along the railway tracks in order to gather and transmit information from and to the different trains at fixed points of the rail tracks, via spot transmission. With this information, the on-board processors can easily calculate parameters such as maximum train speeds and breaking distances at any given time.

ETCS level 2 is a digital radio system that is used to present signalling and other important indications in the cab of the drivers, which, with a few additional on-board equipment may supress the need for trackside signalling. At this level, eurobalises are used as passive positioning locators, that is, they are used exclusively to extract train positioning information, which is continuously transmitted via GSM-R between the train and the Radio Block Centre (RBC), with the absence of direct contact with the on-board train processors. Additional line integrity checkers and train equipment such as accelerometers are needed, to account for the passive behaviour of the eurobalises. Through the use of this ETCS level, the RBC is able to effectively control all trains along the covered area.

The need for trackside equipment (signals, track circuits and axle counters) can be supressed via the use of ETCS level 3. As with the previous levels, the trains' positions are acquired through eurobalises placed along tracks. After finding their location, the trains use their GSM-R antennas to transmit this information to the RBC, which is then able to calculate all possible path information at any given time. With this system, the railway track can be interpreted as a moving block and the positions of the different carriages can be determined with maximum reliability.

The previous points show the importance of coverage along the track. Even though the communications for passengers are usually not critical, this is not the case when dealing with trains, since their signalling and safety systems depend entirely on the availability of wireless communications. With the suppression of track signalling the lack of network coverage can lead to enormous costs in infrastructure, cargo and, ultimately, human lives.

A capacity problem one might face when using the ETCS system is approached in [SnSo12]. The main issue here is that the usual 8 GSM time-slots are sufficient for railway voice communication, however, when using ETCS level 2, the train needs to maintain a permanent data link with RBC, which uses one time-slot. Even though the information sent through this system is not frequent and small-sized, this time-slot is permanently occupied, due to GSM's CS nature, which translates into wasted capacity, leading to capacity constraints in busy stations.

2.5 Scenario Development

Following the scenario description in [AHGZ12], the Viaduct scenario is one of the most common environments when dealing with metallic environments. It consists of long bridge-shaped structures that carry a railway across a valley or another type of uneven ground, with heights usually ranging from 10 to 30 m. They are used due to the fact that tracks are very hard to deploy along uneven ground, in order to smoothen the terrain and allow trains to operate at high speeds. Tx antennas are usually 20 to 30 m above tracks and propagation can involve Line of Sight (LOS) or not (NLOS), depending if the obstructions near the railways are above the tracks or not.

Another technique used to smoothen the terrain is the Cutting seen in Figure 2.10. Even though they are rarer than Viaducts, these are very still commonly found environments for HSR. This type of construction is employed on uneven grounds to overcome large obstacles such as hills, creating reflection and scattering phenomena inside the newly created "container", whose depth can range from 3 to 12 m. When dealing with these scenarios, the most common structure is the regular deep Cutting, in which the walls along both sides of the structure have similar depths and slopes. Usually the train's antenna is located at a much lower distance than the top of the Cutting and therefore a lot of multipath components exist. Furthermore, bridges are commonly found above these locations, which lead to NLOS environments and extra diffraction along the metallic structures.

Figure 2.10 - Terrain Cutting (adapted from [AHGZ12]).

Tunnels are underground structures usually found in cities or near mountains in HSR environments, used to assure high train speeds. They usually consist of vault or semi-circular sections with heights of 5 to 10 m and widths of 10 to 20 m, existing along courses of up to dozens of kilometres. The signal analysis is much easier in this environment, due to the wave guided effect introduced inside the tunnel by the diffractions and scatterings along its smooth walls. Usually, a pair of BSs is employed, one placed at the start of the tunnel and another at its end, however, depending on the tunnel's length, several BSs can be placed along it in order to provide higher levels of coverage.

Railway Stations consist of platforms next to tracks, where the trains stop to load or drop passengers. The levels of speed in this situation are much lower than in the previous situations (from hundreds of

kilometres per hour to a few dozen, at most), however passenger mobility must be taken into account (around 5 km/h for a walking person). Train communications are usually guaranteed here, however, due to the higher number of users, high capacities are needed in order to ensure communications among passengers. Once more, one is usually dealing with NLOS environments since the station's structures that are used to provide shelter and information to passengers can cause shadowing and diffractions. Depending on the size and function of the station, these can be divided into 3 different types:

- Medium or small sized stations are similar to suburban environments. There are little to none awnings atop of the tracks and medium traffic requirements are expected;
- Large stations have a much higher passenger throughput. They can receive orders of a few thousands of trains per day in populated cities and there are usually big awnings atop the rails, as seen in Figure 2.11, making these scenarios similar to indoor ones. Significant wave propagation phenomena are expected when trains enter or leave the station;
- Marshalling stations are the places where carriages are organised before transportation and trains stop to load/unload cargo. The communication requirements here are related to train signalling and, once more, the metal present in the huge number of metallic carriages creates a scenario where multipath components are abundant.

Figure 2.11 - Large Train Station (extracted from [AHGZ12]).

The commonly found scenarios, along with some modelling parameters measured at GSM-R's 930 MHz, can be found in **Error! Reference source not found.**. The known Okumura-Hata model is commonly used in macro-cell scenarios and accurate when describing propagation in Urban, Suburban and Rural environments, however, when dealing with railways one is often interested in typical scenarios such as the Viaduct, Cutting, Tunnel and different types of stations. According to [AHGZ12], the Okumura-Hata model can incur differences of up to around 17 dB for some tracks comparing the predicted losses to the actual existing ones, which is explained by the fact that the former model does not take the diffractions that occur along the cuttings in the terrain into account. Similar discrepancies occur with the majority of commonly used models and therefore scenarios must be carefully defined in order to cover a wide range of possibilities found in railway environments. The previously mentioned scenarios are very common in the railway environment and, not only they have rarely been studied, there was only a small number of channel measurements carried out.

2.6 CST Overview

The ideal way of approaching the metallic bridge problem would be to analyse it as a Frequency Selective Surface (FSS), however, there is little bibliographic material regarding this matter, with the small number of existing papers approaching structures with electrical dimensions way smaller than the problem at hand. Since studying the method of moments is not within the scope of this thesis, the solution found to tackle the lack of bibliographic material regarding FSSs was to analyse the problem by the means of EM simulation software, namely Computer Simulation Software (CST) due to its availability.

CST is a powerful EM simulation software that includes a range of tools including Low/High frequency simulations, Thermal and Mechanical analyses, System Assembly and Modelling, as well as Board/Package/Cable simulations, as shown in Figure 2.12. In this thesis the tool in use is the high frequency simulation, described in [Csts18], which aids the user in creating as well as simulating structures via the use of a user-friendly graphic modelling interface. Depending on the problem being analysed, there are certain methods that are more efficient than others and therefore the software enables the user to choose from different simulators and mesh types in order to suit different problems.

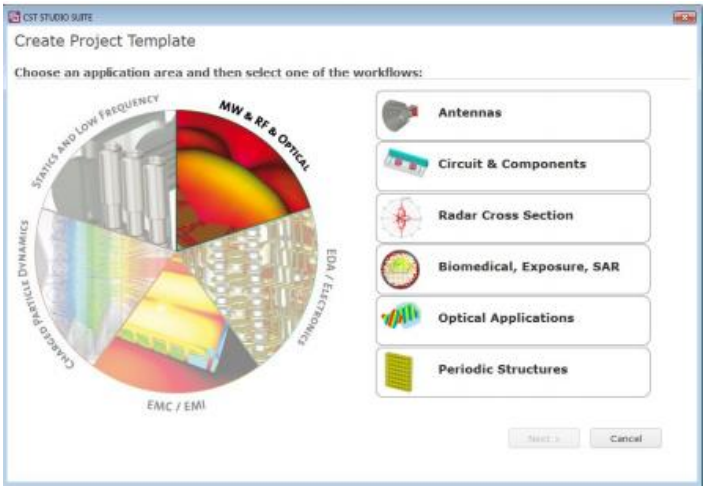

Figure 2.12 - CST's Modelling Tools (extracted from [Csts18]).

The solvers that the user can opt for are the Time and Frequency domain ones, the Integral equation solver, an Asymptotical one, as well as the Multilayer and the Eigenmode solvers. Each solver has different meshing types and approximations that can be used, such as Hexahedral and curved Tetrahedral meshes with the perfect boundary approximation or the thin sheet technique, in order to increase the accuracy of the simulations.

The Time Domain is widely accepted as the most powerful solver, offering the broadest range of tools and having an especially high performance for some high frequency applications such as transmission lines, waveguides and antennas. On the other hand, this solver is not very efficient for electrically small structures, that is, with dimensions much smaller than the wavelength), in which case the Frequency Domain solver is a better option. Apart from electrically small problems, the Frequency Domain solver is also a good choice for filter modelling and problems with very small geometric details.

Should the problem in study involve large structures, the Integral equation solver is an option to consider since the former solvers require very fine meshes that often suffer from dispersion effects when modelling the problems. This type of solver includes both a multilevel multipole method and an iterative method of moments technique.

For extremely electrically large structures one should consider the Asymptotic solver whereas the Multilayer and Eigenmode solvers perform well for mainly planar structures and efficient filter design, respectively. This solver is often used in boat and plane simulations.

When dealing with bridges and trains at frequencies ranging from 900 MHz to 5.9 GHz, dimensions ranging from 10 to a couple of hundred of wavelengths are often encountered. More specifically, the modelling done in this work has a case where the figure of 239 706 λ x 228 291 λ is present, when dealing with the dimensions of the modelled metallic bridge under a BBRS scenario, leading to electrically large structures.

According to the description of the different solvers, the Time Domain and the Integral solvers are the ones that should be first looked at. Should a solver prove inefficient, the next solver should be approached. The Integral solver lacks tools that the Time Domain solver possesses such as broadband frequency sweeping and flexible probes and therefore should not be used on a first approach but as a last resort.

Initially many simulations were performed in order to choose the optimal solver for the current problem. Different configurations were checked, ranging from simpler and more complex bridge models to different EM solvers (mainly Time Domain vs. Integral) and even various meshing settings. With the gradual increase in complexity of the models, it was concluded that a standard personal computer with 8 GB of RAM and a 2 GHz processor is not viable to perform this type of simulation due to hardware limitations. Frequent problems involved exceeded time and memory limits and exceedingly high computational times.

With the specs listed above, a simple 925 MHz simulation with a partial bridge model (around 10 Million mesh cells, Time Domain Solver) took 29 hours and 21 minutes of simulation time to perform. With the introduction of the actual complexity of the bridge this solver led to boundary and memory errors and was promptly discarded since, even if the model was simplified in order for the 925 MHz simulation to be feasible, the LTE simulation (2600 MHz) would never be completed due to the much higher number of wavelengths present in the simulation. In order to tackle this problem, a workstation with large amounts of RAM and a powerful processor was used when performing the simulations. The technical specs of the machine running the software are presented in Table 2.8.

Table 2.8 - Hardware Specification.

Operating System	Windows 7 Professional 64 bit
CPU	Intel Xeon E5620 @2.40 GHz (2 processors)
RAM	44 GB

2.7 State of the Art

The state of the art is analysed in this section in order to provide a brief overview of the work that has been done so far in the different types of structures one can find in the railway communications field.

[GZAB12] carried out a series of measurements at 2.4 GHz in Tunnel environments. The measurements were made in the Line 10 tunnels of Madrid's subway, between the stations of Tribunal and Príncipe Pio. Four tunnel sections were selected, consisting of 3 wide tunnels and one narrow tunnel, with four transmitters, which were installed at a height of 4 m, 25 cm away from the tunnel walls. These were located at 455, 664, 946 and 1128 m along the track, operating at the frequencies of 2481, 2454, 2427 and 2400 MHz, respectively. The receiving antennas were placed in the front and rear cars of the train, 2.2 m away from the nearest wall and 4.5 m above the tracks. The parameters that were analysed are near shadowing, shadow fading, path loss, fast fading and attenuation. The authors calculated values for the standard deviation of shadow fading of 2.75 dB for wide tunnels and 4.17 dB for narrow ones, with path loss exponents of 5.49 and 7.13, respectively. Another important result is that the near-shadowing effect caused by the train passing the base stations can produce attenuations of up to 31.2 dB and can last for up to several seconds.

Still regarding tunnels, [Zhan03] provides a different approach to this type of scenario. A two-way hybrid model is developed in order to estimate the path loss in tunnels. It uses a combination of the free-space and flat earth models: a breakpoint that greatly depends on frequency, antenna position and tunnel dimensions is defined, separating the propagation mechanisms within the two distinct regions. In this work, this methodology is applied to a tunnel and the breakpoint is defined. The authors compare the simulated results with actual measurements and validate their results for different tunnels, for the frequencies of 900 MHz, 1.8 GHz and 2.448 GHz. Finally, it is concluded that factors such as the increase of the work frequencies, the placement of antennas on corner locations and larger tunnel dimensions result in a breakpoint further away from the Tx antenna and that the last one's gain has no significant effect on the breakpoint's location.

In [LZBr11], cutting scenarios are approached with the study of a slope measuring from 7 to 8 m and around 70º of inclination. Viaduct measurements are also obtained as a term of comparison. The data is collected using an antenna on top of a train (3.5 m high) operating on a GSM-R network, which moved at speeds from 240 to 320 km/h. The transmitter antenna was located at a height of 33 m and operated at a frequency of 932.8 MHz. The authors developed tuned path loss models for the cutting and viaduct scenarios, reaching values for path loss exponents of 4.3 for cuttings and 3.5 for viaducts. They found out that the shadow loss could be described by a log-normal distribution, with a standard deviation of 3.5 dB. Additionally, it is seen that bridges built on top of cuttings can yield propagation losses of around 5 dB and concluded that cuttings experience much more fading than viaducts.

In [HZAD11], a path loss model for HSR Viaducts is proposed based on empirical data at 930 MHz. It considers the influence of heights of the viaducts and BSs, which are not well predicted by large scale models, particularly the Hata model, versus which the proposed model is compared. The mean values of the errors between the predicted values and actual measurements are around 0 dB for the proposed

model, whereas the Hata model reaches errors with means from 3 to 8 dB. Values of around 2.5 dB for the path loss exponent and 2.4 dB for the standard deviation error are achieved with this model. The work shows that the fading depth is between 14.38 and 15.96 dB for HSR environments and that the maximum fading depth is between 28.92 and 40.32 dB, values which are unaffected by the viaduct's height.

[WZGA10] carried out a series of measurements at the Zhengxi HSR, which is mainly composed of viaduct and plain environments, with frequencies ranging from 930.2 MHz to 933.4 MHz, with a bandwidth of 200 kHz. The transmitting antennas were placed along the railway and the receiving antennas were placed on top of the train, at a height of 3.5 m. The data was obtained using the power receiver Griffin and Global Positioning System (GPS). After analysing the produced data and comparing it to the Hata model, the authors developed free-space tuned models with errors that decreased by 5.1 dB in the viaduct scenario and 11.0 dB in the plain scenario, compared to the Hata model. The models' Root Mean Square Errors (RMSEs) decreased by 2.5 dB and 7.7 dB, respectively. The authors conclude that their models are useful for predicting propagation behaviours for these two types of scenarios.

In [GZAK14], the losses in train stations are analysed. Based on empirical data measured at 930 MHz in Chinese train stations, this work interprets train stations as a combination of a solid obstacle and a non-existent obstacle, providing two models for path loss in train stations. The conditions which are analysed here are the distance between the Tx and the station, the type of train station, the track on which the train operates and the different propagation mechanism zones. Errors lower than 2 dB for the mean and 5 dB Root Mean Square Errors (RMSEs) are achieved, which show the developed models adapt well to the studied scenario.

Following their previous works, R. He *et al*. developed a standardised path loss model for HSR in [HZAD14]. Based on a series of measurements at 930 MHz, the authors propose an empirical propagation model for the different scenarios that can be present in railway environments via the introduction of two new correction factors. The results obtained with the proposed model were compared against the Hata, Winner, 3GPP and ITU-R models and, based on the different RMSEs, it was concluded that the proposed model outperformed the previously mentioned models for two distinct HSR lines.

Chapter 3

Model Development and Implementation

This chapter presents the different models, methods and software used in this thesis, as well as the explanation of the assumptions and approximations made. Different models are used for path loss and throughput calculation, and important points regarding the specific simulation details are made. The chapter ends with a model assessment.

3.1 Overview

Propagation models must be used so that the performance of any telecommunications system can be estimated. A deterministic model can be employed, where Maxwell equations are numerically solved, but the most common and practical way to do this is via signal measurements at different points of a network. Based on these empirical data, a new model is developed or a previous one is adapted so that one can estimate performance parameters such as path loss and fading.

To do this, different factors have to be taken into account, such as the distance between the transmitter (Tx) and the Rx, the frequencies in use, the type of track that contains the train, the possible environment types and the propagation mechanism zones such as the presence of obstructions in the signals' path. Following this idea, it is important to state that the models accessed in the following subchapters are semi-deterministic, in the sense that they are based on measurement data, however they have the aid of collected site-specific information and data post-processing analysis.

It is also important the fact that most of the models currently used in railway communications were developed and tested for the 900 MHz band. One should be careful when employing these models to higher frequencies, such as the 2600 LTE band or even WiFi ones. Using the models outside of their validity range can produce meaningless results and therefore one should be careful when applying a model originally developed for GSM-R on an LTE-R network without any type of model extension. The present chapter contains an analysis of these situations and details the possible sources that can introduce a degree of error in the calculations.

The specification of these parameters, along with a minimum carrier to noise ratio, which can depend on the parameters themselves, for a given system margin enable the calculation of the maximum propagation losses for a given situation, which will be translated into a maximum distance between BSs, along with the respective achievable data rates for the different systems (GSM-R, LTE-R and BBRS). Even though some of these parameters are intermediate results that ultimately lead to a data rate, they are important enough to be considered output parameters, such as the propagation losses for the different scenarios and the required signal to noise ratio.

Figure 3.1 states the methodology followed along this work, where the most important input parameters are the centre frequency, the type of modulation that is used, M, and the respective coding rate R, the average transmission powers, the heights of both the BS and the MT, as well as the different types of environment at hand.

After the input of all the parameters mentioned in the previous paragraph there are 2 steps that need to be performed in order to obtain the outputs. Firstly, the propagation models that are developed in this section yield parameters such as propagation losses, maximum communication distances and required signal to noise ratios for the different modulations. Along with this procedure, one also needs to account

for the presence of a metallic bridge and therefore an EM simulation is performed in order to obtain an estimate of the additional losses due to the introduction of this metallic structure, which can be considered indoor propagation losses.

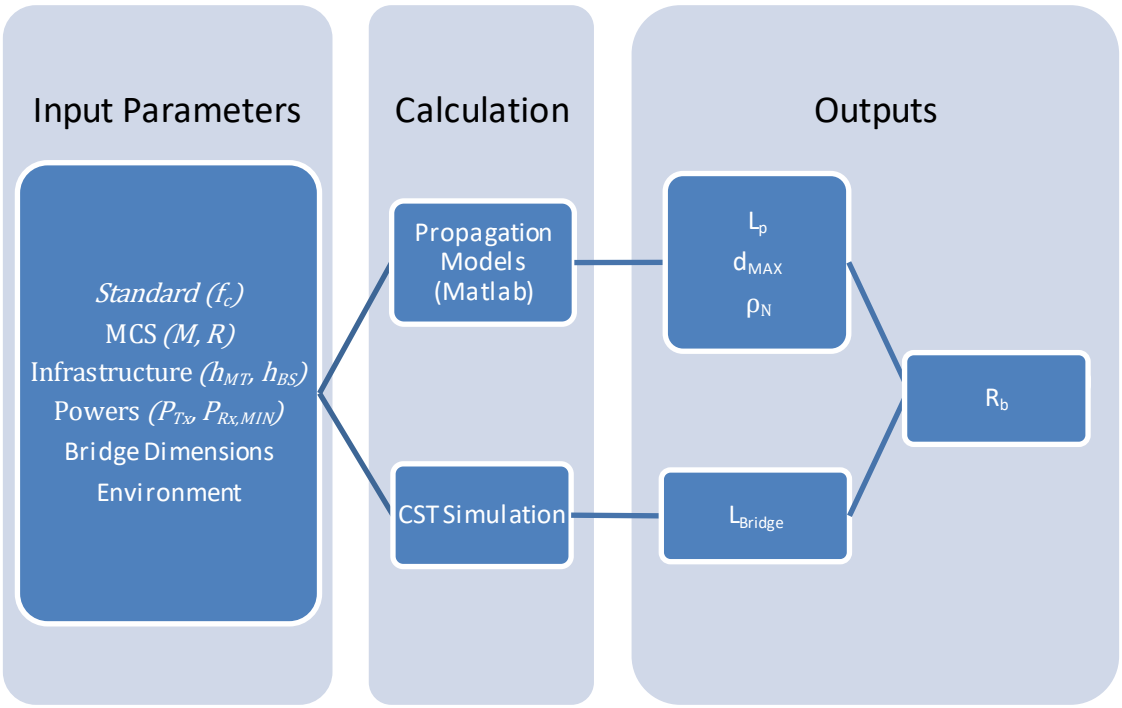

Figure 3.1 - Work Plan.

Finally, all these calculated parameters are taken into account and throughputs are estimated for the different systems and modulations.

According to [Feng13] and [XZZW08], an FSS consists of a periodic array of elements designed to reflect, transmit or absorb EM radiation. These can be very useful when designing multiband systems such as communications and defence applications, antenna radomes, as well as the securing and optimisation of wireless links. This process can isolate different bands of the same system, minimising interference and leading to the possibility of designing each operating band independently, but can also lead to otherwise inexistent difficulties, for instance when broadcasting signals.

Metallic bridges can be interpreted as FSSs and therefore it is important to analyse the signal contribution or attenuation that comes from the reflected and transmitted signals on the metallic surfaces. Depending on the type of link and location of the Receiver (Rx), these can be beneficial or detrimental, that is, in situation where the BS is located outside the bridge this reflection will come as an attenuation. Should one consider another scenario, where the BS is located inside the metallic structure, then the reflected rays on its surface will translate in a higher density of signal confined within the bridge.

The analysis mentioned in the previous paragraph can be done via the interpretation of the reflection coefficients, which can be extracted by means such as the Method of Moments. A useful simplification here is that, since the problem involves metallic structures, one considers the reflectivity of the materials is high enough so that the absorbed EM waves by the metallic interfaces can be neglected.

After extensive reading, no FSS models that could be directly applied to the problem could be found. [Scot98] contains an analysis of Photonic Bandgap Structures, [FFOR01] analyses radar absorbing materials based on polymers, [KiCh94] uses the method of moments to study planar periodic structures, [CWCF08] provides a simplistic approach to the problem considering finite size FSS arrays, [WaZC14] approaches the issue considering periodic conductive patches on dielectric substrates and [Munk00] contains a series of examples ranging from centre connected structures to combinations of loaded elements. The issue found here is that the dimensions of the studied structures often involve symmetry along the different axes and element spacings lower than 1 cm, which are very different conditions than the ones found in metallic bridges, which often possess varied symmetry planes, however with distances between elements in the order of metres.

3.2 Model Development

The following subsections introduce link budget calculation through important parameters such as system losses, gains and radiated powers. Different propagation models are implemented and used to estimate path loss in various environments and the CST modelling process is detailed.

3.2.1 Link Budget

In order to calculate the received power at an antenna, one has to define path loss. According to [Corr15] the path loss can be calculated as

$$L_{p[\mathrm{dB}]} = P_{t[\mathrm{dBm}]} + G_{t[\mathrm{dBi}]} - P_{r[\mathrm{dBm}]} + G_{r[\mathrm{dBi}]} \tag{3.1}$$

where:

- P_r: Power available at the receiving antenna;
- P_t: Power fed to the transmitting antenna;
- G_r: Gain of the receiving antenna;
- G_t: Gain of the transmitting antenna.

Introducing the Effective Isotropic Radiated Power (P_{EIRP}), one has:

$$L_{p[\mathrm{dB}]} = P_{EIRP[\mathrm{dBm}]} - P_{r[\mathrm{dBm}]} + G_{r[\mathrm{dBi}]} \tag{3.2}$$

Depending on the link, different losses have to be considered and therefore

- in DL,

$$P_{EIRP[\mathrm{dBm}]} = P_{Tx[\mathrm{dBm}]} - L_{c[\mathrm{dB}]} + G_{t[\mathrm{dBi}]} \tag{3.3}$$

where:

- P_{Tx}: Transmitter output power;
- L_c: Losses in cable between transmitter and antenna.

- in UL,

$$P_{EIRP[\mathrm{dBm}]} = P_{Tx[\mathrm{dBm}]} - L_{u[\mathrm{dB}]} + G_{t[\mathrm{dBi}]} \tag{3.4}$$

where:

- L_u: User losses.

For LTE, the maximum output power is defined in a different way for UL and DL. In DL it stands for the maximum transmitted power per subcarrier, $P_{Tx/sc,max}$, while in UL it is the total transmitted power for all of the available bandwidth, $P_{Tx,BW,max}$. If Multiple Input Multiple Output (MIMO) is used then, to obtain the power transmitted per antenna, one has to divide the power for the by order of the MIMO system.

Similarly, for purposes of link budget, one has

$$P_{Tx}^{DL} = P_{Tx/sc}/N_{MIMO} \tag{3.5}$$

$$P_{Tx}^{UL} = P_{Tx/sc} \cdot N_{subc}/N_{MIMO} \tag{3.6}$$

where:

- $P_{Tx/sc}$: Transmitted power per subcarrier;
- N_{subc}: Number of subcarriers;
- N_{MIMO}: Order of MIMO system.

For GSM, the receiver sensitivities $P_{Rx,min}$ for the different classes are defined and shown in Table 3.1.

Table 3.1 - GSM receiver Sensitivities.

Class	$P_{Rx,min}$[dBm]					
	BS				MT	
	900	1800	900 µ	1800 µ	900	1800
1	-104	-104	-97	-102	-104	-102
2			-92	-97	-102	
3			-87	-92		

For LTE, $P_{Rx,min}$ depends on the type of link and service. One first needs to calculate the total noise power,

$$N_{[\mathrm{dBm}]} = -174 + 10\log(\Delta f_{[\mathrm{Hz}]}) + F_{[\mathrm{dB}]} \tag{3.7}$$

where:

- F: Noise Figure;

- Δf: Signal bandwidth, with:

$$\Delta f_{[\mathrm{kHz}]} = 15 \cdot N_{subc} \tag{3.8}$$

Knowing the signal to noise ratio, ρ_N, it is possible to calculate the receiver sensitivity for LTE as

$$P_{Rx,\min[\mathrm{dBm}]} = N_{[\mathrm{dBm}]} + M_{S[\mathrm{dB}]} + \rho_{N[\mathrm{dB}]} \tag{3.9}$$

where:

- M_S: System Margin.

It should be noted that (3.9) usually involves an interference margin, M_I, instead of a system one. This is due to the fact that in most telecommunication systems interference has the most severe impact when facing other performance degrading factors such as fading and noise.

In this work, however, the effect of interference is not studied. Instead of this interference margin, the calculations include a base system margin of 10 dB, which accounts for this factor, as well as both the fast and slow fading margins, M_{ff} and M_{sf}, respectively, with the first one being especially predominant due to the high speeds involved. The figure of 10 dB is present in some projects planned by Thales and is consistent with the available literature, as seen in [HZAG15].

One still has to account for the losses due to the insertion of the metallic bridge, L_{bridge}, which should be added to M_S.

3.2.2 Winner II Model

The Winner II model deals with the environments being studied in this work under section D2a (Moving Networks). According to [KMHZ17], the model considers a rural LOS situation where the 2.5 m high trains move at speeds of 350 km/h. The frequencies to be considered are between 2 and 6 GHz. The model considers there are BSs every 1000 to 2000 m along the track and either:

1. 50 m away from the tracks with 30 m high antennas;
2. 2 m away from the tracks with 5 m high antennas (optimal for BBRS).

In a general way, the Winner II model for path loss can be written as seen bellow,

$$L_{p,WinnerII[\mathrm{dB}]} = A\log\left(d_{[\mathrm{m}]}\right) + B + C\log\left(\frac{f_{c[\mathrm{GHz}]}}{5.0}\right) + X \tag{3.10}$$

where:

- A: Fitting Parameter;
- B: Intercept Parameter;
- f_c: Centre Frequency;
- C: Path Loss Frequency Dependence;

- X: Environment-Specific Parameter;
- d: Tx-Rx Separation Distance.

For moving networks,

$$\begin{cases} A = 21.5; B = 44.2; C = 20; X = 0, \ \ 10\,\mathrm{m} < d < d_{BP} \\ L_{p,WinnerII\,[dB]} = 40\log\left(d_{[\mathrm{m}]}\right) + 10.5 - 18.5\log\left(h_{BS[\mathrm{m}]}h_{MS[\mathrm{m}]}\right) + 1.5\log\left(\frac{f_{c[\mathrm{GHz}]}}{5.0}\right), d_{BP} < d < 10\ \mathrm{km} \end{cases} \quad (3.11)$$

where:

- h_{BS}: Actual BS' antenna height;
- h_{MS}: Actual MS' antenna height;
- d_{BP}: Breakpoint distance, with:

$$d_{BP} = 4 \cdot h_{BS} \cdot h_{MS} \cdot \frac{f_c}{c} \quad (3.12)$$

3.2.3 He *et al.* Model (2011)

This model was developed for the 930 MHz band (intended to be applied to GSM-R), specifically for viaducts with heights ranging from 10 to 30 m above ground and cell radii from 2.5 to 4 km. The BS' antennas are positioned 20 to 30 m above the rail surface and 10 to 20 m away from the railway. The MT's antennas are placed on top of the train, 30 cm above its roof, on its middle. The train at study moves at speeds of 200 to 350 km/h and is 204 m long, 3.8 m high and 3.3 m wide.

The relevant dimensions mentioned in model are schematised in Figure 3.2, where:

- H: Viaduct's Height;
- w_t: Train's Width;
- h_t: Train's Height;
- h_{AR}: Antenna's distance to the roof of the train, with:

$$h_{MS} = h_{AR} + h_t \quad (3.13)$$

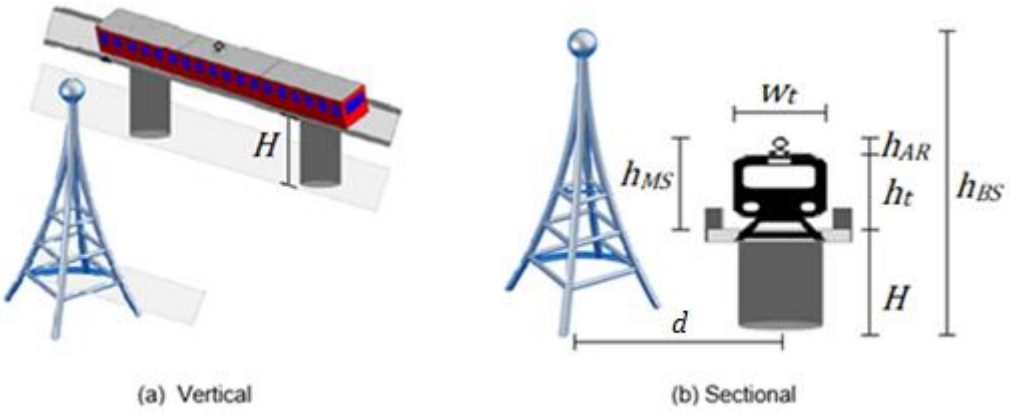

Figure 3.2 - Vertical and Sectional Viaduct Views (adapted from [HZAD11]).

The authors conclude that when the viaduct is low, most obstacles are bellow it and therefore little to no phenomena such as diffraction, reflection and scattering occur, leading to *quasi* free space propagation and a path loss exponent close to 2.

In contrast, when the viaduct is high, these phenomena are present, however, the reflected and scattered components from the rail and the ground below the viaduct have little to no chance of reaching the MT's antenna, leading to a two-ray model with a path loss exponent close to 4.

The path loss exponent increases with the viaduct's height, ranging from 2 to 4 for the tested scenarios. Viaduct heights higher than 30 m lead to bad channel quality. The same happens for heights lower than 10 m, due to the scattering of multipath components.

Based on the effect of the different factors, the proposed model for the path loss has the following expression,

$$L_{p,HZAD11[\mathrm{dB}]} = \left[C_a H_{[\mathrm{m}]} + C_B\left(h_{BS[\mathrm{m}]} - h_{MS[\mathrm{m}]} - H_{[\mathrm{m}]}\right) + \frac{C_C}{h_{BS[\mathrm{m}]} - h_{MS[\mathrm{m}]} - H_{[\mathrm{m}]}} + C_D\right] \cdot \cdot 10\log\left(\frac{d_{[\mathrm{m}]}}{d_{0[\mathrm{m}]}}\right) + 20\log\left(\frac{4\pi d_{0[\mathrm{m}]}}{\lambda_{[m]}}\right) + xy, h_{BS[\mathrm{m}]} - h_{MS[\mathrm{m}]} - H_{[\mathrm{m}]} > 0 \quad (3.14)$$

where:

- C_A = 0.04798;
- C_B = 0.00194;
- C_C = 42.84;
- C_D ~ *N*(-0.266, 0.318), where *N* stands for the Normal Distribution Function;
- x ~ *N*(0,1);
- y ~ *N*(2.319 dB, 0.702 dB);
- λ: Wavelength;
- d_0: Reference distance (around 500 m for HSR viaducts).

3.2.4 He *et al*. Model (2014)

The present model introduces new correction factors to the Hata model. It was tested and validated for HSR scenarios at 930 MHz.

Starting with the Hata path loss model for urban areas, with the large cities correction factor (see (A.1) through (A.3)):

$$L_{p,Hata[\mathrm{dB}]} = 74.52 + 26.16\log\left(f_{c[\mathrm{MHz}]}\right) - 13.82\log\left(h_{BS[\mathrm{m}]}\right) - 3.2log^2\left(11.75h_{MS[\mathrm{m}]}\right) + \left[44.9 - 6.55\log\left(h_{BS[\mathrm{m}]}\right)\right] \cdot \log\left(d_{[\mathrm{km}]}\right) \quad (3.15)$$

R. He *et al*. introduce the correction factors Δ_1 and Δ_2 so that this model translates the propagation in commonly found HSR structures more accurately. This is shown in the following expression:

$$L_{p,HZAD14[\mathrm{dB}]} = \Delta_1 + 74.52 + 26.16\log\left(f_{c[\mathrm{MHz}]}\right) - 13.82\log\left(h_{BS[\mathrm{m}]}\right) - 3.2log^2\left(11.75h_{MS[\mathrm{m}]}\right) + \left[44.9 - 6.55\log\left(h_{BS[\mathrm{m}]}\right) + \Delta_2\right] \cdot \log\left(d_{[\mathrm{km}]}\right) \quad (3.16)$$

The correction factors are derived from the difference between the optimal path loss curve (Least Squares (LS) fit curve of the measurements) and (3.6) and are shown in Table 3.2 for the different types of environments. Δ_1 is used to normalise the constant in the model in order for it to fit the data, while Δ_2 deals with the path loss exponent changes introduced by railway environments and buildings.

Table 3.2 - Correction Factors for the Standardised Path Loss Model (adapted from [HZAD14]).

HSR Environment	Correction Factors [dB]
Urban	$\Delta_1 = -20.47$ $\Delta_2 = -1.82$
Suburban	$\Delta_1 = 5.74\log(h_{BS}) - 30.42$ $\Delta_2 = -6.72$
Rural	$\Delta_1 = 6.43\log(h_{BS}) - 30.44$ $\Delta_2 = -6.71$
Viaduct	$\Delta_1 = -21.42$ $\Delta_2 = -9.62$
Cutting	$\Delta_1 = -18.78$ $\Delta_2 = 51.34\log(h_{BS}) - 78.99$
Station	$\Delta_1 = 34.29\log(h_{BS}) - 70.75$ $\Delta_2 = -8.86$
River	$\Delta_1 = 8.79\log(h_{BS}) - 33.99$ $\Delta_2 = -2.93$

3.2.5 Throughput Models

With propagation losses estimated via the previous models, one still needs to account for losses due to the presence of a metallic bridge in order to correctly calculate levels of attenuation and consequent signal to noise ratios, which are promptly converted into throughputs for the different scenarios and communication systems.

According to [TsVi05], one can define Channel Capacity, C_{ch}, as the maximum rate at which information can be transmitted through a noisy communications channel. For an Additive White Gaussian Noise channel this is given by the Shannon-Hartley theorem,

$$C_{ch[bps]} = B_{W[\mathrm{Hz}]} \cdot \log_2(1 + \rho_{\mathrm{N}}) \quad (3.17)$$

where:

- B_W: Channel's Bandwidth.

Equation (3.17) is only an upper limit for the channel's data rate, which is never achievable since the theorem assumes unrealistic amounts of transmitted bits per modulation symbol. Additionally, any channel is going to be affected by factors such as fading, interference from other devices and noise, which are going to lower the actual achievable data rates. In order for the information to be transmitted over a telecommunications channel, one has to code the bits using a certain modulation (this process is schematised in Figure 3.3). The Coding Rate, R, of the system determines the number of bits per modulation symbol that will be effectively providing information, with the remaining ones providing the possibility of Forward Error Correction. Together with the type of modulation used, these form an MCS, which corresponds to a maximum achievable throughput.

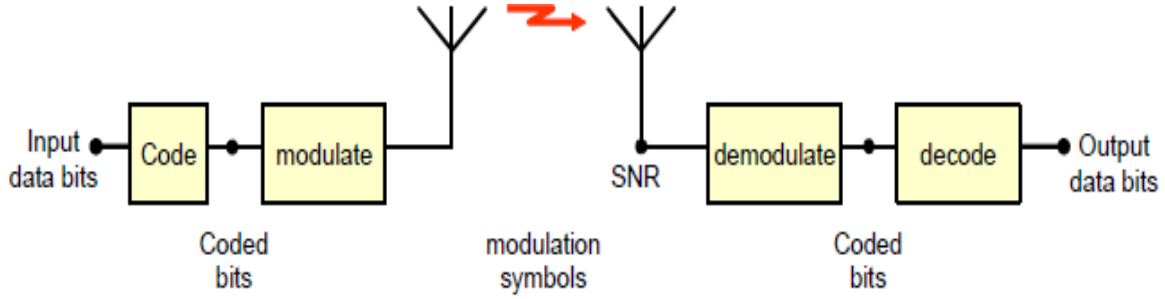

Figure 3.3 - Coding and Modulation of Data over a Radio Link (extracted from [ETSI11]).

Three systems are analysed in this thesis: GSM-R, LTE-R and BBRS. Since these only differ to their standard counterparts (GSM, LTE and 802.1n WiFi, respectively) in the services provided, the data rates are considered to be the same.

With this in mind, GSM-R supports 12.2 kbps (enhanced full rate) voice transmission for any value of ρ_N higher than -102 dBm. In what concerns LTE-R, the bandwidth used to calculate both the data rate and the noise corresponds to the required number of resource blocks. Both GSM-R and WiFi calculations consider the whole bands in use (4 MHz for the former and 20 MHz for the later).

One is mainly interested in data rates when dealing with LTE-R and BBRS, since these are the networks capable of transmitting CCTV footage in real time. In order to analyse the impact of metallic bridges in the different scenarios it is important to define how the data rates are calculated for both LTE and 802.11n WiFi.

Figure 3.4 shows LTE throughputs that are unrealistic when operating in the physical layer, however some of the data contained in this figure can still be used to extract the minimum required signal to noise ratios in order to use each MCS.

Furthermore, it is important to state that these ratios greatly depend on the user equipment that is being used and thus some fluctuations around the observed values are acceptable.

In what concerns the achievable data rates, the model for LTE is adapted from [Alco17]. The expressions for the different modulations are expressed bellow, with slight modifications from the original

ones (introduction of constants) in order to account for single streams of data. These were obtained through experimental measurements of several manufacturers from [3GPP11].

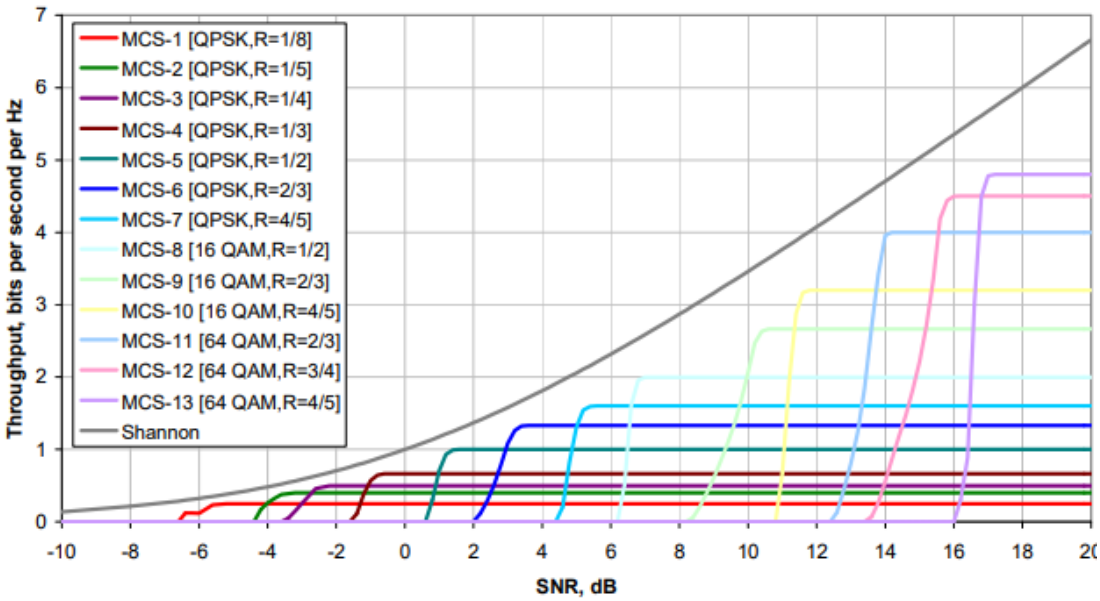

Figure 3.4 - LTE Theoretical Throughput for Different MCSs (extracted from [ETSI11]).

Note that the presented expressions only consider a single data stream scenario with negligible interference and all 100 resource blocks in use.

For QPSK the throughput is given by,

$$R_{b[\text{bps}]}^{QPSK,\frac{1}{3}} = \frac{2.34201 \cdot 10^6}{14.0051 + e^{-0.577897 \cdot \rho_{N[\text{dB}]}}} \cdot 50 \tag{3.18}$$

where:

- R: Coding Rate;
- ρ_N: Signal to noise ratio at receiver.

Similarly, for 16QAM, one can obtain the throughput as:

$$R_{b[\text{bps}]}^{16QAM,\frac{1}{2}} = \frac{47613.1}{0.0926275 + e^{-0.295838 \cdot \rho_{N[\text{dB}]}}} \cdot 50 \tag{3.19}$$

And finally, for 64QAM, the expression is:

$$R_{b[\text{bps}]}^{64QAM,\frac{3}{4}} = \frac{26405.8}{0.0220186 + e^{-0.24491 \cdot \rho_{N[\text{dB}]}}} \cdot 50 \tag{3.20}$$

Figure 3.5 shows throughputs for three sets of MCSs, obtained with (3.18) through (3.20). As expected, using a higher-level modulation does not always translate into a throughput gain. For instance, 64-QAM with a coding rate of ¾ only outperforms 16-QAM with a coding rate of ½ for signal to noise ratios above roughly 13 dB. Looking at this figure, one can clearly see that for the 64-QAM modulation with a coding rate of ¾ the obtained value in the saturation zone is 60 Mbps whereas the data in Figure 3.4 suggests

that a rate of around 90 Mbps is obtainable, which shows the relevance of using actual measurement data instead of basing the model on theoretical calculations.

Overall, through the use of adaptative modulation and coding, the modulation in use should be the one that yields the highest throughput at any given time, that is:

$$R_{b[\text{bps}]}^{LTE-R} = \max\left(\left\{R_{b[\text{bps}]}^{QPSK,\frac{1}{3}}, R_{b[\text{bps}]}^{16QAM,\frac{1}{2}}, R_{b[\text{bps}]}^{64QAM,\frac{3}{4}}\right\}\right) \quad (3.21)$$

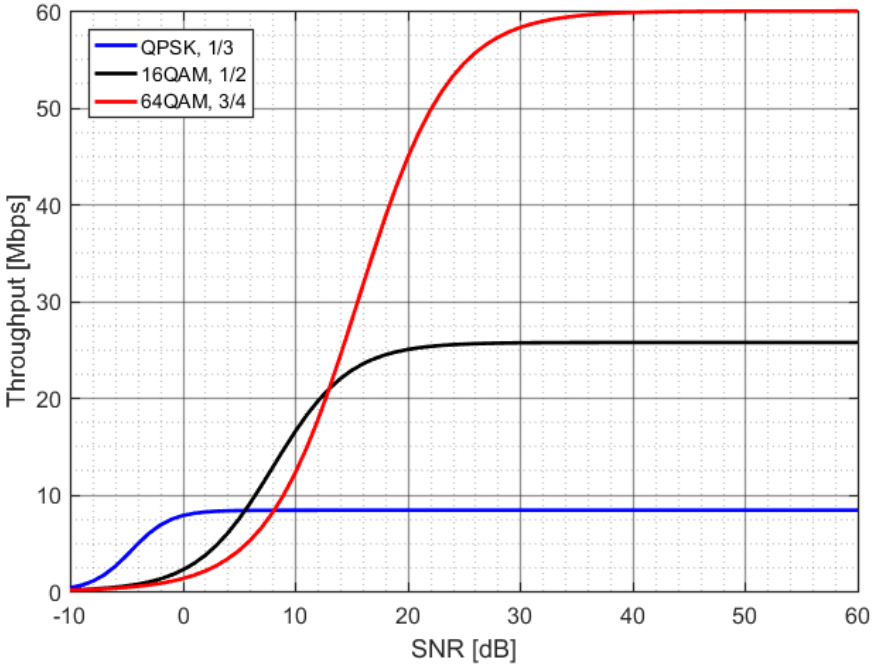

Figure 3.5 - Throughput for some LTE MCSs.

Regarding WiFi, Figure 3.6 contains an example of a real system with achieved data rates.

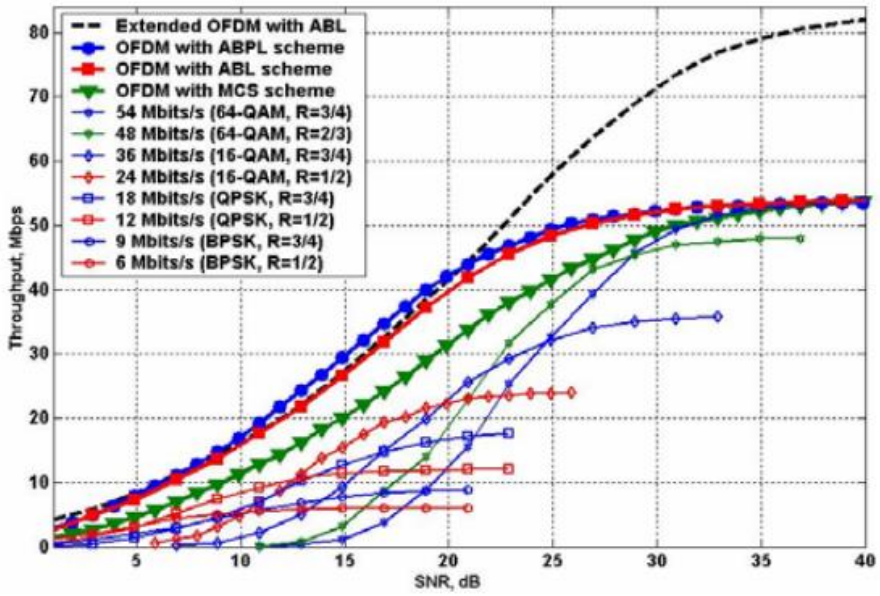

Figure 3.6 - 802.11n's Air Interface Throughput for a 20 MHz Channel (extracted from [BJHS03]).

The idea here is to extract data from this graph using graph digitiser software since no expressions for the curves are given. With this, one is able to interpolate the obtained points and create a model which yields a certain 802.11n throughput based on a given signal to noise ratio.

Once again, considering that the hardware in use is capable of performing adaptative coding and modulation, the available throughput expression contemplates 5 different branches, corresponding to the best available MCS for the current ρ_N. This is done through the use of the MATLAB fitting tool, which is able to interpolate the points with a polynomial approximation. Using the modulation with the highest throughput for a given signal to noise ratio, one can set the modulation boundaries as seen in Table 3.3.

Table 3.3 - BBRS Modulation Boundaries (extracted from [BJHS03]).

Modulation	Condition
64-QAM, ¾	$\rho_N \geq 28.8$ dB
64-QAM, ⅔	$28.8 > \rho_N \geq 22$ dB
16-QAM, ¾	$22 > \rho_N \geq 19.5$ dB
16-QAM, ½	$19.5 > \rho_N \geq 12.3$ dB
QPSK, ½	$12.3 > \rho_N \geq 0$ dB

MATLAB interpolation expresses the different throughputs as follows:

- QPSK, ½:

$$R_{b[\text{Mbps}]}^{QPSK,\frac{1}{2}} = 0.0159\rho_{N[\text{dB}]}^2 + 0.676\rho_{N[\text{dB}]} + 0.523 \tag{3.22}$$

- 16-QAM, ½:

$$R_{b[\text{Mbps}]}^{16-QAM,,\frac{1}{2}} = -0.146\rho_{N[\text{dB}]}^2 + 6.19\rho_{N[\text{dB}]} - 43 \tag{3.23}$$

- 16-QAM, ¾:

$$R_{b[\text{Mbps}]}^{16-QAM,\frac{3}{4}} = 2.33\rho_{N[\text{dB}]} - 22.2 \tag{3.24}$$

- 64-QAM, ⅔:

$$R_{b[\text{Mbps}]}^{64-QAM,\frac{2}{3}} = -0.216\rho_{N[\text{dB}]}^2 + 13.4\rho_{N[\text{dB}]} - 160 \tag{3.25}$$

- 64-QAM, ¾:

$$\begin{cases} R_{b[\text{Mbps}]}^{64-QAM,\frac{3}{4}} = 0.00689\rho_{N[\text{dB}]}^3 - 0.787\rho_{N[\text{dB}]}^2 + 30.1\rho_{N[\text{dB}]} - 334, \rho_N < 40 \text{ dB} \\ R_{b[\text{Mbps}]}^{64-QAM,\frac{3}{4}} = 54, \rho_N \geq 40 \text{ dB} \end{cases} \tag{3.26}$$

3.3 CST Modelling

The task at hand is to derive the attenuation caused by the bridge's metallic beams within the far field region of the antenna, which is a half-wavelength dipole, placed on top of a train. The choice of the field monitor's placement is directly related to the far field limit, R_{ff}, of the antenna. The expression below gives the limit of this boundary,

$$R_{ff} = \frac{2l^2}{\lambda} \tag{3.27}$$

where:

- l: Dipole's Length.

The antennas used in the simulations are half-wavelength dipoles for the different frequencies. For this type of antenna, (3.27) simplifies into:

$$R_{ff} = l = \frac{\lambda}{2} \tag{3.28}$$

Table 3.4 summarises the results for 925 MHz and 5.9 GHz, the lower and upper limits of the frequencies approached in this work, when applying (3.11) with the equivalent dipole's length.

Table 3.4 - Far Field Limits for the Dipole.

	Frequency [MHz]	
	925	**5900**
λ [m]	0.324	0.051
R_{ff} [m]	0.162	0.025

Knowing the far field limit for both cases, in order to avoid multiple time-consuming simulations, one has to decide on a reference distance on which to monitor it. Using spherical coordinates as seen in Figure 3.7, this is done by setting a constant elevation, θ, of 90º (which is a realistic approximation since at large distances the EM waves arrive from a quasi-horizontal direction) and analysing different azimuth angles, or φ, so that the whole extension of the bridge is covered.

The first consideration when analysing the different angles of the problem is that there are some symmetries and therefore one does not need to analyse all range of angles $\varphi \in [0, 360]$ º. The range of $\varphi \in [0, 90]$ º is symmetric to $\varphi \in [270, 360]$ º and the scenario $\varphi \in [90, 180]$ º is the same as $\varphi \in [180, 270]$ º. For these reasons, the only zones that need to be looked at are the first and third quadrants of the problem, that is, $\varphi \in [0, 90]$ º and $\varphi \in [180, 270]$ º.

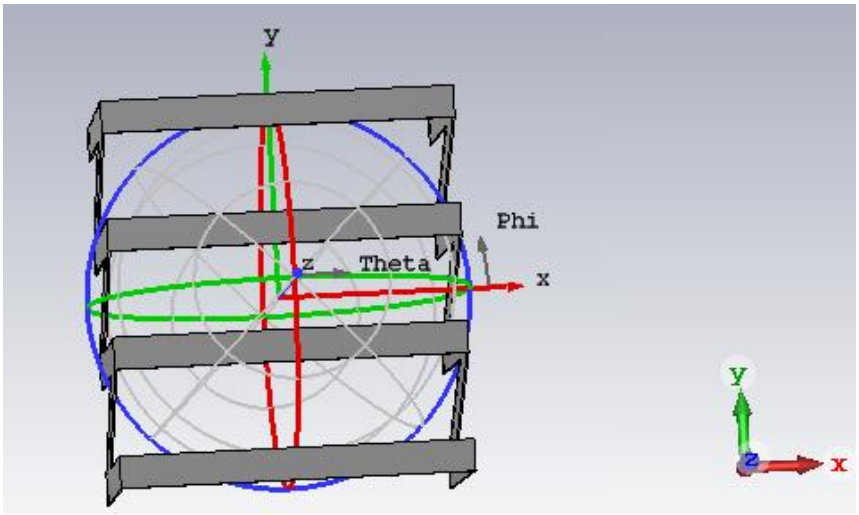

Figure 3.7 - Problem's Angle Definition.

Looking at the first zone, a range of $\rho = 7\ 227$ mm encompasses all of the metallic beams, however, due to the fact that the antenna is not located at the origin of the coordinate system, all the sections of the bridge present in the second zone are outside of this range, with the closest beam being located at $\rho = 7\ 500$ mm. In order to cover the entirety of the bridge, the radius is kept at $\rho = 10\ 000$ mm, which corresponds to the reference distance parameter under far field simulation in CST. Looking at Table 3.4, it can be observed that these ranges are well within the far field of the antenna and therefore suitable for the problem at hand.

Numerous simulation configurations led to the conclusion that the analysis of the current problem with the available computational resources is not feasible. A simulation with the actual bridge model in the 900 MHz band results in more than 2 days of simulation time and increasing the frequency of the problem to 2600 MHz leads to weeks of simulation time. Due to these reasons, the solution to this complexity revolves around CST symmetry planes. These marginally reduce the number of mesh cells at hand, however the cost of this operation comes associated with the fact that the simulated environment does not represent the actual problem exactly as it exists.

The real scenario involves a railway with two tracks and a bridge, which only has symmetry along the ZOY axis, unlike the simulated scenario, a single way track with 3 planes of symmetry. This is an acceptable approximation since the introduction of another rail track should not change the factor one is interested in with this simulation, that is, the bridge penetration losses. Also, this bridge itself does not have symmetry along its metallic beams, however, there are many types of bridges with different symmetries and the objective of this study is not to study this bridge in particular, but to develop a method applicable to any bridge and provide an average value for the losses along the metallic medium. Smaller scale simulations also show that the positioning of the antenna (which is located on the middle of the problem in the simplified scenario) marginally change the value of the electric field but do not justify the increased complexity of the problem.

When one introduces the stated simplifications, the actual range that needs to be analysed is reduced to $\varphi \in [0, 90]$ º. The probe radius, ρ, is the same as stated before, 10 m, which is enough to analyse the

electric field in any point outside the, now symmetric, bridge from any angle of observation.

The process of adding E-field probes in CST requires the user to input the data in cartesian coordinates. With the angle definition in Figure 3.7 these can be obtained with the known spherical to cartesian transformation:

$$(x, y, z) \rightarrow (\rho, \theta, \varphi) \tag{3.29}$$

Figure 3.8 shows the problem's schematic with the placement of the probes. It can be seen that, when using the time domain simulator, the whole bridge is surrounded by E-field probes for the previously defined radius. Although the Integral solver does not have access to these probes, one can manually set the far field reference using the same radii values.

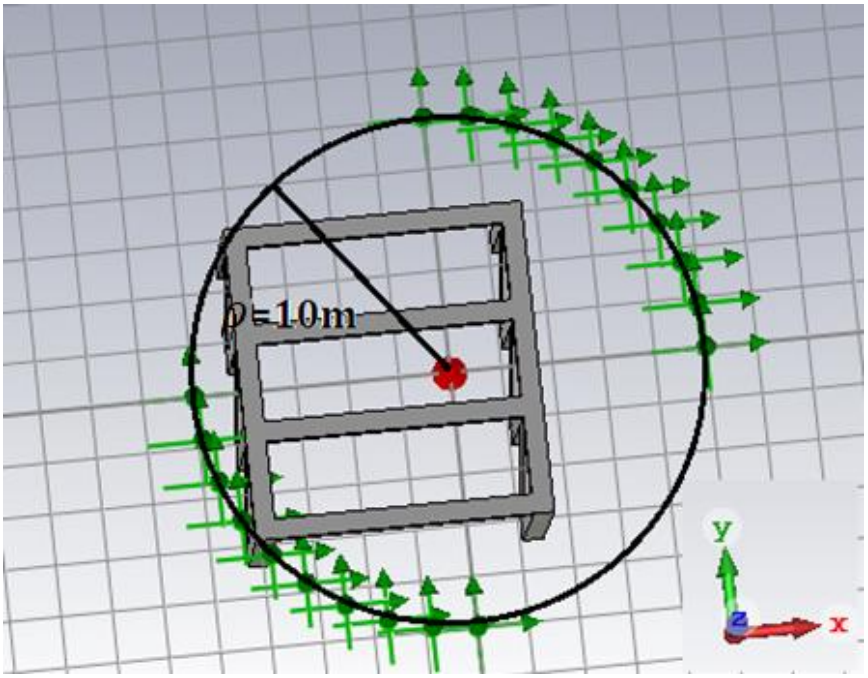

Figure 3.8 - Probes' Placement.

The results from this procedure are mainly interesting in the GSM-R and LTE-R cases, since these are the situations where one has the BS outside the bridge, hence dealing with the highest levels of attenuation on the metallic surfaces. In the BBRS case, the signal is directly fed via optical fibre into the APs, which are usually located inside the metallic structure, a case that has low propagation losses. A BBRS scenario with a metallic bridge obstruction is also analysed due to the fact that surrounding rail track conditions may force the APs to be placed inside the metallic bridge.

Figure 3.9 shows the boundaries defined by CST. YOZ and XOZ planes have Magnetic symmetry, while the XOY plane has Electric symmetry. According to [PDBR15], this means that, using image theory, for an electric current at a given distance above the magnetic plane, this plane can be replaced for another current with the same sign at the same distance, bellow the original plane. Similarly, an electrical current above a perfect electrical conductor plane means that the plane can be replaced by a current with the opposite sign, at the same distance, bellow the original electric plane.

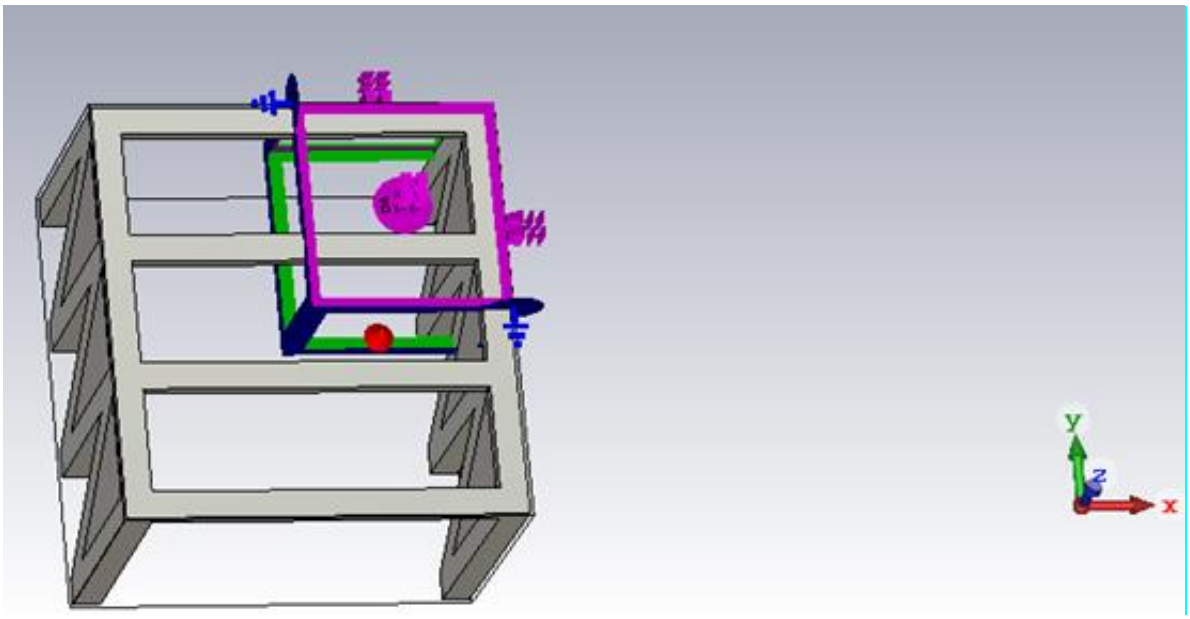

Figure 3.9 - CST's Symmetric Boundaries Definition.

The metallic structure is made of PEC (Perfect Electrical Conductor) or Steel-1010, both found within the CST material options. PEC is studied as an option to steel since it reflects an ideal case, with levels of reflectivity higher than metals'. The schematic of the bridge, along with the antenna placement in red, are shown in Figure 3.10.

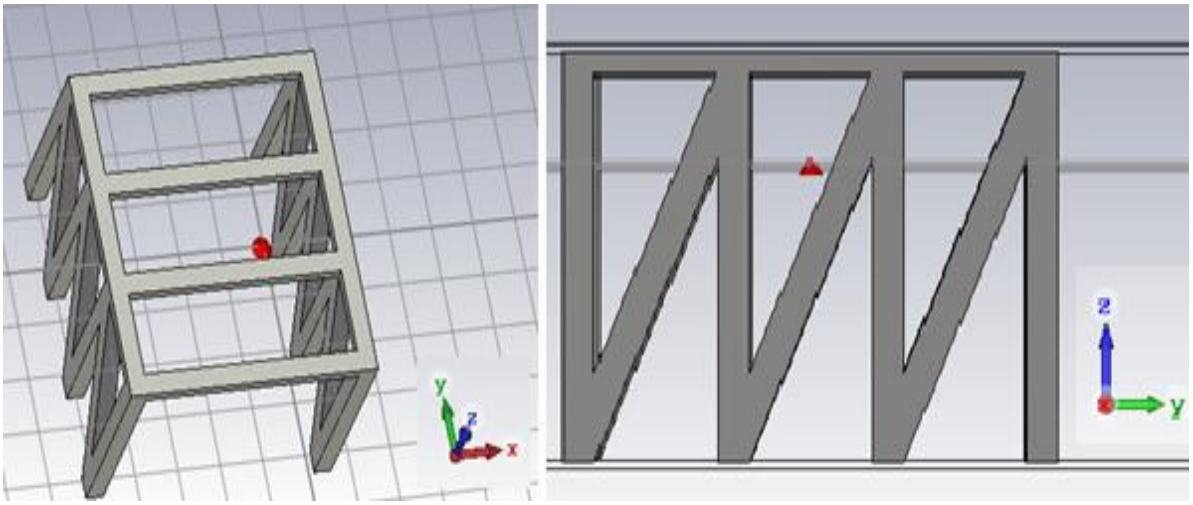

(a) Top View (b) Lateral View

Figure 3.10 - Top and lateral views of the CST simulation schematic.

Figure 3.11 and Figure 3.12 show the dimensions of the models used in CST. Even though the train itself is not modelled in CST, the last figure is useful to define the width and height of the metallic bridge, as well as to provide an estimation of the antenna's placement, which is set at 5 m above the level of the rail track. By looking at Figure 3.10 it is easily observed that only a portion of the metallic bridge was simulated, corresponding to 12.18 m of the bridge's extension. This choice was made in order to include an integer number of metallic beams, while keeping similar bridge dimensions in both length and width.

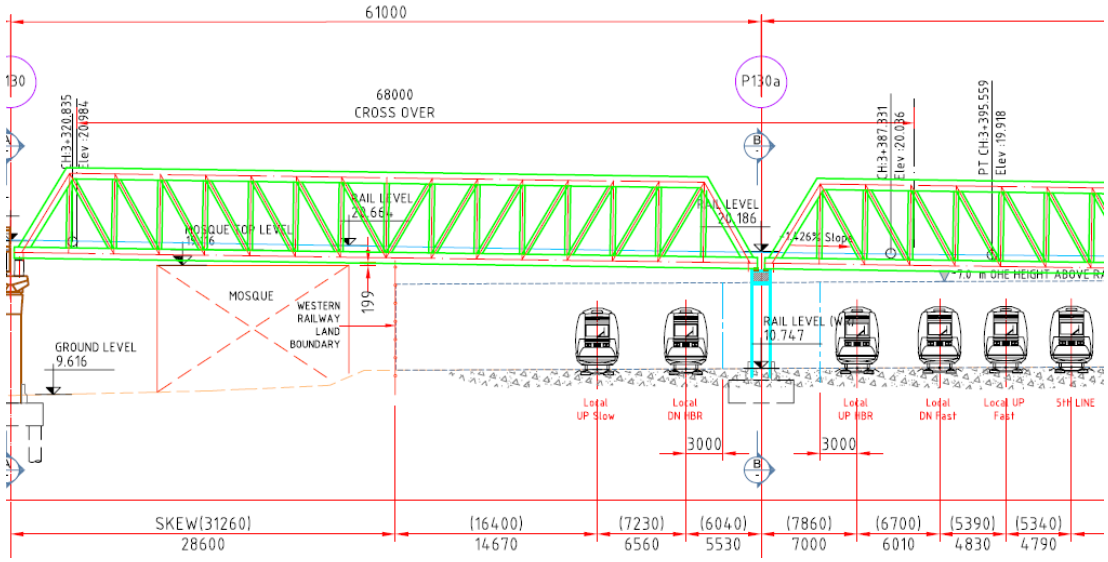

Figure 3.11 - Metallic Bridge's Dimensions (provided by Thales).

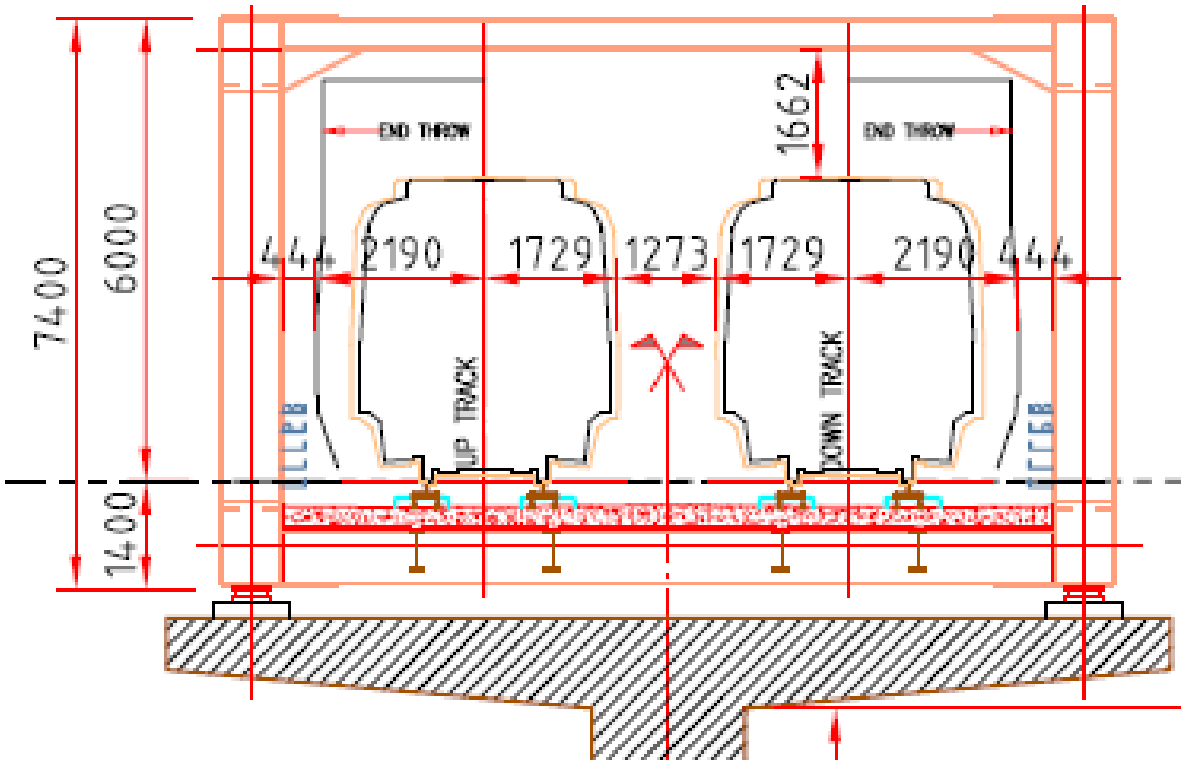

Figure 3.12 - Train's Longitudinal Section (provided by Thales).

The performed simulations contemplate a degree of accuracy of -20 dB, which means the simulation ends when 1/100th of the original energy is available within the simulation, as well as 5 cells per wavelength for both the 925 and the 2600 MHz simulations in what concerns meshing purposes.

Unlike antenna simulations, where a high number of cells per wavelength is needed in order to define the edges of the model (commonly 15 to 20 cells per wavelength are used), this simulation is less demanding in this aspect, since the metallic beams are large enough to allow lower values of this parameter.

With the evaluation of the field outside of the metallic structure, the next step is to compare it with the

field that would result without the presence of the metal beams, given by free-space propagation.

The losses on the metallic bridge can then be expressed, in dB, by the following expression,

$$L_{bridge[\mathrm{dB}]} = 20\log\left(\frac{|E_{fs}|}{|E_{obs}|}\right) = |E_{fs}|_{[\mathrm{dBV/m}]} - |E_{obs}|_{[\mathrm{dBV/m}]} \tag{3.30}$$

where:

- E_{fs}: Electric field in the absence of the metallic bridge (free space);
- E_{obs}: Electric field outside of the metallic beams.

As seen in [Semt18], the root mean square value (RMS) of the electric field's magnitude at a given point is given by the expression bellow,

$$|E_{dir}|_{,RMS[\mathrm{dBV/m}]} = 20\log\left(\frac{\sqrt{30P_t G_t}}{r}\right) \tag{3.31}$$

where:

- r: Distance between the point being evaluated and the antenna.

CST does not present its results in RMS, but in peak values. For comparison purposes it is useful to convert (3.31) with the introduction of a constant:

$$|E_{dir}|_{[\mathrm{dBV/m}]} = |E_{dir}|_{,RMS]} \cdot \sqrt{2} \tag{3.32}$$

3.4 Model Implementation

The MATLAB scripts used in this work are explained here. Depending on the work frequency and the type of environment at hand, different models (Subsections 3.2.2 through 3.2.4) are used in order to estimate path loss. Free space propagation is used as a comparison in all cases as a means of assessment. The flowchart that explains the behaviour of the developed code, as well as the chosen models for each scenario can be seen in Figure 3.13.

The first inputs needed in order to calculate path loss through any of the models are the carrier frequency (925, 2600 or 5900 MHz for GSM-R, LTE-R and BBRS, respectively), the heights of the antennas for both the MT and the BS, and the type of environment being analysed (viaduct, rural, suburban, river, cutting or station). Based on the frequencies at hand as well as the chosen environment, different models are used in order to estimate path loss as accurately as possible.

Should the frequency of work be the 5.9 GHz (BBRS scenario) the chosen propagation model is the Winner II, described in Subsection 3.2.2. This choice is not affected by the type of environment at hand due to the nature of the distances involved in this type of system. For the usual distances between transmitters of around 300 m, the effect of the high frequency on path loss is more relevant than the actual scenario where the BS is located. No additional input is needed from the user, however breakpoint distance must be calculated by (3.12), whereas (3.11) yields the path loss for the current model.

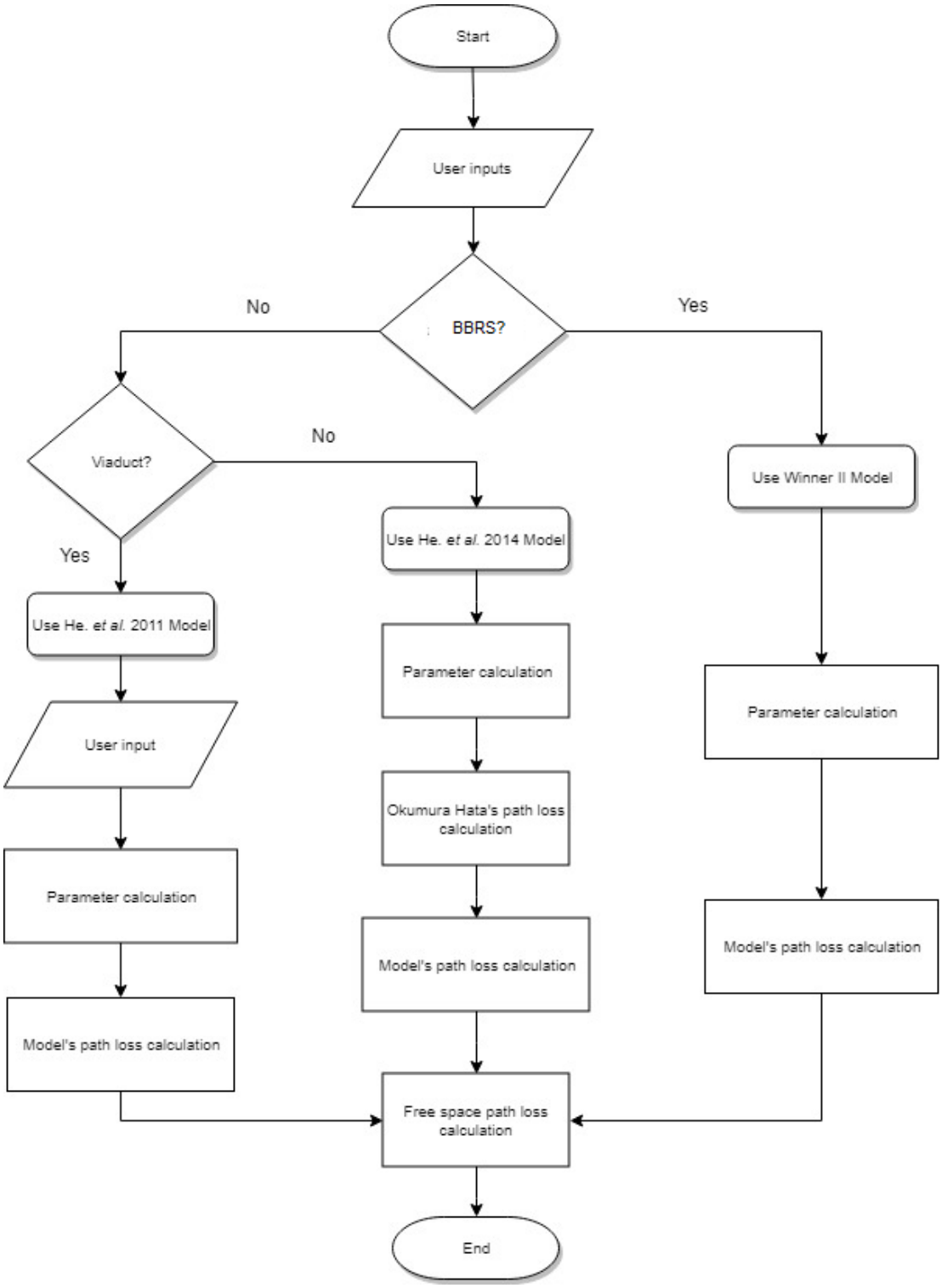

Figure 3.13 - MATLAB scripts' explanation.

For lower frequencies (GSM-R and LTE-R), the model that is employed depends on the scenario at hand. Viaducts are analysed with the He *et al.* 2011 model, which is described in Subsection 3.2.3. In addition to the previous inputs, the user now needs to state the height of the viaduct that is being analysed. The C_D model parameter is calculated for a z-score of 1.282 when using the x and y distributions, in order to cover 90% of the cases. The path loss for this model is calculated using (3.14).

For the other mentioned scenarios, the model to be used is the He *et al.* 2014, mentioned in Subsection 3.2.4, which calculates the correction parameters for the different environments without any additional input from the user through the expressions shown in Table 3.2. The path loss for urban areas with the large cities' correction factor, model on which the former one is based, is also calculated as a means of comparison with the urban path loss for HSR specific scenarios, as well as a means of model assessment, through (3.15). Finally, the model's path loss is calculated with (3.16).

A final and common step to all of these models regards the calculation of the path loss given by free space propagation in order to make sure the obtained values are coherent.

3.5 Model Assessment

The propagation models previously mentioned were developed and tested for specific scenarios, and their results were verified in numerous publications. Thus, their assessment is not done in this work, but instead, a lower level assessment is made, in order to make sure that the model's equations are correctly implemented and the results and meaningful. The list of the actions that were performed in order to check the model's behaviour are present in Table 3.5, which mainly revolves around testing the code's output with the user's calculations and predicting the behaviour of the simulator for low complexity scenarios.

Table 3.5 - Model Assessment Procedure.

Operation	Description
1	Comparison of MATLAB results against calculator ones.
2	Visual analysis of the obtained graphs' shapes
3	Relative analysis of the different environments, *i.e.* Rural vs. Urban losses
4	Analysis of CST behaviour for different accuracies in lower complexity models

Figure 3.14 represents path losses for a given configuration with different propagation models, one of the tests used in order to verify actions 2 and 3. The viaduct configuration is sub-optimal, which shows high levels of path loss compared with the remaining environments. All models show propagation losses higher than free space propagation. One of the performed CST tests consists of measuring the intensity of the electric field at a fixed distance of 45 cm away from the dipole for two distinct situations. Figure 3.15 shows a half-wavelength dipole radiating in both free space and a knife-edge configuration, where there is a metallic surface placed between the dipole and the point where the field is being measured. This test is chosen due to the fact that it involves small structures and consequently fast simulations, while representing the metallic bridge problem accurately.

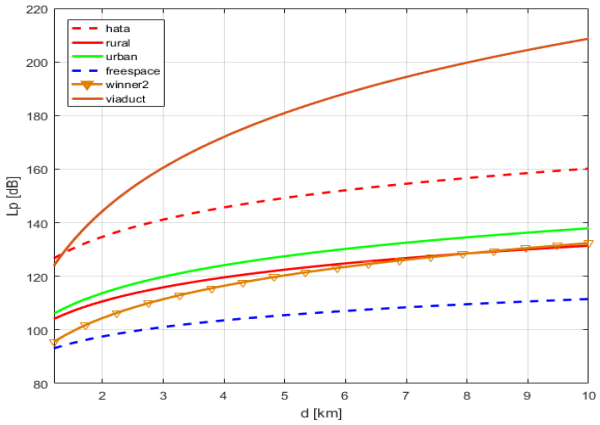

Figure 3.14 - Path Loss Model Assessment Test for 900 MHz.

The main idea behind this test is that one expects EM waves to be reflected when in contact with the metallic walls, which represent the bridge's beams, distorting the expected toroidal radiation pattern of a dipole and affecting the radiated electric field, which can be measured at different points of the schematic.

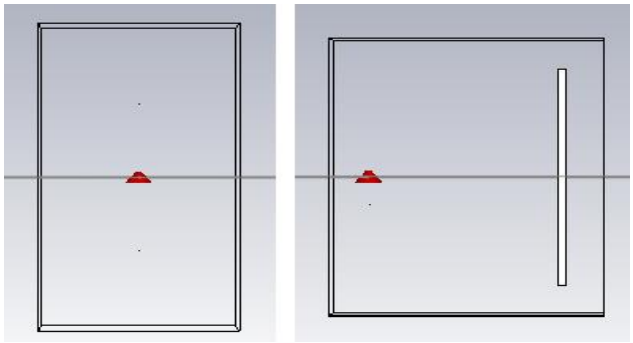

(a) Isolated Dipole (b) Knife-Edge

Figure 3.15 - Simulator Assessment Test.

The results of these simulations are expressed in Figure 3.16. The field pattern is deformed when the metallic wall is inserted since this situation contemplates an obstruction. On the opposite side of the obstruction (φ = 180 º) one can contemplate a higher level of electric field, which is explained by reflections on the metallic surface. The incident rays on the obstruction are reflected and accumulate on the opposite edge of the plane, which sees an increase of around 2 dB in its electric field value.

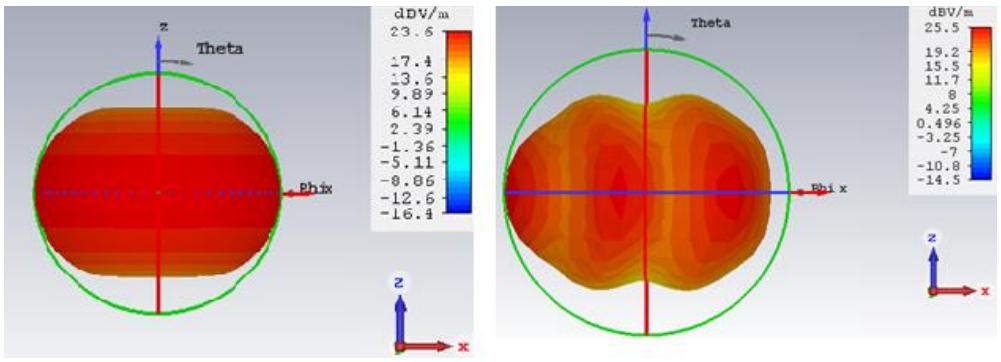

(a) Isolated Dipole (b) Knife-Edge Scenario

Figure 3.16 - Electric field originated by the different configurations.

Chapter 4

Results

The current chapter presents the results obtained when applying the developed models and simulating the previously defined scenarios, as well as their analysis. These are split into the developed bridge attenuation model and the analysis of the different networks' maximum communication distances and throughputs.

4.1 Scenarios and Requirements

In this section, the metallic bridge represented in Figure 4.1 is analysed. Even though this study targets a specific bridge, the objective is not to obtain a very specific model for this bridge but to provide a reference for the losses that can be observed when dealing with this kind of structures.

Figure 4.1, Figure 4.2 and Figure 4.3, all pose examples of metallic bridges that can be commonly found in railway scenarios and involve a high level of reflections, posing possible problems when dimensioning telecommunications systems. Even though they have somewhat different appearances, the process of study and the electromagnetic phenomena existing in any of them are exactly the same.

Figure 4.1 - Metallic Bridge in Study, Mumbai Line 1 (extracted from [MMOP14]).

Figure 4.2 - Another Metallic Bridge in the same Mumbai line (extracted from [MMOP14]).

Figure 4.3 - A Third Example of a Metallic Bridge, Santa Fe (extracted from [Fell13]).

Unlike antennas, where a specific modelling is necessary for each scenario, when dealing with metallic bridges one is interested in a margin for losses, similar to an indoor propagation scenario, which should be accounted for when constructing the link budget.

In GSM-R the only existing requirement is to meet the minimum signal to noise ratio in order for the system to be able to transmit voice. Both in LTE-R and BBRS, this no longer stands true and there are data throughput requirements that must be met so that train functions, mainly CCTV footage uploading, may be possible.

Table 4.1 states typical requirements for BBRS systems. UL rates are always more constraining than DL ones since video upload functions are typically used by the trains and DL is often required by passengers or negligibly small data train commands.

Table 4.1 - Examples of BBRS Requirements (adapted from [Thal17]).

Project Index	Required Throughput [Mbps]		Possible Setup
	UL	DL	
1	12	-	2 permanent stream, 2 station streams
2	12	8	
3	10	-	1 permanent stream, 2 station streams
4	6	-	1 permanent stream, 1 station stream
5	4	4	1 station stream

Trains possess both streams inside their carriages, as well as dedicated streams to capture platform footage specifically when they are arriving or leaving stations. The first type of cameras has a requirement of 2 Mbps per data stream, whereas station streams need at least a throughput of 4 Mbps in order to upload images in real time. This is due to the fact that platform footage is of a crucial importance when dealing with a series of issues that can occur inside the train station, such as human or infrastructural damages.

In these analyses, one assumes the systems are balanced (that is, the same bandwidth is available for both links) and the link budget is done for the more demanding case, that is, the UL. The rates presented refer to single input single output (SISO), that is, no diversity is employed.

Since 20 MHz bandwidth channels are considered both for LTE-R and BBRS, with LTE-R networks being barely existent at the moment, the same requirements are considered for both systems.

Table 4.2 states the link budget parameters for the 3 systems that are being tested in order to provide a reference for future measurements. An UL situation is considered, that is, the transmitter parameters refer to the train antenna whereas the receiver is the BS one.

The cable losses consist of the sum of two parcels. The first one, L_{Cant}, refers to the losses regarding the BS antenna cables and the other, L_{Conb}, accounts for the onboard cable losses. Their constitution is different (different types of cables) and therefore their losses are accounted for separately. It should also be noted that the stated values for these refer to a reference frequency of 5.8 GHz and therefore actual losses for GSM-R and LTE-R are lower, given their lower frequencies of operation.

Finally, two system margins are considered. M_{S1} corresponds to the margin used in a standard scenario where no metallic bridge is present, whereas M_{S2} is a higher margin, which accounts for the losses introduced by the metallic bridge penetration, L_{bridge}.

Table 4.2 - Link Budget Parameters.

P_{Tx}	22 dBm
L_{Cant}	2 dB
L_{Conb}	2.4 dB
G_R	14 dBi
G_t	8.5 dBi
M_{S1}	10 dB
M_{S2}	(10 + L_{bridge}) dB
F	8 dB

4.2 Bridge Attenuation Modelling

The first result has to deal with the materials that are used when simulating the EM behaviour of the bridge. Simulations were made, both for the PEC and a specific type of Steel (Steel-1010 in CST studio), in order to analyse the intensity of the electric field for the whole range of azimuth angles.

Even though Steel-1010, which is actually a real material, is the one considered henceforth, the difference between the two distinct materials is marginal, and therefore it can be argued that the use of either type of material will produce similar results, since the high reflectivity of metallic structures resembles the behaviour of perfect electric conductors. The only noticeable deviations between both cases consist of punctual fluctuations, which pose no interest to the analysed scenarios since the train will be constantly moving through the bridge and therefore a single angle does not provide any meaningful data.

The simulation results from CST show that, at 925 MHz, the magnitude of the electric field follows the behaviour shown in Figure 4.4, where the field originated by the dipole (fed with 0.825 W) at the same distance (10 m), in free space, is shown as a term of comparison. These values can be calculated with (3.12) and (3.13), however marginal differences are observed between the represented values and the theoretical ones due to the efficiency of the antennas.

As stated in the previous chapters, only the values present in the range of $\varphi \in [0, 90]$ º are represented since these repeat themselves over the whole extension of azimuth angles, providing no additional information to the problem.

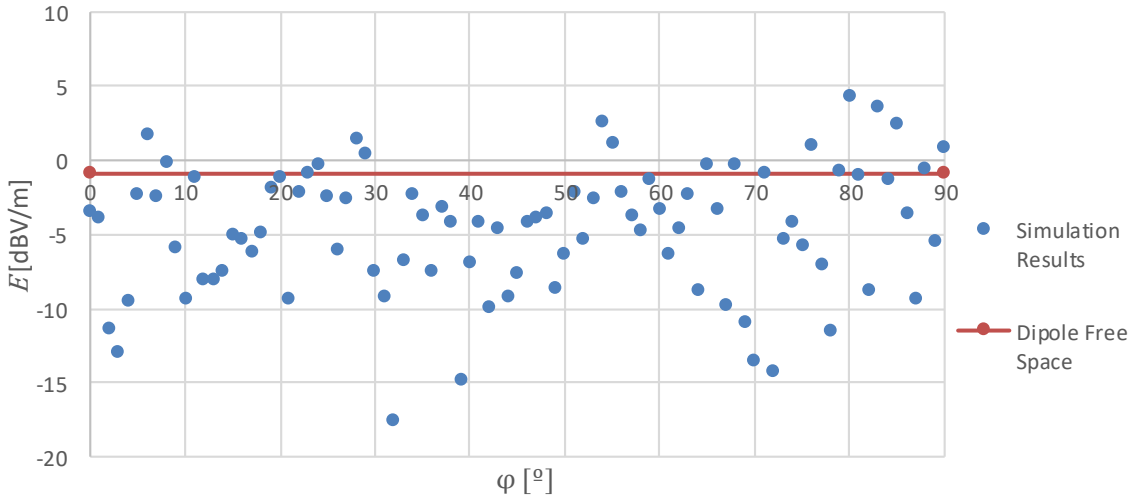

Figure 4.4 - Magnitude of the Electric Field at 925 MHz.

One should proceed to the saturation of outliers originated by constructive reflections of numerical calculations before any further analysis, in a similar procedure as the ones used in other propagation models such as two-ray and knife-edge models. Since the parameter of interest is the average value for the losses (not losses in specific angles of arrival), one considers the situation with no obstruction as the reference for the maximum value of the signal (which corresponds to free space propagation) and

therefore, for the measurements relative to 925 MHz, any point above this value is saturated to the value of E_{MAX} = -0,905 dBV/m.

Likewise, the lower peaks are saturated to the lower limit of E_{MIN} = -12.957 dBV/m, which contains the majority of the lower electric field values. This process is shown in Figure 4.5, which shows the corrected values for the propagation losses in dB for the metallic bridge.

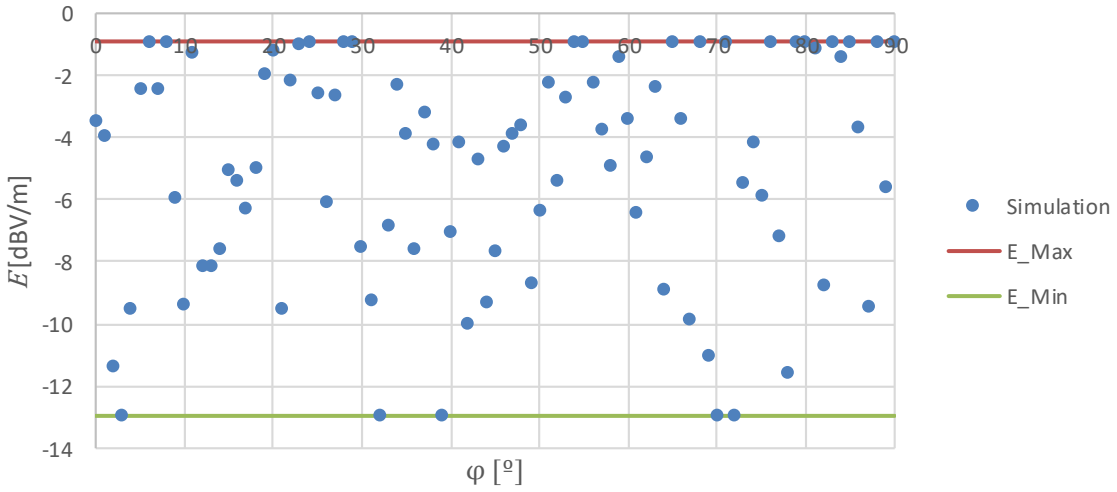

Figure 4.5 - Saturated Field Magnitudes at 925 MHz.

With the use of Excel, it is possible to analyse the data provided by CST and, through the calculation of averages and standard deviations, analyse the respective z-scores, seeing that the simulation results can be approximated by a normal, left-truncated (at zero), distribution curve with an average of 3.5 and a standard deviation of 4.1. Figure 4.6 shows the respective cumulative density function (CDF), both with the simulation results and the normal approximation curve.

The expression for a normal CDF is expressed bellow,

$$P(X \leq x) = \frac{1}{2}\left[1 + \operatorname{erf}\left(\frac{x-\mu}{\sigma\sqrt{2}}\right)\right] \tag{4.1}$$

whereas the specific CDF follows the expression:

$$P(X \leq x) \approx \begin{cases} \frac{1}{2}\left[1 + \operatorname{erf}\left(\frac{x-3.5}{4.1\sqrt{2}}\right)\right], x > 0 \\ 0.2, x = 0 \end{cases} \tag{4.2}$$

where:

- erf stands for the error function;
- σ: Standard Deviation;
- μ: Average.

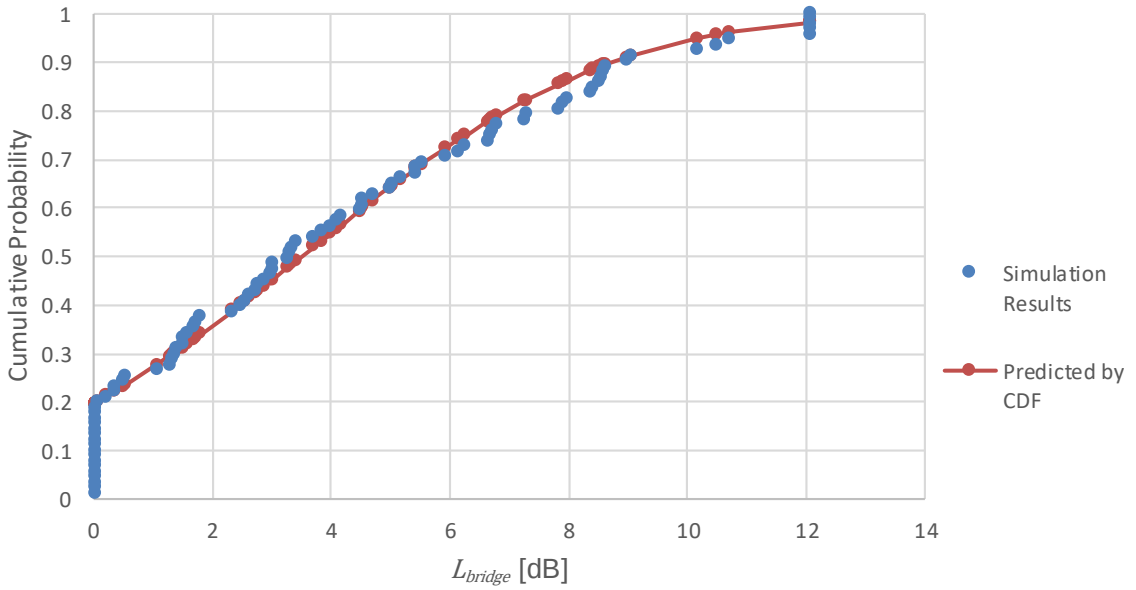

Figure 4.6 - Simulation Results and Normal CDF Approximation at 925 MHz.

In what concerns statistical performance parameters, the obtained correlation coefficient (via Excel Data Analysis toolbox) of 0.99728 shows a strong dependence between the simulation results and the values obtained by the stated CDF.

It is important to state that the accumulation of points corresponding to 0 dB losses is not caused by a lack of resolution from CST, as one would expect when looking at this kind of graph, but by the saturation of points made in the previous step. The normal curve approximation is used henceforth in order to reflect the average scenario in what concerns losses in a metallic bridge environment and not a specific bridge. The graph represented in Figure 4.6 provides L_{bridge} for the forthcoming calculations, allowing one to calculate a new system margin for a case where there is a metallic bridge present in the scenario. For instance, the maximum value of bridge propagation losses for 90% of the cases is defined as the standard value for the scenarios where a metallic bridge is present at 925 MHz and its value corresponds to 8.75 dB. One can write this as:

$$L_{bridge}^{GSM-R,90\%} = 8.75 \text{ dB} \tag{4.3}$$

The same procedure can be followed for the LTE-R scenario, that is, for the 2600 MHz frequency. In this simulation the antenna is fed with 0.814 W. The obtained electric field for the same extension of φ, along with the field produced by the dipole in free space are represented in Figure 4.7. One can state that a higher number of electric field values are above the free space value, indicating that the frequency raise brings additional scattering and diffraction phenomena, resulting in areas with additional accumulation of signal, however that analysis is not going to be approached within this work.

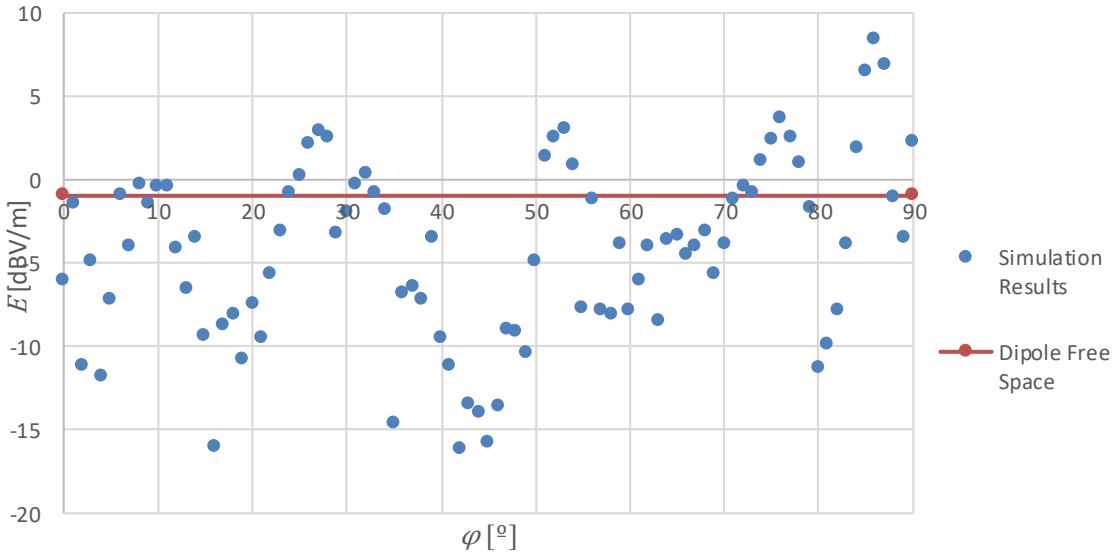

Figure 4.7 - Magnitude of the Electric Field at 2600 MHz.

Once more, the higher bound of the problem becomes the field generated by the dipole in free space, that is, E_{MAX} = -0.961 dBV/m whereas the lower limit is set at E_{MIN} = -14.579 dBV/m. This process is shown in Figure 4.8, which contains the saturated values for the LTE-R simulation.

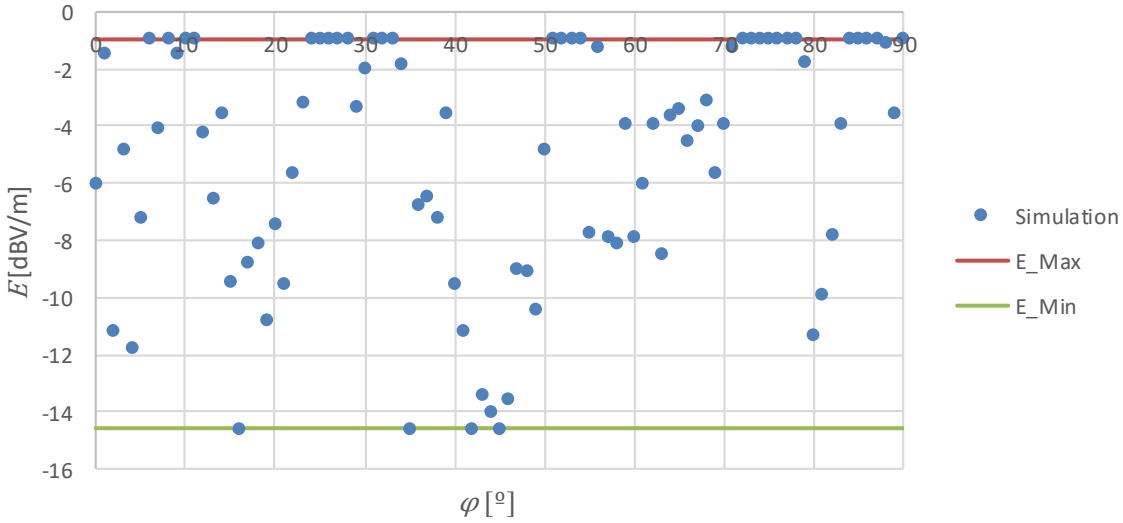

Figure 4.8 - Saturated Field Magnitudes at 2600 MHz.

The analysis of the present data shows that, for this case, the simulation results can be approximated by a left-truncated (at zero) normal CDF with an average of 2.7 and a standard deviation of 5.8. The obtained results are expressed in Figure 4.9 and the specific obtained CDF follows the expression:

$$P(X \leq x) \approx \begin{cases} \frac{1}{2}\left[1 + \operatorname{erf}\left(\frac{x - 2.7}{5.8\sqrt{2}}\right)\right], x > 0 \\ 0.3, x = 0 \end{cases} \quad (4.4)$$

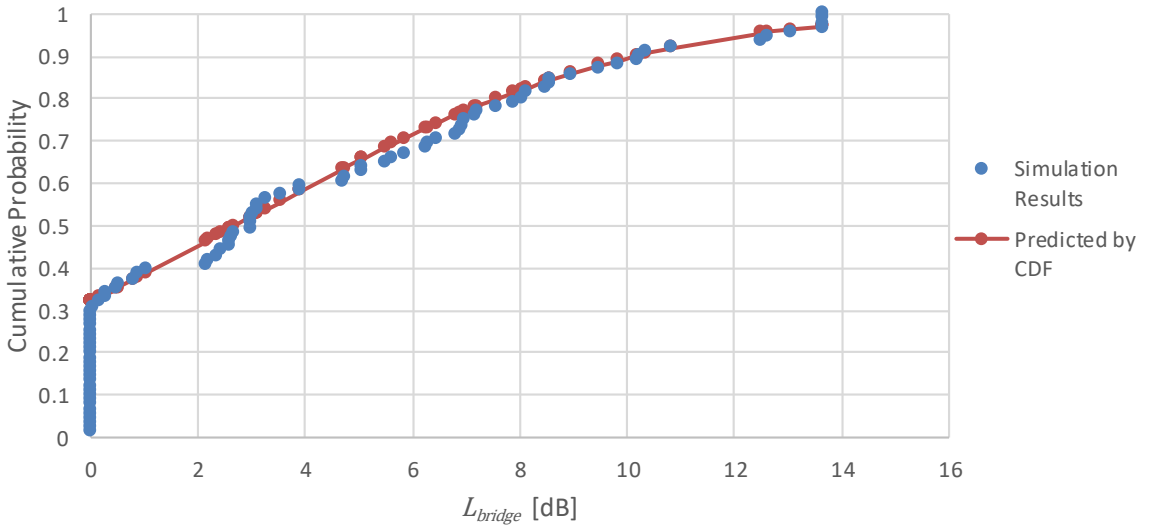

Figure 4.9 - Simulation Results and Normal CDF Approximation at 2600 MHz.

This time, the correlation coefficient's value is 0.99827, which also shows a strong correlation between the observed data and the normal prediction.

With the graph in Figure 4.9 providing L_{bridge} for the scenarios at 2.6 GHz where a metallic bridge is present, the same parameter, which translates the maximum propagation losses for 90% of the cases, is retained, this time corresponding to a value of 10.13 dB.

$$L_{bridge}^{LTE-R,90\%} = 10.13 \text{ dB} \tag{4.5}$$

Finally, the remainder parameter to obtain is related to the propagation losses in a metallic bridge scenario at 5.9 GHz, that is, for a BBRS system. Due to the high frequency at hand and the limited hardware available, CST simulation is not a viable strategy since it would result in weeks of simulation. For this reason, the procedure to obtain the losses for this last scenario is through the linear approximation involving the values obtained in the GSM-R and LTE-R simulations. Of course, the higher frequency can change the behaviour of the EM signals and one must be conscious that the best method to obtain these values would be through diffraction analyses such as ray-tracing techniques, which would introduce another degree of complexity in the current work. Nonetheless, works such as [Chen70], [KiCh94], [Scot98] and [CWCF08] show that both losses and reflection coefficients are somewhat linear and monotonous when operating with frequency selective structures up to 10 to 20 GHz, frequencies that are still quite above the one at hand. This is also the case when dealing with metallic walls.

With this is mind $L_{bridge}^{BBRS,90\%}$ is the parameter one is looking for in order to calculate the penetration losses in the BBRS metallic bridge scenario, which can be obtained with a simple linear approximation, which is shown in Figure 4.10.

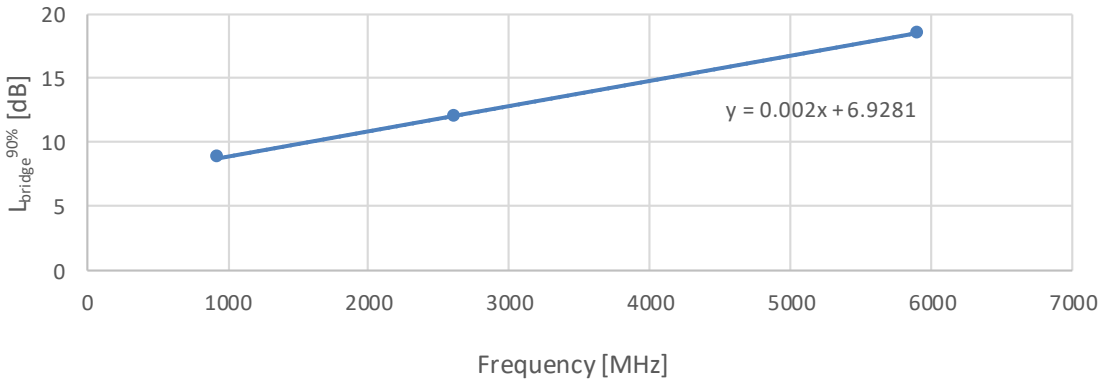

Figure 4.10 - Linear Approximation for BBRS' Bridge Losses.

The linear equation contemplates a slope of 0.002 and a value of 6.9281 for the y-intercept parameter, resulting in the value of:

$$L_{bridge}^{BBRS,90\%} \approx 18.55 \text{ dB} \tag{4.6}$$

4.3 GSM-R Analysis

In this section, a different set of environments is analysed. GSM-R is not capable of reaching data rates high enough to support video transmission and therefore the performed analysis regards the maximum distance one can support in order to guarantee voice transmission, that is, the maximum distance that guarantees the system sensitivity of -102 dBm.

4.3.1 Viaducts

Table 4.3 synthetises the most important parameters and results for this system. The presented signal to noise ratio accounts for a situation where no metallic bridge is present, thus, the margin in use is M_{SL}.

Table 4.3 - GSM-R System Parameters and Results.

f_c	925 MHz
$P_{Rx,MIN}$	-102 dBm
Δ_f	4 MHz
N	-100 dBm
$\rho_{N,MIN}$	-12 dB
$L_{p,MAX}$	132.1 dB

The data in this section were obtained using the model descripted in Subsection 3.1.2. Sources of error include the height of the trains and the placement of the antennas. On the model the trains are 3.8 m high and the antennas are placed 30 cm on top of them, resulting in a MT height of 4.1 m, whereas all the situations bellow simulate an environment where the receiver antenna is 5 m above the rails. Instead of 10 to 20 m away from the railway, as stated in the model, the antennas are closer, distancing around 5 m from the rails. All the heights (of the BS and the viaducts) used in this section are within the validity range of the model, and so is the used frequency of 925 MHz.

With the intent of analysing different viaducts behaviour, the first result shows the effect of the height of the viaduct itself. Figure 4.11 shows the path losses for different heights of viaducts when the height of the base station is fixed at 30 m.

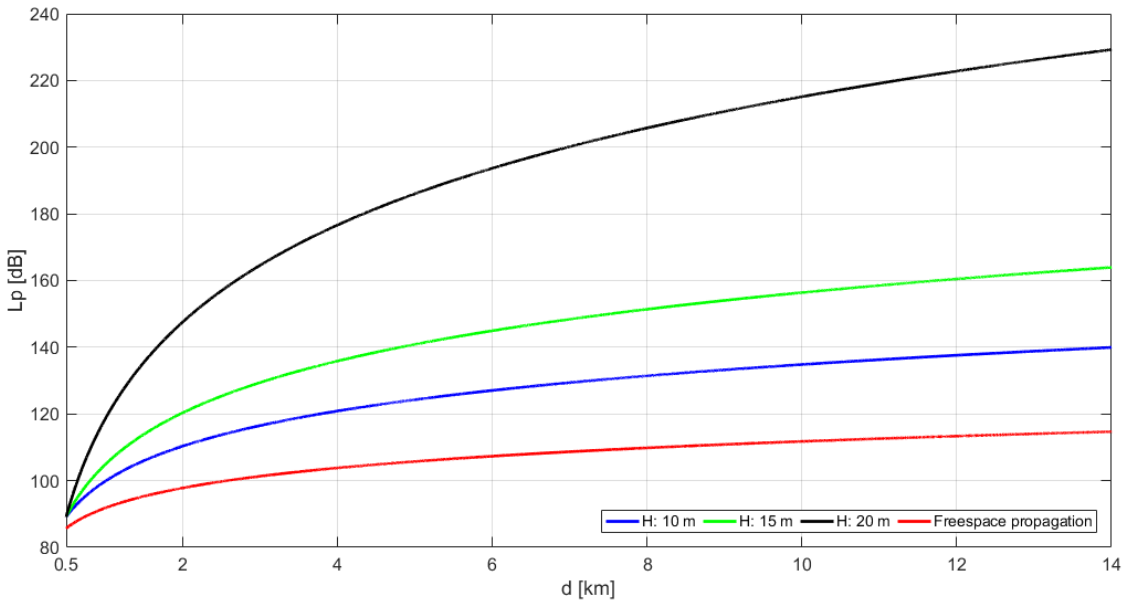

Figure 4.11 - Effects of the Viaduct's Height.

One can see that the losses increase with the height of the viaduct, which is explained by the fact that the reflected and diffracted components of the transmitted signals both on the ground and the surface of the have difficulty reaching the receiver's antenna.

One would expect that higher heights of the viaducts would lead to lower obstacles present in the signals' paths and therefore better performance, however, with a viaduct's height starting at 10 m, on top of the antenna being placed on top of the train, most obstacles are already below the rails and lower viaduct heights will actually provide the best clear LOS situations between the transmitter and the receiver.

Another phenomenon related to the height of the viaducts is that when they are tall, due to the aforementioned scattered components having trouble reaching the receiver, there will also be a low number of multipath components present, leading to lower levels of fading, which is a key effect mentioned in [HZAD11].

One could also analyse the higher levels of interference produced in this situation, however, these metallic environments are often present in areas where there are little to no other systems operating,

and often using different frequencies. Should the viaduct be present in an area with other systems of communication operating in the same frequencies, their height would pose a problem in what concerns to interference. Additionally, tests show that viaduct heights beyond 30 m lead to bad channel behaviour.

Another result has to deal with the height of the BS used to communicate with the trains' antennas. Figure 4.12 shows some variations of this parameter when the viaduct's height is fixed at 10 m, a commonly found value in HSR scenarios.

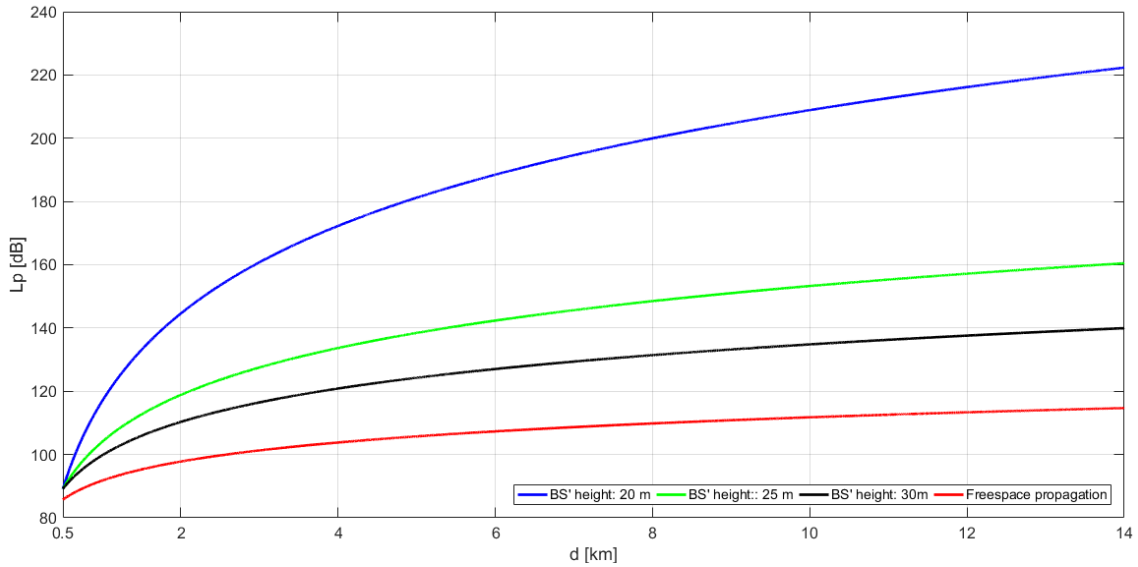

Figure 4.12 - Effects of the BS' Height.

Naturally, due to the chosen parameters, one configuration (viaduct height of 10 m and BS antenna's height of 30 m) is represented twice. As expected, higher BS heights lead to a decrease in what concerns to propagation losses. This is explained by the fact that this results in situations with clearer LOS and therefore lower attenuation from obstructions. Table 4.4 shows the maximum distances supported in each of the presented cases. It can be seen that one configuration (30 m high BS with a 10 m viaduct) vastly outperforms the others, which is a clear indicator that network planning is essential when dealing with viaducts.

Table 4.4 - Maximum BS Distances for Different Viaduct Configurations.

h_{BS} [m]	H [m]	d_{MAX}		
		w/o bridge [km]	w/ bridge [km]	Relative Decrease [%]
20	10	1.464	1.178	19.5
25		3.711	2.470	33.4
30		8.377	4.711	43.8
	15	3.381	2.298	32.0
	20	1.386	1.129	18.5

4.3.2 Other Scenarios

In this subsection the model detailed in Subsection 3.2.4 is used to study other railway scenarios apart from viaducts. These were already introduced in the scenario development and are the urban, rural and suburban ones, as well as the cuttings, stations and rivers.

The model is based on the Hata model for Urban environments with the large cities' correcting factor, which is included as a term of comparison between specifically developed HSR scenario models and standard ones.

Even though the frequency band matches the one studied in the model, the dimensions of the trains are not specified, the MT's antenna is fixed at a height of 4 m and the placement of the antennas is not specified, therefore one should expect a degree of deviation between the obtained results via the model and the actual behaviour of a real system.

Figure 4.13 shows the propagation losses for the first set of environments analysed in this subsection when the height of the BS' antenna is set at 20 m.

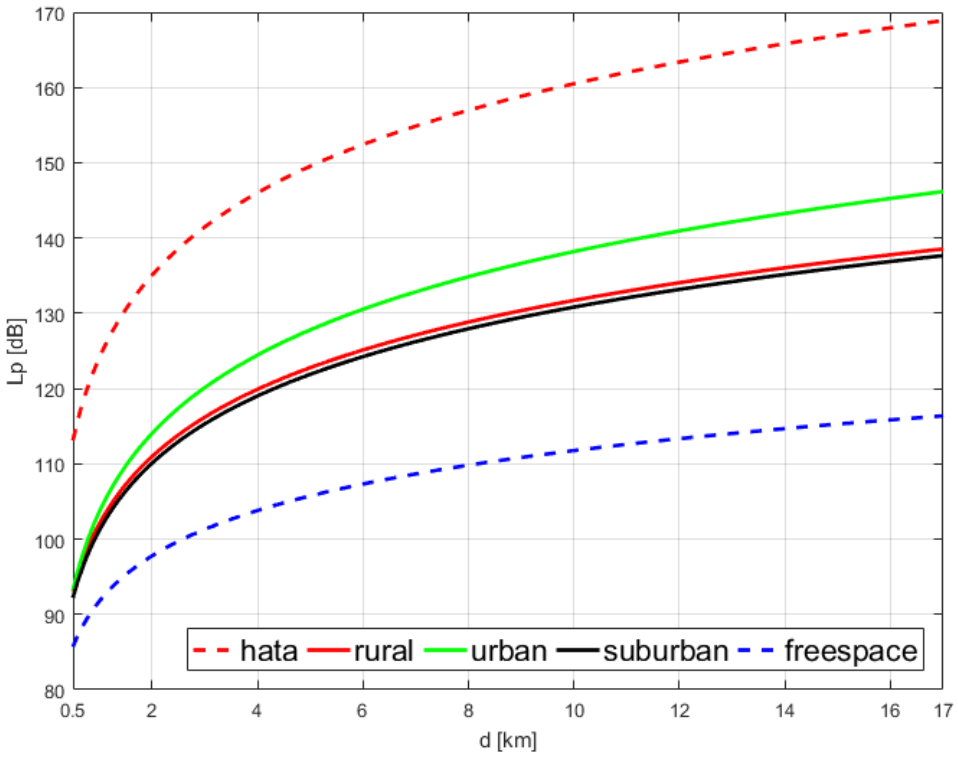

Figure 4.13 - Path Losses for Urban, Suburban and Rural Environments.

When comparing the Hata model with for urban scenarios with the large cities' correction factor against the urban HSR scenario, the immediate drawn conclusion is that the use of a standard path loss model instead of an HSR one can lead to differences in path loss higher than 20 dB. With system margins in the order of 10 dB, this is an exceptionally high value that most certainly impacts on the development of any telecommunications system.

Apart from the previous result, one can still see that the difference between Rural and Suburban scenarios is very small, leading to differences of, at most, 1 dB between each other, whereas the Urban

scenario can incur losses up to 7 dB higher than the rural case. As mentioned in [HZAD14], this often occurs in most HSR models, with some of them not even distinguishing between these 2 environments since, as seen with these results, the differences are negligible. By looking at the expression of the Δ_1 coefficient for both of these environments it is very evident that these deviate by a factor of around 0.69log(h_{BS}), which is rarely noticeable due to the heights of the antennas used in these environments, often ranging from 20 to 30 m, up to 50 m, as seen in Table 4.5.

Table 4.5 - Differences in Δ_1 for Suburban and Rural Scenarios.

h_{BS} [m]	0.69log(h_{BS})
20	0.898
30	1.019
50	1.172

For these reasons, as well as a matter of consistency, the suburban scenario is not going to be analysed since its losses should be higher than the rural case and additionally no populational density indexes are given by the original authors, which makes the difference between the suburban and rural environments hard to quantify.

The remaining set of scenarios, consisting of Cuttings, Stations and Rivers, is presented in Figure 4.14. Even though the original paper does not specify this, these stations are most likely Large Stations, due to the dimensions of their awnings.

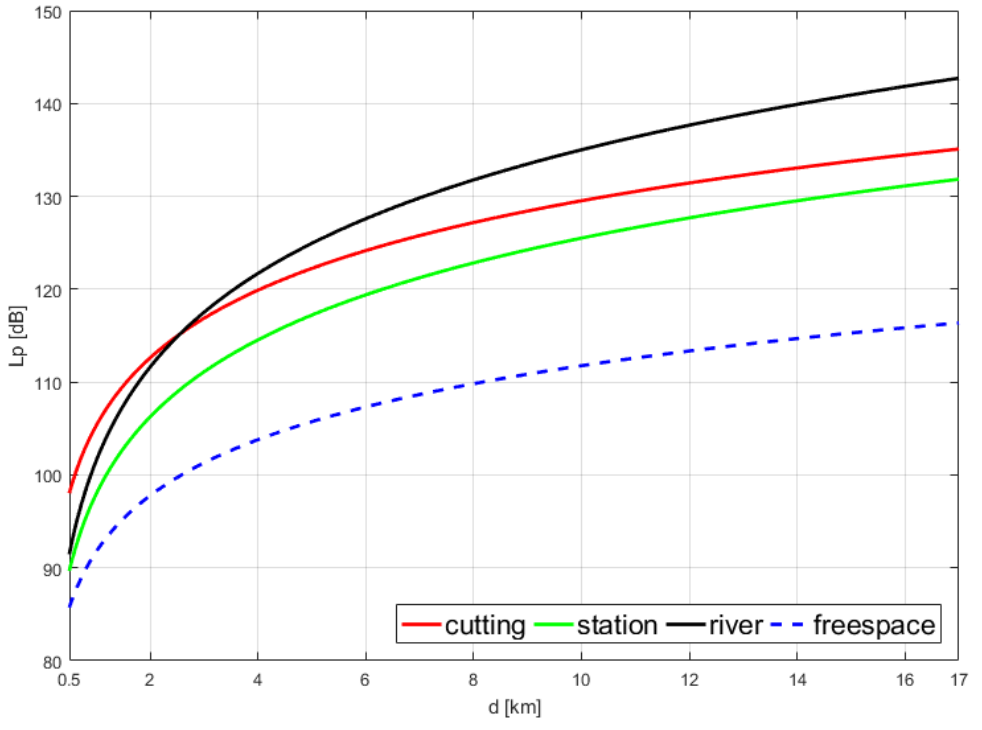

Figure 4.14 - Path Losses for Cuttings, Stations and Rivers with h_{BS}= 20 m.

An interesting result appears with the increase in the height of the BSs from 20 to 30 m. Figure 4.15 and Figure 4.16 show the propagation losses for the previous environments when the height of the BS is set at 30 m. The first set of scenarios, consisting of Urban, Suburban and Rural propagation are expressed in Figure 4.15, whereas the later set of scenarios is shown in Figure 4.16, containing the Cutting, Station and River propagation scenarios.

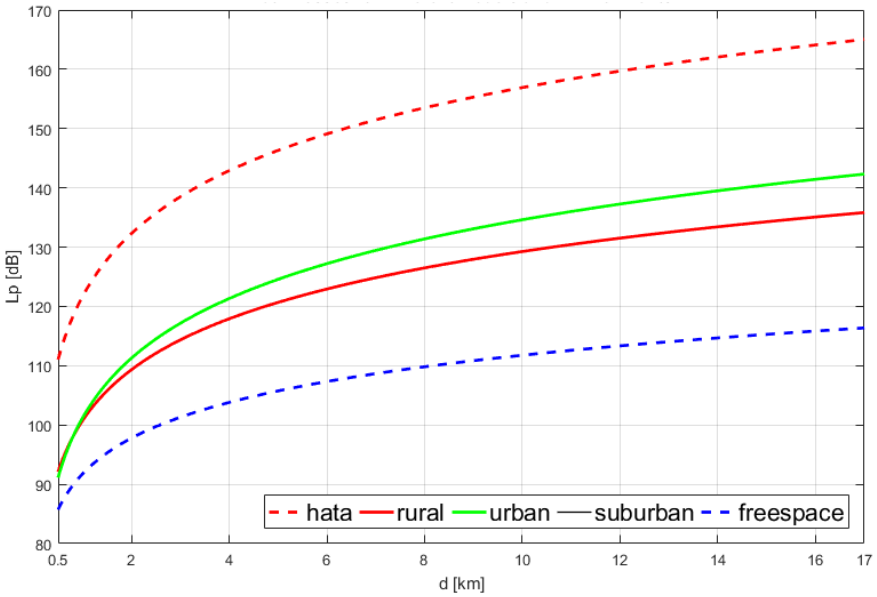

Figure 4.15 - Path Losses for the Rural, Urban and Suburban scenarios with h_{BS} = 30 m.

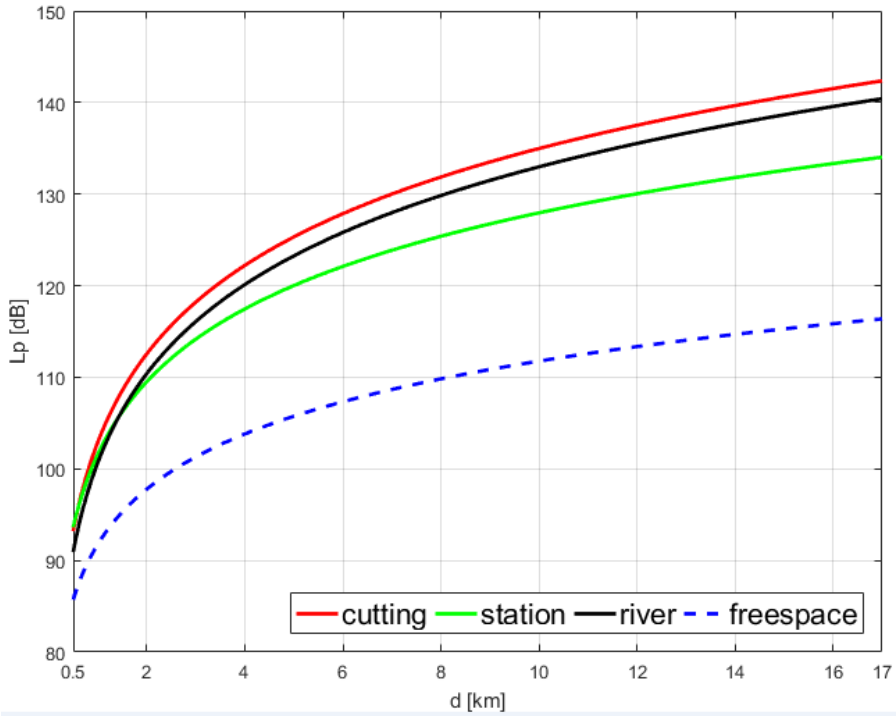

Figure 4.16 - Path Losses for Cuttings, Stations and Rivers with h_{BS} = 30 m.

Table 4.6 translates the behaviour of the previous figures into maximum communication distances. It also presents a relative analysis, stating whether the increase of the BS height is beneficial or not for the different analysed environments.

Table 4.6 - Maximum Communication Distances for Different Scenarios.

Scenario	d_{MAX} w/o bridge [km]			d_{MAX} w/ bridge [km]		
	h_{BS} = 20 m	h_{BS} = 30 m	Relative Change [%]	h_{BS} = 20 m	h_{BS} = 30 m	Relative Change [%]
Urban	6.7	8.4	25.4	3.7	4.3	11.6
River	8.2	9.4	14.6	4.5	5.0	11.1
Rural	10.3	12.6	22.3	5.1	6.2	21.6
Cutting	12.8	8.1	**- 36.7**	5.6	4.4	**- 21.4**
Station	17.4	14.4	**- 17.2**	8.4	6.7	**- 20.2**

With the raise in height of the BS, every scenario besides the Cuttings and Stations notices a decrease in propagation losses. One would expect, similarly to previous situations, that a higher height of the BS would result into a clearer LOS with less obstructions and therefore less propagation losses. The behaviours of these environments are explained by the expressions for Δ_1 in Stations and Δ_2 in Cuttings, which show that these parameters greatly depend on the height of the BS.

In what concerns stations, a higher BS height means that more components of the transmitted signals will be retained in the awnings on top of the station and other obstacles such as information panels, leading to signal scattering and consequent higher losses. In what concerns the Cutting, a possible explanation is that a higher number of multipath components that are reflected along its walls have trouble reaching the receiver antenna, often getting confined within the valley. The restructuration of the previous data results in Table 4.7, showing that the insertion of a metallic bridge in GSM-R scenarios yields degradations in communication distances ranging from, roughly, 45 to 56%.

Table 4.7 - Maximum Communication Distances for Different Scenarios.

Scenario	d_{MAX} (h_{BS} = 20 m)			d_{MAX} (h_{BS} = 30 m)		
	w/o bridge [km]	w/ bridge [km]	Relative Decrease [%]	w/o bridge [km]	w/ bridge [km]	Relative Decrease [%]
Urban	6.7	3.7	44.8	8.4	4.3	48.8
River	8.2	4.5	45.1	9.4	5.0	46.8
Rural	10.3	5.1	50.5	12.6	6.2	50.8
Cutting	12.8	5.6	56.3	8.1	4.4	45.7
Station	17.4	8.4	51.7	14.4	6.7	53.5

4.4 LTE-R Analysis

Unlike the previous system, the 4G LTE-R is capable of handling the required throughputs to transmit video. Even though the specifications for LTE-R are not totally defined yet, the 900 and the 2600 MHz bands are the most likely contenders for this system. Only the later band is analysed in this section since the results for the first band are very close to the ones expressed in the 925 MHz GSM-R section.

The models seen in Subsection 3.1.3 are suitable for the first band, however works verifying their validity for the later band have not been published yet. Nonetheless, the models are still used in this study and one must be aware of the error which is introduced by their use. The extended Hata model is valid for frequencies up to 2000 MHz unlike the standard, non-extended Okumura-Hata version, which act as a basis for the present models that is designed for frequencies up to 1500 MHz.

The analysis made in this section is not as linear as in Section 4.3, in the sense that the powers and throughputs depend on the modulations and coding rates that are used. Adaptative Coding and Modulating (ACM) is hard and expensive to implement in HSR scenarios due to the low coherence times that lead to channel instability, as previously explained. It is essential to know beforehand which options are available for each scenario in what concerns throughputs and available MCSs so that one knows the complete range of possibilities that can be used in the coder.

Lower level MCSs require additional bandwidth for a given data rate when compared against higher modulations, due to their lower spectral efficiency, but allow higher levels of path loss since the required signal to noise ratio for the modulator to work is also lower. Bearing this is mind, using the highest available MCS is not always advantageous.

Table 4.8 states the minimum signal to noise ratios needed in order to use different LTE modulation and coding schemes as seen in Figure 3.5 efficiently, that is, a value that enables an acceptable (near the saturation zone) throughput for QPSK, 16-QAM with a better performance than QPSK and 64-QAM with a throughput higher than 16-QAM's.

Table 4.8 - LTE's MCS' Signal to Noise Ratios.

MCS	$\rho_{N,MIN}$[dB]
QPSK, ⅓	- 8.0
16-QAM, ½	5.5
64-QAM, ¾	13.0

With this in mind, one can define maximum communication distances in order to achieve specific throughputs for different train camera setups. Using (3.18) through (3.20), it is possible to assign a required level of signal to noise ratio for a specific throughput. (3.1) and (3.9) allow one to calculate maximum path loss for a given system margin. Table 4.9 shows these values, where no metallic bridge is being considered, that is, the margin in use is M_{S1}.

Table 4.9 - Maximum Allowed Path Losses for LTE Configurations.

Throughput Requirement [Mbps]	MCS	ρ_N [dB]	$L_{p,MAX}$[dB]
4	QPSK, ⅓	- 4.7	131.8
6	QPSK, ⅓	- 2.9	130.0
10	16-QAM, ½	6.6	120.5
12	16-QAM, ½	7.6	119.5
20	16-QAM, ½	12.3	114.8
30	64-QAM, ¾	15.6	111.5

A quick comparison with the maximum path loss for the GSM-R case (132.1 dB, no bridge) shows that all LTE schemes are more demanding in what concerns propagation losses, a factor which is further aggravated by the increase of the work frequency from 925 to 2600 MHz and consequent higher attenuation.

The results expressed in the following tables contemplate a viaduct height of 10 m, whereas the heights of the BS' and the MT's antennas are fixed at 30 m and 5 m, respectively. This is due to the fact that the effect of these parameters has already been analysed in the previous section.

Table 4.10 shows the maximum communication distances, with and without the presence of a metallic bridge, in order to obtain a throughput of 4 Mbps. The relative decrease in distance due to the insertion of the bridge is also stated in these results.

Table 4.10 - LTE-R's Maximum Communication Distances for Different Environments @4 Mpbs.

Environment	d_{MAX}		Relative Decrease [%]
	w/o bridge [km]	w/ bridge [km]	
Viaduct	4.56	2.33	48.9
Urban	3.66	1.83	50.0
River	3.98	1.94	51.2
Rural	4.76	2.11	55.7
Cutting	3.42	1.66	51.5
Station	5.04	2.08	58.7

Table 4.11 presents results for the highest rate (20 Mbps) where the model is still accurate, that is, the

distances involved start to drop below the reference distance of the model (500 m) in cases where a metallic bridge is present.

Table 4.11 - LTE-R's Maximum Communication Distances for Different Environments @20 Mpbs.

Environment	d_{MAX}		Relative Decrease [%]
	w/o bridge [km]	w/ bridge [km]	
Viaduct	1.49	0.77	48.3
Urban	1.14	**< 0.50**	–
River	1.19	0.58	51.2
Rural	1.21	0.52	57.0
Cutting	1.01	**< 0.50**	–
Station	1.14	**< 0.50**	–

The results for the remainder throughputs can be seen in Table B.1 through Table B.3, which contain results for the 6, 10 and 12 and Mbps rates. The results for the highest rate that is analysed, of 30 Mbps, are expressed in Table 4.12. One can consider this throughput is only attainable for a scenario with no metallic obstructions.

Table 4.12 - LTE-R's Maximum Communication Distances for Different Environments @30 Mpbs.

Environment	d_{MAX} w/o bridge [km]
Viaduct	1.20
Urban	0.90
River	0.94
Rural	0.92
Cutting	0.80
Station	0.85

With the shown data, it can be concluded that the presence of a metallic bridge in LTE-R scenarios yields reductions from roughly 49 to 57% in what concerns maximum communication distances, which are in the same order of the ones observed in the GSM-R scenarios, albeit a bit more severe.

As expected the distances reduce dramatically (reductions from around 67 to 77%) when enhancing the

throughput from 4 Mbps to the 20 Mbps rate for different scenarios. Distances for the 30 Mbps scenario with the presence of a metallic bridge are not shown since these would result in values lower than the model's reference distance of 500 m, rendering it inaccurate. The same happens, to some extent, to the 20 Mbps rates metallic bridge scenario. Actual measurements may show these data rates are unattainable given the current conditions.

Another interesting case that one can analyse is the effect on system throughput when the link between the Tx and the Rx is temporarily obstructed by the metallic bridge. Table 4.13 states different possible cases, where the system is operating with a certain signal to noise ratio, which suddenly drops due to the presence of the obstruction and the consequences on the resulting throughputs. Three examples are analysed, one where the signal to noise ratio decrease is still high enough to maintain the same MCS, and two that force the modulation level to drop, one from 64-QAM to 16-QAM and another from 16-QAM to QPSK.

Table 4.13 - Effect of the Presence of a Metallic Bridge in Throughput Levels for LTE-R.

ρ_N	MCS in use	Normal throughput [Mbps]	ρ_N after drop	Resulting MCS	Throughput after drop [Mbps]	Throughput decrease [%]
40.0	64-QAM, ¾	59.8	29.9	64-QAM, ¾	58.2	**2.7**
20.0	64-QAM, ¾	44.8	9.9	16-QAM, ½	16.3	63.6
10.0	16-QAM, ½	16.5	- 1.1	QPSK, ⅓	7.4	55.2

Looking at the results stated in Table 4.13, one can see that the effect of the signal to noise ratio decrease in what concerns throughput is intimately related to what happens to the MCS. In the first case the throughput is barely affected since the system is able to maintain the same modulation and coding rate as before. On the remaining cases, however, drops in throughputs range from 55.2% to 63.6% since the system is forced to lower, less efficient modulation levels.

4.5 BBRS Analysis

As previously stated, the requirements for the BBRS system and the LTE-R one are the same, which are specified in Section 4.1. The analysis of the achievable throughputs follows the same bandwidth considerations as LTE's, that is, only 20 MHz channels are considered, with the full band being used by the telecommunications system.

In order to know beforehand which levels of signal to noise ratios one is aiming at, an analysis on the different 802.1n's modulation and coding schemes is necessary.

Using (3.22) through (3.26) one is able to convert different levels of system throughputs as a function of required signal to noise ratios and consequently, through link budget, into maximum allowed path losses. Similarly to the process depicted in Table 4.9, the maximum path loss values for a scenario without any metallic bridge are present in Table 4.14.

Table 4.14 - Maximum Allowed Path Losses for BBRS Configurations.

Throughput Requirement [Mbps]	MCS	ρ_N[dB]	$L_{p,MAX}$[dB]
4	QPSK, ½	4.6	118.5
6	QPSK, ½	7.0	116.1
10	QPSK, ½	11.1	112.0
12	16-QAM, ½	12.7	110.4
20	16-QAM, ½	17.0	106.1
30	64-QAM, ⅔	22.0	101.1
40	64-QAM, ⅔	25.8	97.3
54	64-QAM, ¾	40.0	83.1

Comparing the values of path loss shown in Table 4.14 against the ones present in Table 4.9 shows that, regardless of the modulation in use, WiFi is more demanding than LTE in what concerns the required signal to noise ratios. Even though the maximum path loss values are lower than the ones allowed by LTE, the distances between base stations in BBRS are also smaller in order to account for this requirement.

Before moving on to the calculation of the corresponding maximum transmission distances for each case, it is necessary to state that the used model for this system (Winner II) considers a rural LOS scenario, however, in this work, the model is used for any scenario with this work frequency, as stated in model implementation. This is due to the fact that the distances in use are so low (around 300 m) that the impact of the surrounding terrain is not going be noticeable in what concerns propagation losses.

The resulting cases are, again due to the low distances in play, going to be LOS scenarios and, due to the same arguments, free space propagation would also be an acceptable approximation. The most important parameters here are the high frequencies in use (contemplated by the model) and the fact that the carriages are moving, which is the main focus of the model.

Figure 4.17 shows path loss for BBRS when both the MT's and the BS' antennas are located at a height of 5 m. This BS height is different from the previous ones since, in a BBRS setting, the APs are to be located alongside the railway, at approximately the same height as the receivers. One can clearly see the breakpoint distance, which is located at 1968 m and given by (3.12).

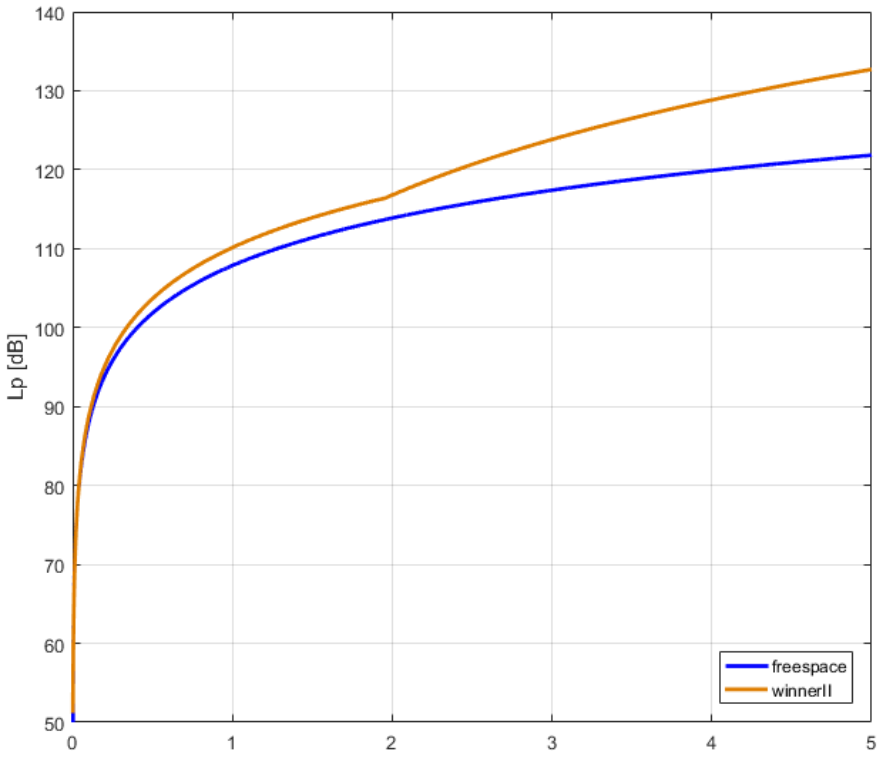

Figure 4.17 - BBRS path loss for BS and MT heights of 5 m.

With this in mind the maximum communication distances for the different throughputs are shown Table 4.15.

Table 4.15 - BBRS' Maximum Communication Distances for Different Throughputs.

Throughput [Mbps]	d_{MAX}		Relative Decrease [%]
	w/o bridge [m]	w/ bridge [m]	
4	2207.3	333.7	84.9
6	1893.7	261.1	86.2
10	1220.7	168.3	86.2
12	1028.5	141.8	86.2
20	648.9	89.5	86.2
30	379.9	52.4	86.2
40	252.9	34.1	86.5
54	55.3	7.6	86.3

Placing the APs 300 m apart from each other guarantees a 4 Mbps rate, even with a metallic bridge obstruction between the Tx and the Rx, however, for higher rates, the system notices a severe

degradation. This performance decrease is somewhat constant through all of the rates and yields a communication distance decrease around 86% in order to maintain the same throughput. One can also see that the distance of 300 m is conservative when providing rates of 20 Mbps, however this study does not account for interference providing from other nearby communication systems. The maximum rate of 54 Mbps for a single data stream is especially difficult to provide, needing distances of 55.3 m between the AP and the train in a scenario without a metallic bridge and becoming impossible to provide should the bridge exist.

Finally, similarly to the process done for LTE-R, one still has to analyse examples of the effect of the inclusion of the obstruction in what concerns throughputs. Again, in Table 4.16, a case where the resulting MCS after the signal to noise ratio drop remains the same is presented, as well as examples for the remainder modulation scheme drops.

Table 4.16 - Effect of the Presence of a Metallic Bridge in Throughput Levels for LTE-R.

ρ_N	MCS in use	Normal throughput [Mbps]	ρ_N after drop	Resulting MCS	Throughput after drop [Mbps]	Throughput decrease [%]
48.0	64-QAM, ¾	54.0	29.5	64-QAM, ¾	46.0	14.8
42.0	64-QAM, ¾	52.4	23.5	64-QAM, ⅔	35.6	32.1
32.0	64-QAM, ¾	49.0	13.5	16-QAM, ½	13.4	72.7
25.0	64-QAM, ⅔	40.0	6.5	QPSK, ½	5.6	86.0
20.0	16-QAM, ¾	24.4	1.5	QPSK, ½	1.6	93.4

In contrast with the results shown for the LTE-R scenarios, where only two MCS changes caused severe degradation of the system, the examples referred in Table 4.16 show that, due to the high value of attenuation for the BBRS caused by the metallic bridge, performance is severely deteriorated for all cases. Even when operating under the same MCS, one can see decreases of around 14.8% and in more severe cases, such as when dealing with lower signal to noise ratios, one can see decreases in the order of 93.4%, which render the system unusable. These results are purely academical and assume the hardware in use implements ACM instantly and without using any additional resources. Also, no system margins are considered here since one considers extreme situations in order to see the effect of changes in MCSs in what concerns to throughputs. Some of the stated signal to noise ratios may even be unattainable in normal conditions.

Chapter 5

Conclusions

This chapter provides a summary of the work developed in all previous chapters and details the work's most important aspects to retain. It ends with suggestions for future works, in order to enhance certain details of the developed thesis, as well as explore new ones which were not approached.

This work addresses a specific problem, which has to do with the presence of an obstruction in the form of a metallic bridge between the transmitter and the receiver of a telecommunications system. Its objective was to develop and implement a model capable of analysing the problem in the form of maximum allowed communication distances and obtainable throughputs. The model itself was developed with EM simulation via CST software and all the numerical analysis and propagation model implementation was done with MATLAB.

The first section of this work gives an overview of the current needs in what concerns telecommunications systems in railway scenarios, as well as their evolution along the years, stating the different systems that are analysed in the work. The motivation of the current work is also stated in this session, which has to deal with the high levels of attenuation present when dealing with these types of environments.

In what concerns the second chapter, it states the fundamental aspects required in order to understand the developed work. It starts with an introduction to the different approached telecommunication systems, stating their network interfaces and architectures and gives ideas of the special needs one has to deal with when operating in railway scenarios. Initial scenario definitions are stated here and an overview regarding the used simulator is given. The chapter ends with the current state of the art, where different works in the railway field are enunciated.

The third chapter contains the core ideas of this thesis. It begins with an overview of the framework that is followed along this thesis and states the main modules of the model, as well as the parameters that are obtained. After this introduction, the development of the adopted model begins. Basic notions regarding link budget are given and the main propagation models that are studied and implemented are presented. These involve a specific model developed for viaducts in the 900 MHz band, a more general model, by the same authors, for other railway scenarios that are typically encountered in the same environments and the Winner II model section that approaches moving networks, a model specially chosen to deal with the highest frequency cases (BBRS).

Throughput models are developed in order to estimate one of the performance parameters of this thesis for LTE and WiFi, whereas CST is used to model the specific metallic bridge problem and yield the second needed parameter in order to analyse communication distances, the penetration loss of a metallic bridge. The MCSs that are analysed in the results section are stated here, as well as a statement regarding the signal to noise ratio boundaries for each MCS.

The CST section explains the modelling of the problem, stating parameters such as probe locations, bridge and train dimensions, plane symmetries, approaches the used solvers, problems encountered when using the software and respective simplifications and states the general strategy in order to obtain the penetration losses of the metallic bridge. The most important simplification adopted in this section has to deal with the fact that computational capability is limited and therefore one has to make the model as symmetric as possible in order to reduce the number of cells (and therefore wavelengths) which need to be modelled and solved.

The behaviour of the developed MATLAB scripts is also covered in this section, where the main modules and propagation models of the work are approached. The section ends with a model assessment, which is crucial in order to test the model and make sure one's assumptions are correct.

The developed work is therefore separated into two main modules. The first is a block of code that enables the user to input the scenario's characteristics, such as the location of the antennas and the frequency of work and extract propagation losses as a function of distance, whereas the second one is a software model of the problem with the objective of providing the losses due to the metallic bridge obstruction in a railway scenario. In conjunction, these allow one to translate the bridge into an additional propagation loss, which is combined with the standard path loss to analyse the problem in terms of obtainable throughputs.

The fourth chapter shows the different scenarios that are analysed and states the link budget parameters that are used, based on real projects. The results obtained from the EM simulator are presented here, where one finds that the penetration losses in a metallic bridge for the GSM-R and LTE-R cases can be modelled under a truncated normal distribution with correlation factors between the simulations and the approximations around 0.99. A metric of this attenuation, which covers the maximum attenuation for 90% of the possible azimuth angles along the metallic bridge is chosen. The procedure that culminates in this parameter is explained, as well as the assumptions which are made. The previously stated parameter corresponds to 8.75 dB for the GSM-R system, 10.13 dB for LTE-E one and 18.55 dB for the last approached system, BBRS.

The first set of propagation results has to deal with the 925 MHz frequency, where one can see that the presence of a metallic bridge in viaduct environments yields communication distance decreases from 18.5% to 43.8%, depending on the viaduct configuration. Still working in the same band, another set of scenarios, consisting of Urban, River, Rural, Cutting and Stations, is approached, where one can see the impact of changing the heights of the BS's antenna and, once more, the performance decrease caused by the presence of the metallic obstruction. It is seen that Cuttings and Stations do not behave as expected compared to other scenarios, that is, an increase in this parameter from 20 to 30 m does not yield a better system performance, but instead diminishes the obtainable communication distances from roughly 17% to 37%. The presence of the metallic bridge has a rougher impact, decreasing the maximum allowed distances from around 45% to 56%, depending on the environment at hand. One concludes the commonly used Hata model results in overestimations in what concerns path loss in railway scenarios, a factor which is also stated in [HZAD14] and that there exists room for improvement when planning the location of BSs in HSRs.

Unlike the GSM-R scenarios, the 2600 MHz LTE-R results contain an approach regarding MCS, which affect the obtainable throughputs, the main focus in both LTE-R and BBRS results. Minimum signal to noise ratios for rates of 4, 6, 10, 12, 20 and 30 Mbps are calculated based on the previously defined throughput models, as well as maximum allowed path loss for each of the given rates. It is suspected that the 30 Mbps distance is only reachable in a scenario where a metallic bridge is not present, however, due to model limitations, however, actual signal measurements can lead to a different

conclusion. It is seen that raising the required throughput from 4 to 20 Mbps comes with reductions from 67% to 77% in what concerns communication distances and that the introduction of a metallic bridge in this frequency deteriorates the achievable communication distances from roughly 49% to 57%, which are in the same order of the ones observed in the previous case. Finally, it is shown that sudden drops in signal to noise ratios can have quite different effects in the resulting throughputs. On the one hand the reduced signal to noise ratio can allow the modulator to work with the same MCS, resulting in a low performance decrease, of around 2.7% for the analysed case. On the other hand, should the drop be high enough to force the system to work in a lower MCS, one can see performance degradations of around 55% to 64%.

Finally, the 5900 MHz BBRS scenario is studied. The same statements regarding system signal to noise ratios are made, however different throughput levels are defined. This is due to the fact that the used model (Winner II) does not have a reference distance limitation and the APs in BBRS are placed at low distances from each other, resulting in less demanding cases in what concerns path loss. It is seen that this scenario contains the cases where the metallic bridge obstruction has the highest impact, with decreases around 86% for all analysed throughputs. This study shows that the theoretical maximum rate of 54 Mbps is very hard to provide, even without a metallic bridge obstruction, and becomes impossible should it be present since this case would result in distances between the train and the APs of around 8 m. It can be concluded that the commonly used distance of 300 m for the BBRS' AP placement in order to guarantee rates below 20 Mbps is somewhat conservative, however one has to remember this study does not account for interference providing from other communication systems. Similarly to LTE-R, throughput performance is analysed as a function of decreases in signal to noise ratio caused by the introduction of the metallic bridge. Performance deterioration is more severe in this system due to the high frequencies in play and consequent higher attenuation caused by the metallic bridge. Unlike the LTE-R examples, all situations that are analysed here see a significant performance drop, ranging from around 14.8% where the same MCS is available after the inclusion of the obstruction, to a high 93.4% decrease in a situation where the used MCS is forced to a less complex one.

In what concerns future work, several aspects can be explored. The first has to deal with the simplifications made during the CST modelling of the metallic bridge. Due to computational and time constraints, the studied case contemplates a totally symmetric bridge, which is not the real case. Of course the objective of this work is not to study the penetration losses of a specific bridge, but instead to provide a general model that can be followed for other scenarios, however, this can be useful in order to model different types of bridges and see if their shapes and symmetries have a significative impact on the obtained results. One can argue that an important point was missed with this work, which is the impact that a two-way railway and the presence of another train have on telecommunications systems, which is a point that could be enhanced.

Signal to noise requirements can greatly vary between different providers and therefore a more specifically target analysis towards BBRS could be studied, with data prevenient from actual hardware measurements. The same can be said for LTE, however a factor which would probably produce better

results is the use of another model, specifically developed for the 2600 MHz band. Unfortunately, these types of models could not be found, and the used model was one designed for the 900 MHz band, which may render the data inaccurate.

Instead of CST EM modelling one could use an analytical model in order to solve the problem recurring to reflection factors. This is certainly a more complex way of approaching the current problem, however it could yield interesting results.

Finally, the most interesting and originally planned idea revolves around the use of FSSs in order to analyse the problem, as stated previously in this work. The limitation here is that the currently existing and publicly available FSS models are designed to work with very small structures compared to metallic bridges such as arrays of dipoles or resonators. Even though some of the work developed in these models can be used, such as the general behaviour of metallic structures with frequency, using these types of models will certainly provide meaningless results.

Annex A

Okumura-Hata Model

This annex contains the definition of the Okumura-Hata model with the relevant correction factors for this work. The complete model can be seen in [Corr15].

The Hata model is among the most used models which predict path loss in exterior environments. It is valid for the following parameters:

- $f_c \in$ [150, 1500] MHz;
- $\underline{d} \in$ [1, 20] km;
- $h_{BS} \in$ [30, 200] m;
- $h_{MS} \in$ [1, 10] m.

Under these conditions, the median value of the path loss is given by:

$$L_{p[\mathrm{dB}]} = 69.55 + 26.16\log\left(f_{c[\mathrm{MHz}]}\right) - 13.82\log\left(h_{BS[\mathrm{m}]}\right) + \left[44.90 - 6.55\log\left(h_{BS[\mathrm{m}]}\right)\right]\log\left(d_{[\mathrm{km}]}\right) - H_{mu[\mathrm{dB}]} - \sum c_f \quad \text{(A.1)}$$

with:

$$H_{mu[\mathrm{dB}]} = \begin{cases} \left[1.10\log\left(f_{[\mathrm{MHz}]}\right) - 0.70\right]h_{MS[\mathrm{m}]} - \left[1.56\log\left(f_{[\mathrm{MHz}]}\right) - 0.80\right], & \text{small city} \\ 8.29\log^2\left(1.54h_{MS[\mathrm{m}]}\right) - 1.10, & f \leq 200 \text{ MHz} \\ 3.20\log^2\left(11.75h_{MS[\mathrm{m}]}\right) - 4.97, & f \geq 400\ MHz, \text{large city} \end{cases} \quad \text{(A.2)}$$

$$c_{f[\mathrm{dB}]} = \begin{cases} 4.78\log^2\left(f_{c[\mathrm{MHz}]}\right) - 18.33\log\left(f_{[\mathrm{MHz}]}\right) + 40.9, & \text{Rural} \\ 2.00\log^2\left(\frac{f_{c[\mathrm{MHz}]}}{28}\right), & \text{Suburban} \end{cases} \quad \text{(A.3)}$$

Standard deviations for urban, σ_u, and suburban, σ_s, environments are given by:

$$\sigma_{u[\mathrm{dB}]} = 0.70\log^2\left(f_{c[\mathrm{MHz}]}\right) - 2.50\log\left(f_{c[\mathrm{MHz}]}\right) + 11.10 \quad \text{(A.4)}$$

$$\sigma_{s[\mathrm{dB}]} = 0.98\log^2\left(f_{c[\mathrm{MHz}]}\right) - 3.40\log\left(f_{c[\mathrm{MHz}]}\right) + 11.88 \quad \text{(A.5)}$$

Annex B

LTE-R Throughputs

This annex contains tables with the values for LTE-R throughputs which were not presented in section 4.4.

Figure B.1 expresses the path loss as a function of distance when analysing viaducts with a height of 10 m, 30 m high BS antennas and MT antennas located at a height of 5 m.

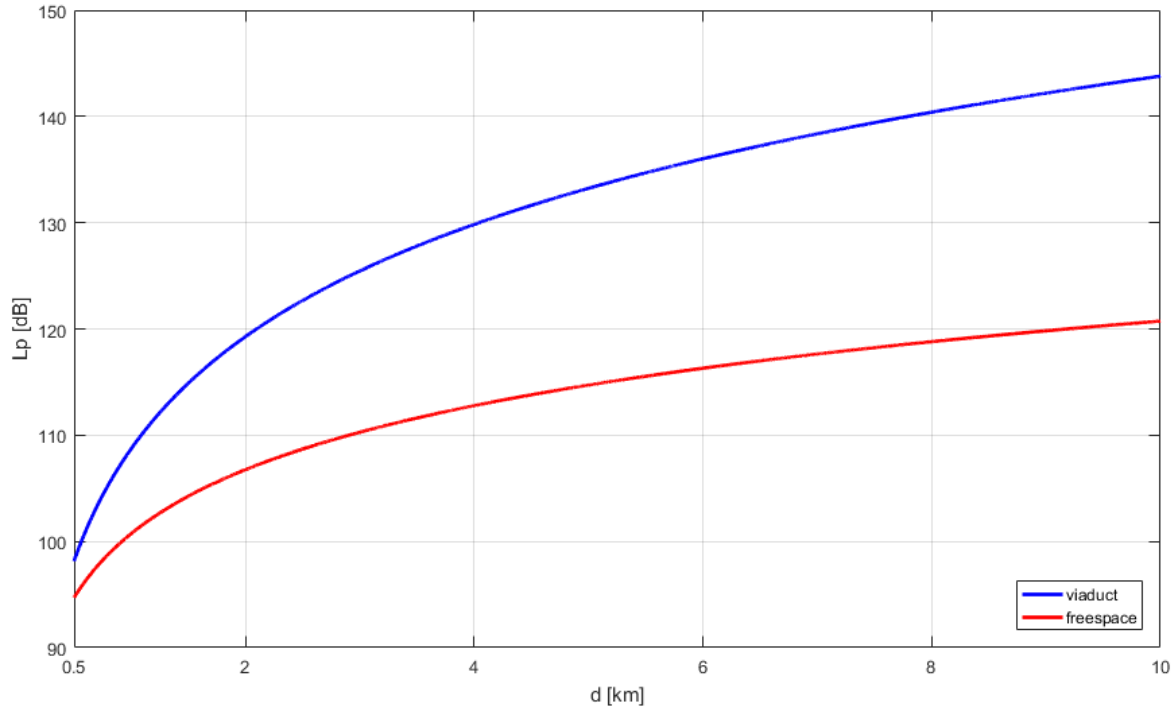

Figure B.1. Viaduct Path Loss at 2600 MHz for Viaduct Heights of 10 m, 30 m high BS, 5 m high MT.

The same parameters are used in Figure B.2, this time for urban and rural scenarios.

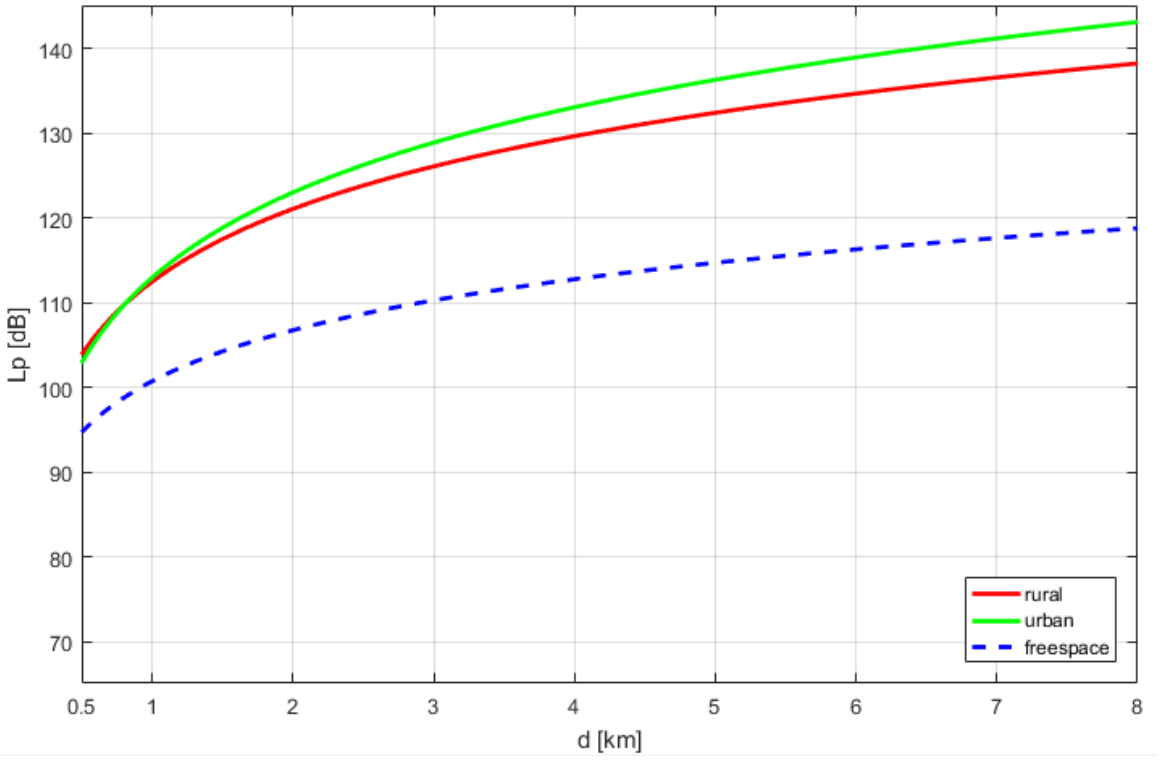

Figure B.2. Path Loss at 2600 MHz for Rural and Urban Scenarios.

Finally, Figure B.3 shows the path loss for the last set of scenarios, consisting of cuttings, rivers and stations.

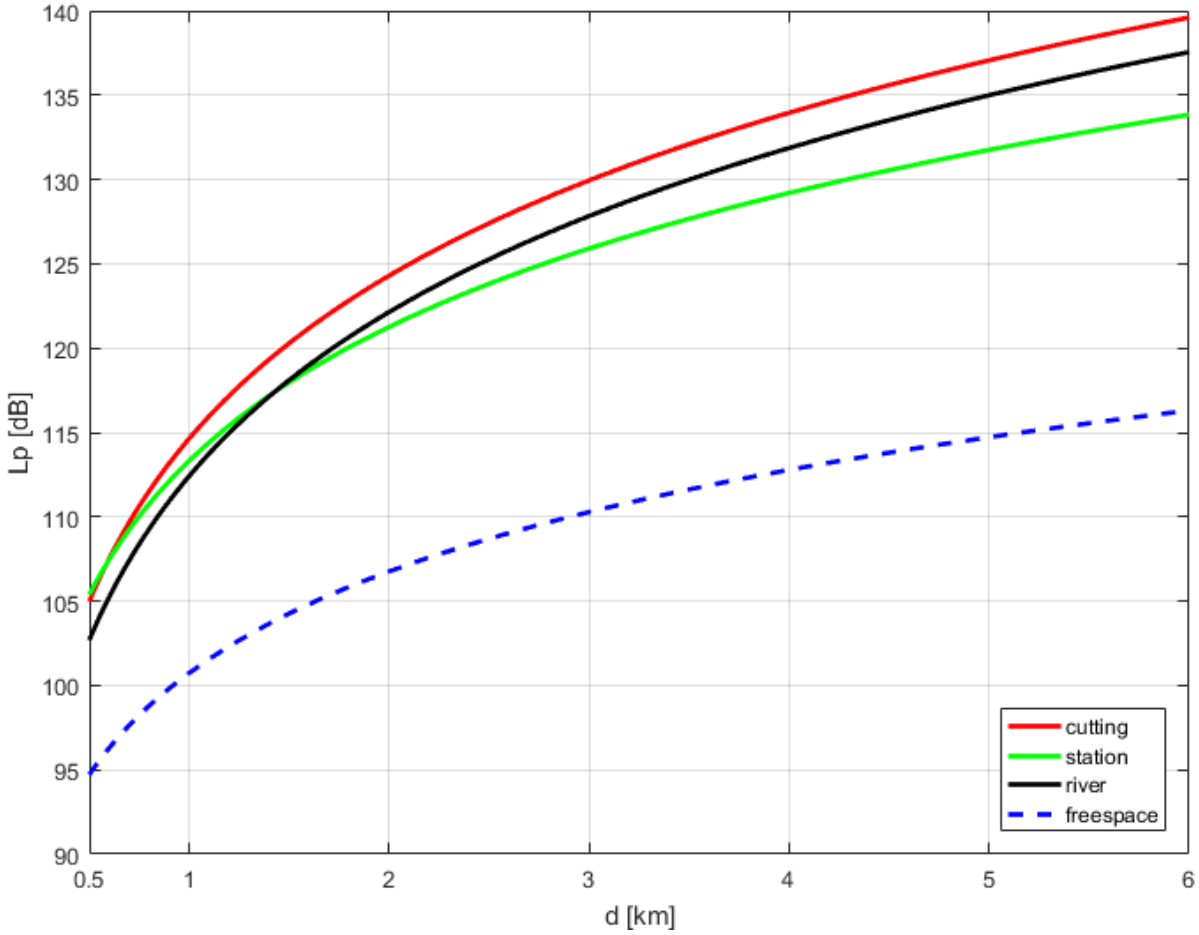

Figure B.3. Path loss at 2600 MHz for Cuttings, Rivers and Stations.

Table B.1; Table B.2 and Table B.3 show the results for the 6, 10 and 12 Mbps throughputs, respectively.

Table B.1.LTE-R's Maximum Communication Distances for Different Environments @6 Mpbs.

Environment	d_{MAX}		Relative Decrease [%]
	w/o bridge [km]	w/ bridge [km]	
Viaduct	4.05	1.21	70.1
Urban	3.24	0.91	71.9
River	3.49	0.95	72.8
Rural	4.13	0.93	77.5
Cutting	3.02	0.81	73.1
Station	4.28	0.86	73.2

Table B.2.LTE-R's Maximum Communication Distances for Different Environments @10 Mpbs

Environment	d_{MAX}		Relative Decrease [%]
	w/o bridge [km]	w/ bridge [km]	
Viaduct	2.17	1.12	48.4
Urban	1.68	0.84	50.0
River	1.78	0.87	51.1
Rural	1.91	0.85	55.5
Cutting	1.52	0.74	51.3
Station	1.87	0.78	58.3

Table B.3.LTE-R's Maximum Communication Distances for Different Environments @12 Mpbs

Environment	d_{MAX}		Relative Decrease [%]
	w/o bridge [km]	w/ bridge [km]	
Viaduct	2.03	1.05	48.3
Urban	1.57	0.78	50.3
River	1.66	0.81	51.2
Rural	1.76	0.78	55.7
Cutting	1.42	0.69	51.4
Station	1.71	0.71	58.5

.

References

[3GPP11] 3GPP – Technical Specification Group – RAN WG4, Summary of alignment and impairments results for eDL-MIMO demodulation requirements, Report R4-112713, May 2011 (http://3gpp.org).

[3GPP17] 3GPP – The Evolved Packet Core, http://www.3gpp.org/technologies/keywords-acronyms/100-the-evolved-packet-core, Dec. 2017.

[AHGZ12] B. Ai, R. He, Z. Zhong, K. Guan, B. Chen, P. Liu, Y. Li, "Radio Wave Propagation Scene Partitioning for High-Speed Rails", *International Journal of Antennas and Propagation*, Vol. 2012, 2012, pp. 1-7, (https://www.hindawi.com/journals/ijap/2012/815232/).

[Alco17] B. Alcobia, *LTE radio network deployment design in urban environments under different traffic scenarios*, M. Sc. Thesis, Instituto Superior Técnico, Lisbon, Portugal, May 2017.

[Alme13] D. Almeida, *Inter-Cell Interference Impact on LTE Performance in Urban Scenarios*, M. Sc. Thesis, Instituto Superior Técnico, Lisbon, Portugal, Oct. 2013.

[Bani14] A. Baniya, *Assessment of Frequency Selective Surface for Improving Indoor Cellular Coverage*, M. Sc. Thesis, Tampere University of Technology, Pirkanmaa, Finland, 2014.

[BJHS03] B. Bangerter, E. Jacobsen, M. Ho, A. Stephens, A. Maltsev, A. Rubtsov, A. Sadri, "High-Throughput Wireless LAN Air Interface", *Intel Technology Journal,* Vol. 7, Issue 3, Aug. 2003, pp. 47-57.

[Chen70] C. Chen, "Scattering by a two-dimensional periodic array of conducting plates", *IEEE Transactions on Antennas and Propagation*, Vol. 18, Issue 5, Sep. 1970, pp. 660-665, (https://ieeexplore.ieee.org/document/1139760/).

[ChSh14] R. Chisab, C. Shukla, "Performance Evaluation of 4G-LTE-SCFDMA Scheme under SUI and ITU Channel Models", *International Journal of Engineering & Technology IJET-IJENS*, Vol. 14, no. 01, Feb. 2014, pp. 58-69, (https://www.researchgate.net/publication/262374272_Performance_Evaluation_of_4G-LTE-SCFDMA_Scheme_under_SUI_and_ITU_Channel_Models)

[Cisc10] CISCO, *Cisco 1140 Series Access Point Deployment Guide*, Cisco Product Support, 2010, (https://www.cisco.com/c/en/us/td/docs/wireless/technology/1140/deployment/guide/1140dep.html).

[Cons17] Construction Intelligence Center – Russia leads investment in road and railway construction in Europe, https://www.construction-ic.com/pressrelease/russia-leads-investment-in-road-and-railway-construction-in-europe-5721072, Jan. 2017.

[Corr15] L.M. Correia, *Mobile Communications Systems – Lecture Notes*, Instituto Superior Técnico, University of Lisbon, Lisbon, Portugal, 2015.

[Cort17] D. Cortez, "(Some) Railway Mobile Communications", *25th Lectures on Mobile Communications* (in Portuguese), Instituto Superior Técnico, Portugal, Jun. 2017, (http://grow.tecnico.ulisboa.pt/wp-content/uploads/2017/07/PalestrasComMov_2017_THALES.pdf)

[Csts18] CST Help, *CST Studio Suite – High Frequency Simulation,* 2018.

[CWCF08] M. Chen, S. Wang, R. Chen, Z. Fan, "Electromagnetic Analysis of Electrically large and Finite periodic Frequency Selective Surfaces", *2008 Asia-Pacific Microwave Conference*, Macau, China, Dec. 2014, pp. 1-4, (https://ieeexplore.ieee.org/document/4958590/).

[DuGI99] J. Dunlop, D. Girma, J. Irvine, *Digital Mobile Communications and the TETRA System*, John Wiley & Sons, Chichester, West Sussex, England, 1999.

[ETSI11] ETSI TR 136 942 – LTE; Evolved Universal Terrestrial Radio Access (E-UTRA); Radio Frequency (RF) system scenarios, Technical Report V10.2.0, May 2011.

[Fell13] Flickr Photo – Former Santa Fe Railroad Through Truss Bridge over Trinity River on Santa Fe Trestle Trail, Dallas, Texas 1306141015BW, photography by Patrick Feller, https://www.flickr.com/photos/nakrnsm/9263674064, Apr. 2018.

[Feng13] D. Feng, "Design of a New Active Frequency Selective Surface (FSS)", *2013 IEEE 5th International Symposium*, Chengdu, China, 2013, pp. 601-603, (http://ieeexplore.ieee.org/abstract/document/6689910/)

[FFOR01] M. Franchitto, R. Faez, A. Orlando, M. Rezende, I. Martin, "Electromagnetic Behaviour of Radar Absorbing Materials Based on Conducting Polymers", *Proceedings of the 2001 SBMO/IEEE MTT-S International Microwave and Optoelectronics Conference*, Vol. 1, Aug. 2001, pp. 137-140, (https://ieeexplore.ieee.org/document/1008736/).

[Gast12] M. Gast, *802.11n: A Survival Guide*, O'Reilly Media, Sonoma County, California, United States, 2012.

[Gold05] A. Goldsmith, *Wireless Communications*, Cambridge University Press, Cambridge, UK, 2005.

[Gsmr17] Gsmr – GSM-R Technology at a Glance, http://gsmr-info.com/gsm-r_history.html, Oct. 2017.

[GZAK14] K. Guan, Z. Zhong, B. Ai, T. Kürner, "Empirical Models for Extra Propagation Loss of Train Stations on High-Speed Railway", *IEEE Transactions on Antennas and Propagation*, Vol. 62, no. 3, Mar. 2014, pp. 1395-1408.

[HaRM13] T. Halonen, J. Romero, and J. Melero, *GSM, GPRS and EDGE Performance: Evolution Towards 3G/UMTS*, John Wiley & Sons, Chichester, West Sussex, England, 2013.

[Hart04] L. Harte, *Introduction to Private Land Mobile Radio: Dispatch, LTR, APCO, MPT1327, iDEN, and TETRA*, Althos Publishing, United States, 2004.

[HAWG16] R. He, B. Ai, G. Wang, K. Guan, Z. Zhong, A. Molisch, C. Briso-Rodriguez, C. Oestges, "High-Speed Railway Communications: From GSM-R to LTE-R", *IEEE Vehicular Technology Magazine*, vol. 11, no. 3, Sep. 2016, pp. 49-58, (http://ieeexplore.ieee.org/stamp/stamp.jsp?arnumber=7553613)

[HoTo11] H. Holma, A. Toskala, *LTE for UMTS: Evolution to LTE-Advanced*, Wiley, Chichester, UK, 2011.

[HZAD11] R. He, Z. Zhong, B. Ai, J. Ding, "An Empirical Path Loss Model and Fading Analysis for High-Speed Railway Viaduct Scenarios", *IEEE Antennas and Wireless Propagation Letters*, vol. 10, 2011, pp. 808-812, (http://ieeexplore.ieee.org/stamp/stamp.jsp?arnumber=5981374)

[HZAD14] R. He, Z. Zhong, B. Ai, J. Ding, W. Jiang, H. Zhang, X. Li, "A Standardized Path Loss Model for the GSM-Railway Based High-Speed Railway Communications Systems", *IEEE 79th Vehicular Technology Conference (VTC Spring)*, Seoul, South Korea, 2014, pp. 1-5, (http://ieeexplore.ieee.org/stamp/stamp.jsp?arnumber=7022797)

[HZAG15] R. He, Z. Zhong, B. Ai, K. Guan, "Reducing the Cost of High-Speed Railway Communications: From the Propagation Channel View", *IEEE Transactions on Intelligent Transportation Systems,* vol. 16, No. 4, 2015, pp. 2050-2060, (https://ieeexplore.ieee.org/document/7052340/)

[KiCh94] R. Kipp, C. Chan, "A Numerically Efficient Technique for the Method of Moments Solution for Planar Periodic Structures in Layered Media", *IEEE Transactions on Microwave Theory and Techniques,* vol. 42, No. 4, Apr. 1994, pp. 635-643, (https://ieeexplore.ieee.org/document/285070/)

[KMHZ07] P. Kyösty, J. Meinilä, L. Hentilä, X. Zhao, T. Jämsä, C. Schneider, M. Narandzić, M. Milojević, A. Hong, J. Ylitalo, V. Holappa, M. Alatossava, R. Bultitude, Y. Jong, T. Rautiainen, *Winner II Channel Models*, IST-4-027756 WINNER II, Deliverable D1.1.2 V1.2, Sep. 2007, (https://cept.org/files/8339/winner2%20-%20final%20report.pdf)

[LIEB11] D. Liebl, *WLAN 802.11n: From SISO to MIMO*, Application Note 04_2011-1MA179_10e, Rohde & Schwarz, 2011.

[LZBr11] J. Lu, G. Zhu, C. Briso-Rodriguez, "Fading Characteristics in the Railway Terrain Cuttings", *2011 IEEE 73rd Vehicular Technology Conference (VTC Spring)*, Yokohama, Japan, May 2011, pp. 1-5.

(https://ieeexplore.ieee.org/document/5956605)

[Mcsi18] Mcsindex – MCS Table, http://mcsindex.com/, Jul. 2018.

[MMOP14] MMOPL Mumbai – Video regarding Mumbai Metro Line 1:Ghatkopar-Versova route, Mar. 2004.

[Munk00] B. Munk, *Frequency Selective Surfaces: Theory and Design*, John Wiley & Sons, New

Jersey, United States, 2000.

[Nati18] National Instruments, Introduction to Wireless LAN Measurements From 802.11a to 802.11ac, 2018, (http://download.ni.com/evaluation/rf/Introduction_to_WLAN_Testing.pdf)

[PDBR15] A. Passarelli, A. Danisi, H. Bartosik, G. Rumolo, C. Zannini, "Using symmetries for wakefield calculation of driving and detuning impedances", CST European User Conference, Technische Universitat Darmstadt, Darmstadt, Germany, April 2015.

[Sams17] Samsung News – World's First LTE-Railway Service Goes Live on New High-speed Train Line in Korea, Supplied by Samsung and KT, https://news.samsung.com/us/lte-railway-service-korea-samsung-kt/, Dec. 2017.

[Scot98] C. Scott, "Analysis, Design and Testing of Integrated Structural Radomes Built Using Photonic Bandgap Structures", *1998 IEEE Aerospace Conference Proceedings*, Vol. 3, Mar. 1998, pp. 463-479, (https://ieeexplore.ieee.org/document/685860/)

[SnSo12] A. Sniady, J. Soler, "An overview of GSM-R technology and its shortcomings", *2012 12th International Conference on ITS Telecommunications*, Taipei, Taiwan, Nov. 2012, pp. 626-629, (http://ieeexplore.ieee.org/stamp/stamp.jsp?arnumber=6425256)

[Stal05] W. Stallings, *Wireless Communications & Networks (2nd Edition)*, Prentice Hall, New Jersey, United States, 2005.

[Stav07] P. Stavroulakis, *Terrestrial trunked radio – TETRA – A global security tool*, Springer, New York, United States, 2007.

[Thal12] Thales – Definitive Design Plan – Technical Specification – Video Transfer System – MMOPL Line 1, Revision No A06, August 2012.

[Thal17] Thales – Broadband Radio System (BBRS), June 2017.

[Thal18] Thales – European Train Control System (ETCS), https://www.thalesgroup.com/en/european-train-control-system-etcs, Nov. 2017.

[TrSS12] T. Tran, Y. Shin, O. Shin, "Overview of enabling technologies for 3GPP LTE-Advanced", *EURASIP J. Wireless Communications and Networking*, vol. 2012, no. 2, Feb. 2012, pp. 1-12, (https://jwcn-eurasipjournals.springeropen.com/articles/10.1186/1687-1499-2012-54)

[TsVi05] D. Tse, P. Viswanath, *Fundamentals of Wireless Communications*, Cambridge University Press, Cambridge, UK, 2005.

[WaZC14] Q. Wang, H. Zhu, R. Chen, "Computation of Reflection and Transmission Coefficients of Frequency Selective Surfaces Using Sub-Entire-Domain Basis Function Method", *2014 2nd International Conference on Systems and Informatics (ICSAI 2014),* Shanghai, China, Nov. 2014, pp. 559-563, (https://ieeexplore.ieee.org/document/7009349/)

[Wlan18] Wikipedia – List of WLAN channels, https://en.wikipedia.org/wiki/List_of_WLAN_channels.

[XZZW08] R. Xu, H. Zhao, Z. Zong, W. Wu, "Dual-Band Capacitive Loaded Frequency Selective

Surfaces With Close Band Spacing", *IEEE Microwave and Wireless Components Letters*, Vol. 18, No. 12, Dec. 2008, pp. 782-784, (http://ieeexplore.ieee.org/document/4686771/)

[ZAZW17] Z. Zhong, B. Ai, G. Zhu, H. Wu, L. Xiong, F. Wang, L. Lei, J. Ding, K. Guan, R. He, *Dedicated Mobile Communications for High-Speed Railway*, Springer, Berlin, Germany, 2017.

[Zhan03] Y. Zhang, "Novel Model for Propagation Loss Prediction in Tunnels", *IEEE Transactions on Vehicular Technology*, Vol. 52, No. 5, Sep. 2003, pp. 1308-1314, (http://ieeexplore.ieee.org/abstract/document/1232695/)